Metabolic stress and tumor progression

A role for glutamine in fibroblast migration

Aida Mestre-Farrera

DOCTORAL THESIS UPF / 2019

Work performed under the supervision of Dr. Antonio García de Herreros in the Mechanisms of Tumorigenesis and Tumor Progression group, from the Cancer Research Program in Institut Hospital del Mar d'Investigacions Mèdiques (IMIM).

Barcelona 2019

Antonio García de Herreros
Thesis Director

Aida Mestre-Farrera
PhD student

DEPARTMENT OF EXPERIMENTAL AND HEALTH SCIENCES

Universitat Pompeu Fabra Barcelona

IMIM Parc de Salut MAR Barcelona
Institut Hospital del Mar d'Investigacions Mèdiques

Senda de otoño
por la que nadie pasa
salvo el ocaso.

MATSUO BASHŌ

ACKNOWLEDGEMENTS

Durant aquests quatre (intensos!) anys he rebut molt suport per part de molta gent. Així doncs, vull agrair a tots aquells que, ja sigui a nivell científic, en forma de bons moments o en *tuppers* han contribuït a que el doctorat hagi estat una etapa molt feliç (tot i l'estrès!).

En primer lloc, vull agrair-te Antonio que em donessis l'oportunitat de quedar-me al laboratori a fer el doctorat. Gràcies per proposar-me aquest projecte i per guiar-me sempre que fes falta. Gràcies per la paciència, els consells, per la teva fe en aquells experiments que jo creia impossibles i per la "canya" (dubto que cap més *jefe* em persegueixi amb un bastó!). La llibertat que m'has donat al laboratori semblava terrible al principi, però m'ha empès a créixer, a entendre i a estimar la ciència. D'aquí m'emporto molts coneixements i ganes de seguir investigant.

D'altra banda, aquest projecte no hauria estat possible sense el suport econòmic de la Secretaria d'Universitats i Recerca del Departament d'Empresa i Coneixement de la Generalitat de Catalunya, que em va concedir l'ajut per a la contractació de personal investigador novell (FI).

Vull donar les gràcies a tot els que m'han ajudat durant el dia a dia al laboratori. Als antics *Snails* (Núria, Jou, Jelena, Àlex, Lorena, Txell, Rocco, Guillem, Rumi, Rubén i Jordi) i als *Chromatins* (Sandra, Joan Pau, Laura, Ane, Jess i Gemma), que em van acollir de la millor manera. Gràcies per crear un ambient immillorable en el grup amb el taxi, les bromes telefòniques, la xocolata pels drames, el *LOOOX* i infinitat de coses més. También a nuestro lab manager súper enrollado: Raúl, muchas gracias por los momentos *Spielberg*, la divagación científica, la ayuda con el Photoshop, los *coffee breaks* y los cotilleos. Hiciste que inventar ensayos raros de migración fuera más divertido que frustrante. Al Jepi i al Víctor els he d'agrair tota l'ajuda, els consells i la discussió científica (i l'haver-me refrescat la bioquímica). Gràcies Mireia per seguir de ben a prop el meu projecte als seminaris de grup i,

junt amb l'Antonio, per les barbacoes a Mieres.

Lorena, gracias por todo lo que me enseñaste al llegar al laboratorio, por la paciencia, por todos tus consejos y por seguir acordándote de mí y mandándome *papers* años después. Este proyecto habría resultado muchísimo más difícil sin el conocimiento, las técnicas y las células que heredé de ti. Sin la ayuda y buen rollo del *in(en)vasion team* mi entrada en el grupo no habría sido igual. Rubén, hem passat de *mindus* a saber-ne una mica més pràcticament plegats. Moltes gràcies per tots aquests anys, per "encriptar-me" tants assajos d'invasió i fer-me les quantificacions una mica més entretingudes, per cantar Queen a cultius i per promoure el *team-building*.

Jordi, a part de tots els moments compartits al laboratori, a tu t'he d'agrair sobretot, sobretot, el viatge a Cuba (i Santa Clara!!!), que va ser la millor manera per carregar-me d'energia per afrontar l'últim any.

També vull donar les gràcies a tots els que han sigut *Snails* de passada: Andrea, Nancy, Nacho, Hernán, Ramona, Rian, Martina, Mees, Kati, Mireia, Laura, Maria, Neus, Carmen i Asya. Especialment a la Maria Val, per l'alegria al lab i pels vespres de *body combat*, i als que m'han patit com a *jefa* i s'han implicat en el meu projecte (Kevin i Alba).

A tots els *Snails* que queden, us desitjo molta sort dins i fora del lab! Marina, mil gràcies per ajudar-me en la recta final del doctorat i per la paciència de fer "reunions" per *whatsapp* i de desxifrar els meus protocols. David, echaré de menos tus fantasías y tu arte, e ¡incluso tus bucles de OT y Rosalía! Estoy segura de que, después de todo el esfuerzo e implicación en el laboratorio de estos años, tendrás muy buen final de tesis. Héctor, les teves ganes de trobar un laboratori amb bon rotllo per fer el doctorat ja apuntaven maneres. Gràcies pels bons moments i per comprar pernils! Raulillo, gràcies pel teu interès en la meva feina i per ajudar-me, tot i que no formés part de les teves pràctiques. Estic contentíssima de que hagis tornat al grup! Santi, gràcies per la xocolata d'alemanya (que ha sigut ideal en els últims

mesos d'experiments) i per ser tant atent amb tots nosaltres. Gràcies també als *catenins*, Willy (strongs) i Bea. Després d'anys de demanar-vos algun reactiu de tan en tan, he descobert lo divertit que és tenir-vos a prop!

No només he estat envoltada de bons *Snails*, sinó que aquests anys al PRBB m'han permès conèixer, compartir i col·laborar amb moltíssima altra gent. No em puc oblidar dels nostres veïns de passadís: els PNs, els Bigas i els Albanells, els Celians i els Calons, amb qui he compartit molt més que protocols i reactius. A Pili y a Rosi por el cariño, los ánimos y las risas con las que me han acompañado cada tarde. També al personal de recerca i de serveis de l'IMIM, així com als serveis de genòmica de la UPF, de citometria i microscòpia del CRG, especialment a l'Arrate, la Raquel i el Xavi per estar sempre disposats a ensenyar-me i resoldre els meus problemes tècnics.

Quan marxi del PRBB una de les coses que trobaré a faltar més és, sens dubte, les tardes a la coral. Gràcies Òscar per plantejar uns assajos tan dinàmics i divertits i per convidar-me a participar en els teus altres projectes. Gràcies a tots els cantaires pels concerts viscuts, sobretot al Rocco, que em va animar a apuntar-me, a les sopranos (especialment l'Erika, la Maria F., la Laura, la Lídia, la Maria M. i l'Elisabeth), a l'Aleix, pel S*omebody to Love*, a l'Imma pels pica-piques i les partitures, i als que sempre estan disposats a sortir a sopar.

Gràcies Pere, Mas, David, Pol, Alba, Mireia, Elena i Marta pels retrobaments al Penedès, les festes majors i les calçotades, que m'han servit per desconnectar, de tan en tan, del món científic.

Finalment, vull agrair a la meva família tot el que ha fet per mi. Als meus pares, per creure'm capaç i per cuidar-me sempre. A la meva àvia, per animar-me (i per alimentar-me!). Al meu avi, per estar tan orgullós del que faig. A la Teresa i l'Enric, pels sopars i el *comté*, i per estar sempre pendents de mi. A la Pumi, que m'ha vigilat mentre escrivia i ha defensat la meva tesi amb ungles i dents de gatet.

Tampoc puc oblidar-me de la que ha estat la meva família a Barcelona. Lídia, va ser una súper casualitat que ens poséssim en contacte i un gran encert venir a viure a casa teva. Amb tu he compartit l'afició per la música i incomptables històries del PRBB. Gemma, m'has fet riure infinitament amb els teus drames diaris i les anècdotes de l'hospital. Marta, ¡eres el ingrediente que nos faltaba en el piso! Y no lo digo sólo por tus ataques de limpieza… Tot i que cada vegada visquem més lluny, em quedo amb les sorpreses d'aniversari (i tenir-vos no se quantes hores esperant amb el llum apagat), els viatges a Alemanya i els sopars d'hummus de supervivència.

I (com dirien els *yankees) and last but not least*, gràcies Guillem. A tu no et puc escriure res que no sàpigues ja. Ets la persona que més m'ha ajudat dins i fora del laboratori. M'has resolt mil dubtes sobre pull-downs i ubiqüitines i m'has esperat pacientment i amb el sopar a punt quan arribava tard (fins i tot t'has llegit la tesi!). M'has alegrat els dies dolents i has multiplicat els bons. Has estat el millor d'aquesta etapa i no puc esperar a començar-ne la següent a San Diego!

ABSTRACT

Tumors are complex tissues composed by multiple cell types, such as cancer associated fibroblasts (CAFs), that facilitate the invasive behavior of tumor cells. When we examined their nutrient requirements, we observed that CAFs rely much more on glutamine than epithelial tumor cells; consequently, they are more sensitive to glutaminase inhibition. Glutamine-dependence in CAFs promotes their migration and invasion towards this amino acid when challenged with a gradient of glutamine. Moreover, fibroblasts support the collective invasion of epithelial tumor cells towards glutamine, a process that is governed by TGF-β/Snail1-dependent fibroblast activation. Fibroblasts migrating towards glutamine present a polarized distribution of Akt2, that is modulated by the E3 ubiquitin ligase TRAF6 in response to TGF-β stimulation and glutamine availability. In addition, the depletion of this Akt isoform prevents the effect of these cells on epithelial tumor invasion. Therefore, these results demonstrate that the high dependence on glutamine of CAFs promotes nutrient-driven tumor invasion.

RESUM

Els tumors son teixits complexos compostos per diversos tipus cel·lulars, així com els fibroblasts associats a tumors (CAFs), que fomenten un comportament invasiu en cèl·lules canceroses. A l'examinar els requeriments nutricionals d'aquestes cèl·lules, vàrem observar que els CAFs són molt més dependents a glutamina que les cèl·lules tumorals epitelials. En conseqüència, els CAFs són més sensibles a la inhibició de l'enzim glutaminasa. La seva dependència a glutamina promou tant la migració com la invasió dels CAFs cap a aquest aminoàcid. A més, els fibroblasts promouen la invasió col·lectiva de cèl·lules tumorals epitelials cap a un gradient de glutamina, en un procés governat per l'activació de fibroblast depenent de TGF-β i Snail1. Al migrar cap a glutamina, els fibroblasts presenten una distribució polaritzada d'Akt2, que està regulada per la ubiqüitina-lligasa TRAF6 en resposta a TGF-β i la disponibilitat de glutamina. La depleció d'Akt2 prevé l'efecte dels CAFs en la invasió de cèl·lules canceroses. Així doncs, aquests resultats demostren que l'alta dependència a glutamina promou la invasió tumoral estimulada per nutrients.

TABLE OF CONTENTS

TABLE OF FIGURES

INTRODUCTION

RESULTS

LIST OF TABLES

RESULTS

MATERIALS AND METHODS

ACRONYMS AND ABBREVIATIONS

ACL: ATP-citrate lyase

ADAM: A Disintegrin and metalloproteinase

ATP: Adenosine triphosphate

BSA: Bovine serum albumin

CAFs: Cancer associated fibroblasts

CAR: Coxsackie-and-adenovirus receptor

CAV1: Caveolin 1

CCL5: Chemokine (C-C motif) ligand 5

CTCs: Circulating tumor cells

CTGF: Connective tissue growth factor

Ctl: Control

CXCL12: Chemokine C-X-C motif ligand 1

DAB: 3,3'-diaminobenzidine

DMEM: Dulbecco's modified Eagle medium

DMSO: Dimethyl sulfoxide

DNA: Deoxyribonucleic acid

DUB: Deubiquitinating enzyme

EBSS: Earle's balanced salt solution

ECM: Extracellular matrix

EGF: Epidermal growth factor

eIF4E: Eukaryotic translation initiation factor 4E

ELISA: Enzyme-linked immunosorbent assay

EMT: Epithelial-to-mesenchymal transition

FA: Focal adhesion

F-actin: Fibrillar actin

FAFs: Fibrosis-associated fibroblasts

FAP: Fibroblast-associated protein

FBS: Fetal bovine serum

FBXL5/14: F-box leucine-rich-repeat protein 5/14

FGF: Fibroblast growth factor

FN1: Fibronectin 1

GFP: Green fluorescent protein

Glc: Glucose

GLS1: Glutaminase 1

Gln: Glutamine

Glu: Glutamate

GLUD: Glutamate dehydrogenase

GLUT1: Glucose transporter 1

GM: General metalloprotease inhibitor

GS: Glutamine synthetase

GSK-3β: Glycogen synthase kinase 3β

HE: Hematoxylin & Eosin

HGF: Hepatocyte growth factor

HIF-1α: Hypoxia-inducible factor 1α

HK: Hexokinase

ICAM1: Intracellular adhesion molecule 1

IF: Immunofluorescence

IGF: Insulin-like growth factor

IHC: Immunohistochemistry

IL: Interleukin

KD: Knock-down

KO: Knock-out

Lac: Lactate

MAPK: Mitogen-activated protein kinase

Mdm2: Murine/human double minute 2

MEFs: Mouse embryonic fibroblasts

MEM: Minimum essential medium

MMPs: Matrix metalloproteases

MMTV-PyMT: Mammary mouse tumor virus polyoma middle-T

MSCs: Mesenchymal stem cells

mTOR: Mammalian/mechanistic target of rapamycin

NAFs: Normal-associated fibroblasts

NEAA: Non-essential amino acids

NF-κB: Nuclear factor κB

Ni-NTA: Nickel nitrilotriacetic acid

OAA: Oxaloacetate

PARP1: Poly(ADP-ribose) polymerase 1

PBS: Phosphate buffer saline

PDGF: Platelet-derived growth factor

PDGFRβ: PDGF receptor β

PDL1 / 2: Programmed cell death protein ligand 1 / 2

PFA: Paraformaldehyde

PFK: Phosphofructokinase

PGE_2: Prostaglandin E_2

PGI: Phosphoglucose isomerase

PI3K: Phosphatidylinositol-3-kinase

PTEN: Phosphatidylinositol 3,4,5-trisphosphate 3-phosphatase

RAGB / C: Ras-related GTP-binding protein B / C

RC: Reductive carboxylation

RFP: Red fluorescent protein

RhoA: Ras homolog family member A

RNA: Ribonucleic acid

ROS: Reactive oxygen species

RT-qPCR: Reverse transcription quantitative polymerase chain reaction

SB: Laemmli sample buffer

SDF1: Stromal cell-derived factor 1

SDS-PAGE: Sodium dodecyl sulfate polyacrylamide gel electrophoresis

shRNA: Short-hairpin RNA

SLC: Solute carrier transporter

S6: Ribosomal protein S6

S6K1: Ribosomal S6 kinase

TAK1: TGF-β-associated kinase 1

TAMs: Tumor associated macrophages

TBS-T: Tris buffer saline – Tween

TCA: Tricarboxylic acid

TFs: Transcription factors

TGF-β: Transforming growth factor β

TGFbRI and II: TGF-β receptor I and II

TGS: Tris-Glycin-SDS

TME: Tumor microenvironment

TNF-α: Tumor necrosis factor α

TRAF6: TNF receptor associated factor 6

TBS-T: Tris-buffered saline-Tween

TWIST1: Twist family BHLH transcription factor 1

UDP-GlcNAc: Uridine diphosphate N-acetylglucosamine

USP27X: Ubiquitin specific peptidase 27 X-Linked

VCAM1: Vascular adhesion molecule 1

VEGF: Vascular endothelial growth factor

WT: Wild-type

Zeb: Zinc finger E-box-binding homeobox

α-KG: α-ketoglutarate

α-SMA: α-smooth muscle actin

β-TrCP1: β-transducin-repeat containing protein

4EBP: eIF4E-binding protein

INTRODUCTION

1. CANCER

1.1. A general overview

Cancer (from the Greek *karkinos* – crab and *-oma* – growth) is a general term for a complex collection of genetic diseases that are characterized by the over-proliferation of abnormal cells and their spread to other tissues and organs[1]. Importantly, cancer is the second cause of death worldwide and it will be likely developed by one in two men and three women during their life[2].

In cancer, dysfunction of normal cell homeostasis has many origins[3]. The characteristics of each case and even within cells from the same tumor are very diverse; thus, complicating its diagnosis and treatment[4,5]. It is also for this reason that the classification of cancer types represents a great challenge[4]. Nowadays, simplistic classifications that were based on the tissue or organ of origin, the onset and the histopathological characteristics of tumors are being substituted with a more complex molecular profiling[6], arisen from the development of genomic sequencing and other high-throughput techniques.

In an effort to connect all types of malignant growth, Hanahan and Weinberg defined a series of traits that are commonly acquired in all tumors regardless their heterogeneity. These hallmarks initially consisted in 1) self-sufficiency in growth signals, 2) insensitivity to growth suppressors, 3) evasion of apoptosis, 4) limitless replicative potential, 5) sustained angiogenesis and 6) tissue invasion and metastasis[7]. Years later, they were extended by the addition of two new characteristics: 7) reprogramming of energy metabolism and 8) evasion of immune destruction[8] **(Fig. I1)**. All these shared capabilities are acquired by different mechanisms among tumors, yet they derive from an accumulation of somatic mutations that is caused by genomic instability. In some cases, these mutations promote a gain of function in genes involved in cell proliferation and survival (also known as oncogenes); in others, there is a loss of function of genes that regulate cell cycle progression and apoptosis (tumor suppressor genes)[9].

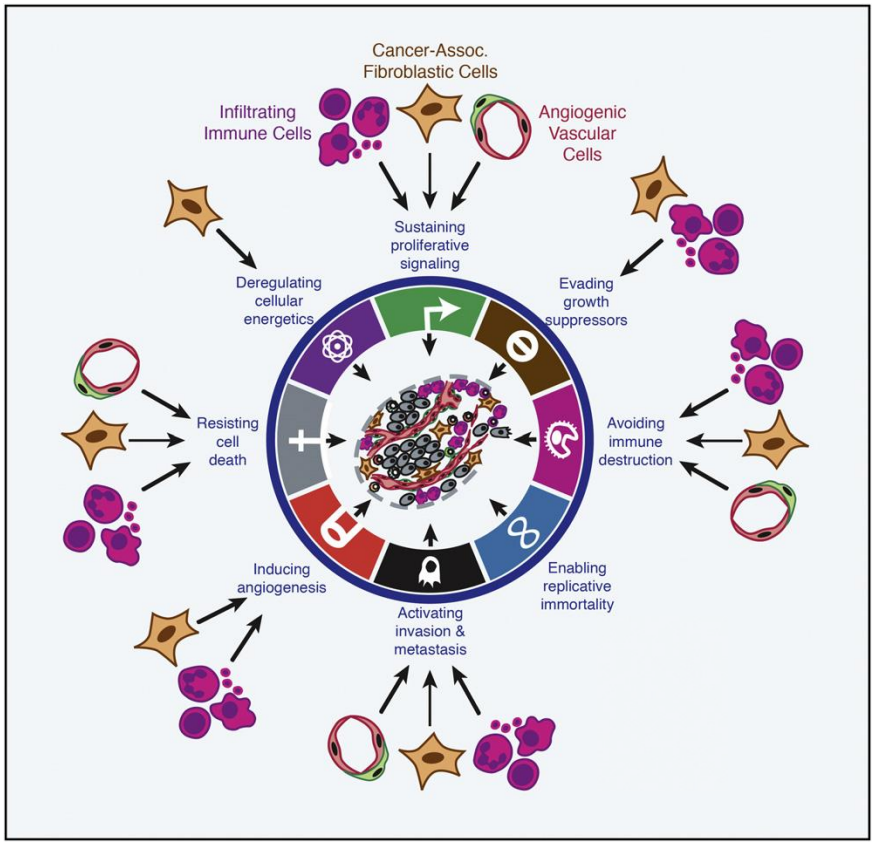

Figure I1. Contributions of stromal cells to the hallmarks of cancer[11]. Connection between some of the stromal components (infiltrating immune cells, cancer associated fibroblasts and angiogenic vascular cells) with the different hallmarks of cancer.

Most importantly, the definition of these hallmarks implied that tumors are not only formed by cancer cells, but they are composed by other normal tissue and bone marrow-derived cells, also known as tumor stroma[8]. These specialized cell types are in constant cross-talk with tumor cells, which modulate their recruitment to the tumor site and their reprogramming towards new tumor-supporting functions[10]. Tumor stroma is mostly comprised by cancer associated fibroblasts, infiltrating immune cells and angiogenic vascular cells. Although the specific contributions of each cell type are tumor class and organ-specific, there is evidence of their influence in seven of the eight hallmarks of cancer[11] **(Fig. I1)**.

For instance, immune cells encompass a broad heterogeneous population of different cell types that can have either anti-tumorigenic or pro-tumorigenic roles and play decisive functions at different stages of tumor progression[12]. They maintain high levels of inflammation that can trigger tumor initiation, promote cell growth and influence cancer cell dissemination[13]. In the case of vasculature, its most important functions are sustaining tumor cell proliferation and preventing cell apoptosis by the transport of oxygen and nutrients into the tumor[11].

Notably, cancer associated fibroblasts (CAFs) are the most abundant cell type in the stroma and modulate tumor progression by their multiple interactions with tumor cells and other stromal components[14]. By the secretion of signaling molecules and matrix remodeling enzymes, they influence several processes including tumor cell proliferation, apoptosis resistance, metastasis, neoangiogenesis or immune suppression[15]. The contributions of CAFs to invasion and metastasis will be further examined in the following chapters, since this has been the main objective of this thesis.

1.2. Metastasis is a multistep process

Despite being considered a very inefficient process, metastatic dissemination represents the major cause of mortality in cancer patients[16,17]. This process can be divided in two major phases, beginning with tumor cell dissemination from the primary tumor to distant tissues and followed by their adaptation to a foreign tissue microenvironment and its colonization[16].

Metastatic dissemination starts when tumor cells acquire enhanced motility, which promotes their invasion to the surrounding tissues and their intravasation (as single cells or clusters) to the tumor vasculature[18,19]. To survive in the bloodstream, tumor cells need to overcome *anoikis* (programmed cell death induced by the lack of attachment) and immune attack[20,21]. Circulating tumor cells (CTCs) are then mechanically arrested in small capillaries and extravasate into the parenchyma of target organs[22]. This process is influenced by the presence of organ-specific circulatory patterns and the morphology of the capillary walls[23]; for instance, fenestrated endothelium from liver and bone marrow capillaries facilitate tumor cell extravasation in these organs, since they present a high permeability[24]. After their extravasation, tumor cells must evade the innate immune response in order to successfully establish in supportive niches[25], which are often generated before the arrival of cancer cells by signals derived from the primary tumor[26]. Once in the secondary niche, tumor cells can remain dormant as single cells or small nodules of cancer cells (micrometastasis) for months or decades, and finally reinitiate their growth into macroscopic lesions[27]. All the steps in metastatic colonization are represented in **Fig. I2.**

Importantly, metastatic dissemination is modulated by therapy-induced cellular stress[16]. After therapy, residual metastatic cells exhibit an enhanced secretion of survival-related signals and form supportive interactions with the tumor microenvironment[28], which leads to the emergence of drug-resistant cells and the outgrowth of a resistant tumor[16] **(Fig. I2)**.

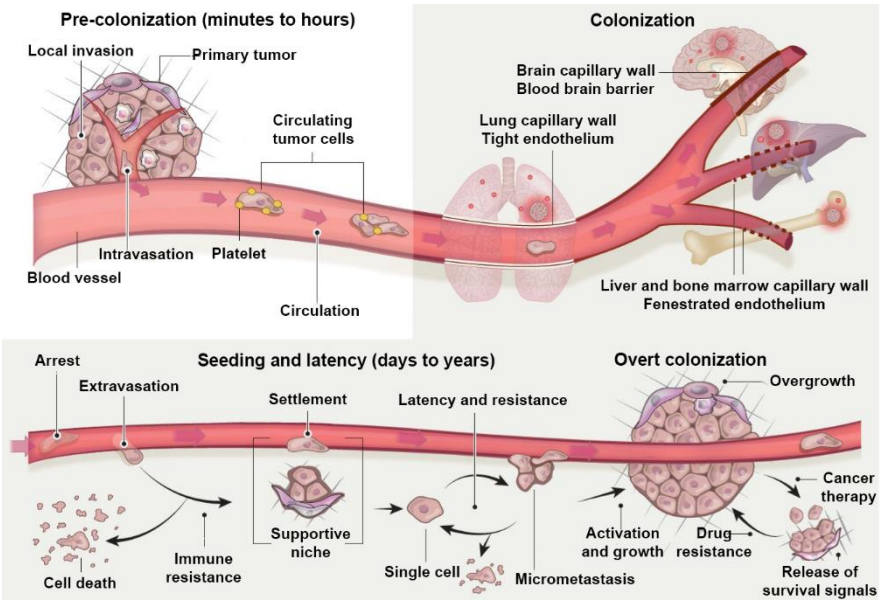

Figure I2. Steps in metastatic colonization[16]. Motile tumor cells invade adjacent tissues and enter the circulatory system. After overcoming *anoikis* and immune attack in the blood stream, circulating tumor cells (CTCs) are arrested in small capillaries of target organs. The dissemination of CTCs is influenced by the structure of the capillaries in each tissue. Following their extravasation and immune resistance, tumor cells settle in supportive niches as single cells or in small groups (micrometastasis). After a variable period, tumor growth into macroscopic lesions can be restarted (macrometastasis). Metastatic colonization is often influenced by cancer therapies, which promote the appearance of resistant phenotypes if they are not completely efficient.

1.3. Mechanisms of tumor migration and invasion

As aforementioned, tumor cell invasion is a fundamental part in metastatic dissemination. This process is defined by the capability of cancer cells to disrupt the basement membrane and to migrate, first, to the stromal compartment and, finally, to the adjacent tissues and vasculature[29]. During invasion, tumor cells undergo major changes in morphology, cell-cell contacts and cell-matrix interaction, which involve a coordinated regulation of extracellular matrix (ECM) degradation by tumor-derived matrix metalloproteases (MMPs)[30]. Several mechanisms of cell invasion have been described[31].

1.3.1. Mesenchymal invasion

Epithelial tissue homeostasis is maintained by the formation of different types of contacts between adjacent cells (tight junctions, gap junctions, adherens junctions and desmosomes) and the union with the basal lamina through hemidesmosomes and α6β4 integrins[32]. To become invasive, epithelial cells need to detach from their counterparts by breaking these interactions[33]. In a process called epithelial-to-mesenchymal transition (EMT), epithelial cells lose their characteristic apicobasal polarity and acquire new mesenchymal traits, displaying front-rear polarity and actin reorganization into stress fibers[34]. EMT is a reversible mechanism (being mesenchymal-to-epithelial transition its opposite) that was first defined in embryonic development, since it plays an important role in gastrulation and neural crest formation[35]. In adult tissues, it is restricted to some specific situations as wound healing and to pathologies such as fibrosis or cancer[35,36]. In any of these situations, EMT rarely advances to its completion; for instance, it is mainly presented as a collection of intermediate phenotypes, characterized by the expression of both epithelial and mesenchymal markers[37].

The most important feature of the EMT is the repression of the E-cadherin-encoding gene *CDH1*[36]. E-cadherin is an essential component of adherens junctions, where it connects the cytoskeleton of adjacent cells by its association with β-catenin and actin filaments[38]. Upon its cleavage and degradation, there is a release of β-catenin and other transcription factors such as the p65 subunit of NF-κB, that translocate to the nucleus and participate in the transcriptional activation of other mesenchymal markers[39,40]. EMT is characterized by the up-regulation of mesenchymal proteins such as fibronectin (FN1), which mediates ECM assembly by its binding to α5β1 integrins and collagen[41]; vimentin, involved in microtubule polarization and focal adhesion (FA) maturation[42]; or the pro-invasive signal transducer N-cadherin[43] **(Fig. I3)**.

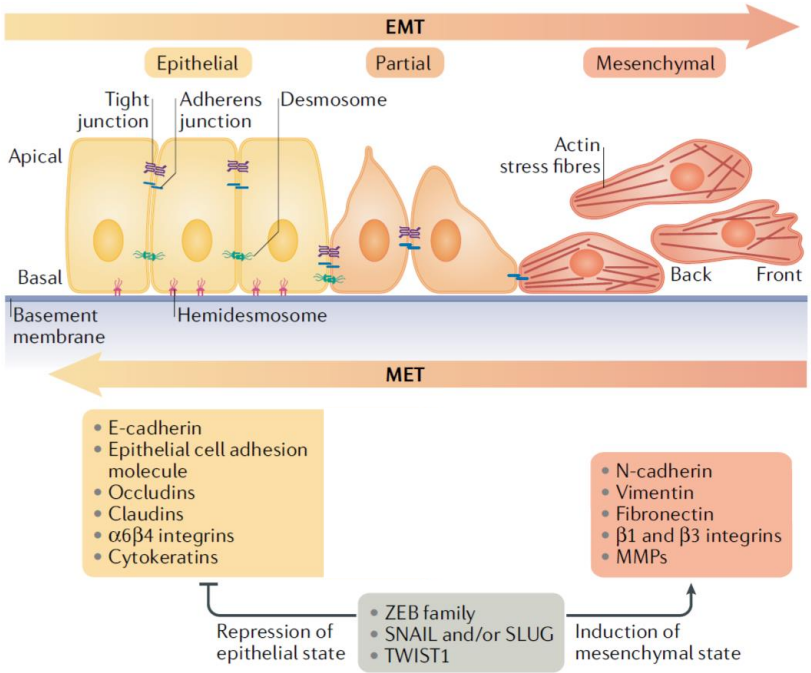

Figure I3. Cellular events during epithelial-to-mesenchymal transition (adapted from[34]). During EMT, epithelial cell-cell contacts (tight junctions, ahderens junctions and desmosomes) and cell-matrix contacts (hemidesmosomes) are disassembled and cell polarity is lost. Invasive properties are then acquired by actin reorganization into stress fibers and MMPs-stimulated matrix degradation. Mesenchymal markers up-regulation (listed in the orange box) and repression of epithelial genes (in the yellow box) are regulated by the EMT-inducing transcription factors Snail (Snail1), Slug (Snail2), Twist1 and Zeb1/2. Between these two states there is a spectrum of partial-EMT phenotypes expressing both epithelial and mesenchymal markers. EMT can be reverted through a process known as mesenchymal-to-epithelial transition (MET), that promotes E-cadherin up-regulation.

Changes in gene expression during the EMT are regulated by different transcription factors (EMT-TFs) including Snail1, Snail2, Twist and Zeb1/2[44] **(Fig. I3)**, which are induced by tumor or stromal-derived growth and differentiation factors such as Wnt, Notch or transforming growth factor β (TGF-β)[45]. Snail1 is the most studied EMT-TF. By its binding to E-boxes (sequences with a 5'-CACCTG-3' core located in

gene promoters), it acts as a transcriptional repressor of epithelial genes such as *CDH1*[46]. Snail1 function is closely related to Akt2, as both proteins are co-regulated: Snail1 increases Akt2 activity, whereas Akt2 controls Snail1 expression[47–49]. Moreover, Snail1 and Akt2 interact increasing the activity of the kinase towards histone H3[47]. Snail1 also interacts with Smad2/3 to repress the transcription of *CDH1* and the tight-junction components occludin, claudin and coxsackie-and-adenovirus receptor (CAR)[50]. Snail1 function is not limited to the repression of epithelial genes, since it also acts as an activator of mesenchymal marks; for instance, it is responsible of the transcriptional up-regulation of *FN1* acting in coordination with p65-NF-κB and Poly(ADP-ribose) polymerase 1 (PARP1)[40]. In addition, Snail1 also increases the expression of other EMT-TFs as Zeb1 and Zeb2, that further extend the repression of E-cadherin[51,52].

Snail1 expression is controlled at multiple levels[53]. It is remarkable that Snail1 RNA and protein do not always associate, since Snail1 is a very unstable protein[51]. In normal conditions, it is sensitive to ubiquitination and proteasomal degradation, a process that is mediated by several ubiquitin ligases, such as β-transducin-repeat containing protein 1 (β-TrCP1), F-box leucine-rich-repeat protein 5 and 14 (FBXL5; FBXL14) or murine double minute 2 (Mdm2)[51,54–56]. Snail1 half-life is also modulated by phosphorylation, being glycogen synthase kinase 3β (GSK-3β) its paradigmatic protein kinase. GSK-3β phosphorylates Snail1 in two different residues, triggering its nuclear export and β-TrCP1-mediated proteasomal degradation[57]. Besides GSK-3β, Snail1 is also phosphorylated by other kinases, either positively or negatively regulating its stability[51,53].

Snail1 expression is modulated by many stimuli, being TGF-β the most relevant in processes such as EMT or fibroblast activation[58]. TGF-β increases Snail1 protein stability by the action of different mechanisms including the activation of Phosphoinositide 3-kinase (PI3K)-Akt pathway, which phosphorylates and inhibits GSK-3β[59]; and the up-regulation of ubiquitin specific peptidase 27 X-linked (USP27X), a deubiquitinating enzyme (DUB) that counteracts the action of Snail1

ubiquitin ligases[60]. Moreover, TGF-β controls *SNAI1* transcription through the activation of its canonical effectors. In this process, TGF-β ligand binds to its heterodimeric receptor complex (formed by TGFbRI and II) and induces the phosphorylation of SMAD2 and SMAD3, which then bind to SMAD4 and translocate to the nucleus[61]; there, the SMAD complex recruits other co-factors to the promoter of *SNAI1* and other target genes[50,53].

The effects of TGF-β are very diverse and depend on the prevalence of different SMAD co-factors and the interaction with other non-canonical signaling cascades[61]. For instance, the activation of non-canonical TGF-β signaling pathways, involving mitogen-activated protein kinase (MAPK) or nuclear factor κB (NF-κB), also increase Snail1 transcriptional regulation of epithelial and mesenchymal genes[40,62]. Some of the non-canonical effectors of this pathway are modulated by the E3 ubiquitin ligase tumor necrosis factor receptor-associated factor 6 (TRAF6), which interacts with TGFbRI and activates several substrates through Lys63-linked polyubiquitination. TGF-β-dependent TRAF6 activity is required for TGF-β-associated kinase 1 (TAK1)[63] and p38 MAPK activation, that promotes c-Jun expression and its activation and binding to *SNAI1* promoter[64]. TRAF6 also polyubiquitinates the PI3K regulatory subunit p85α, leading to the activation of PI3K-Akt axis[65]; and directly binds to Akt, promoting its cytoplasmatic localization and facilitating its activation via phosphorylation[66].

1.3.2. Other modes of invasion

In addition to mesenchymal invasion, other modes of tumor cell migration and invasion have been described. Actually, invasion strategies can be classified in two major groups: single-cell invasion, when cell-cell junctions are absent, or collective cell invasion, when these adhesions are maintained[67] **(Fig. I4)**. The first group includes the paradigmatic mesenchymal cell migration (characteristic of cells with an elongated “spindle-shaped” cell body presenting long protrusions)[68], but also other subtypes, as different types of ameboid-like invasion (typical of cells with low adhesion force, in which motility is driven by short

protrusions or by blebbing)[69]. Collective invasion is characterized by the movement of neighboring cells either as narrow linear strands, as irregularly shaped sheets or as cohesive aggregates depending on the number of leader cells on each case and the stiffness of the matrix[70]. In some cases, these populations can be constituted by a mixture of mesenchymal *leader* cells and epithelial *follower* cells[71] **(Fig. I4)**. There is also the possibility that individual cells that are chemoattracted by the same source move one after each other using the same tracks, in a process that is called *multicellular streaming*[72,73].

The molecular mechanisms of each mode of invasion depend on many signaling pathways as well as on cell-cell, cell-stroma and cell-substrate interactions[73]. Often, the different modes of tumor invasion are interchangeable and respond to local variations in tissue microregions and therapeutic challenge. This plasticity allows a rapid adaptation to environmental changes[67].

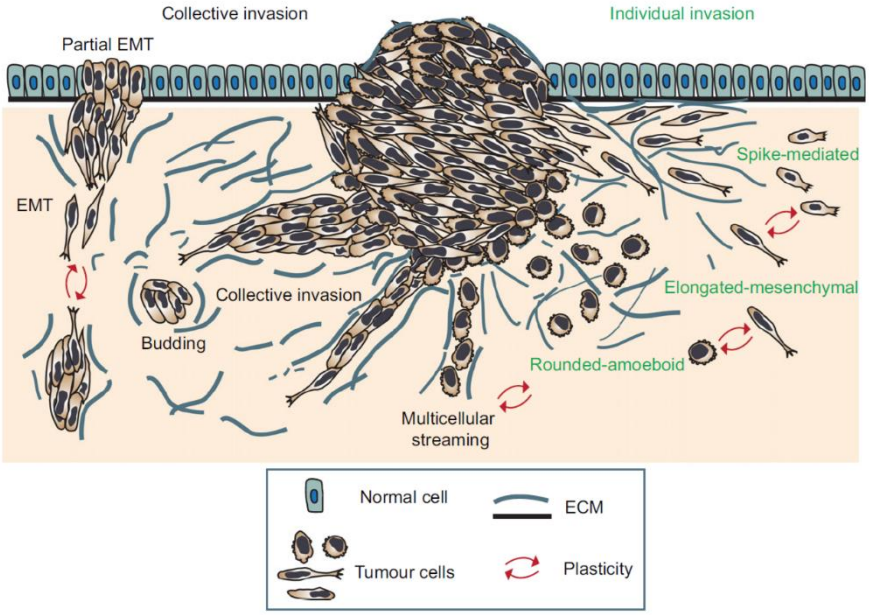

Figure I4. Modes of tumor invasion[72]. Representation of the main individual and collective modes of tumor cell invasion. The plasticity of tumor cells promote that different parts of a tumor invade following different mechanisms.

1.4. Tumor microenvironment

Tumor cells actively modify their context creating a microenvironment of non-transformed cells, also known as tumor stroma, which is mainly composed by immune inflammatory cells, CAFs, endothelial cells, pericytes and ECM[74]. All these components play an important role in the architecture of tumors by remodeling their structure and composition, releasing growth factors and cytokines and influencing tumor cell functions[11]. Hence, it is very difficult, if not impossible, to understand tumor progression and metastasis without considering the contributions of tumor microenvironment (TME).

At the onset of tumors, cancer cells recruit and reprogram many stromal cell types, fostering the formation of a permissive pro-tumorigenic microenvironment that promotes cell growth and dissemination[13]. Nevertheless, this aberrant proliferation causes a decrease in oxygen and nutrients that compromises tumor cell survival and could lead to a massive tumor cell dead (necrosis)[75]. To sustain the nutrient requirements of highly proliferative cells, there is a need to increase intratumor blood supply[76]. Unlike normal tissues, in which vasculature is mostly quiescent, tumors develop a dynamic disorganized vessel network[77]. This process (termed *angiogenic switch*) is triggered by hypoxia[78]. Sensing of hypoxic signals by tumor cells and other stromal types as CAFs and tumor associated macrophages (TAMs) triggers the production of chemokines and pro-angiogenic factors[13,79]. Importantly, increased permeability of the tumor vasculature together with the secretion of MMPs by CAFs and immune cells, facilitates intravasation of tumor cells and their metastatic spread[11].

Besides, stromal cells are crucial for tumor invasion, contributing with growth factors and proteases to this process. CAFs and TAMs promote ECM degradation and remodeling by their enhanced production of MMPs, that are necessary for breaking tumor cell interaction with the basement membrane[80,81]; moreover, they reorient collagen and fibronectin fibers providing tracks for cancer cells migration[73]. In the TME, CAFs, mesenchymal stem cells (MSCs) and immune cells secrete

high amounts of TGF-β and other factors that induce an EMT in the tumor cells, thus promoting mesenchymal-like invasion[82,83]. In addition, local gradients of stromal-derived growth factors and cytokines attract tumor cells, further directing their invasion[11]. There is also evidence that cancer cells are more motile in the proximity of blood vessels[84]; however, it is unclear if this effect is due to signaling molecules, differential ECM stiffness or the abundance of metabolites.

Tumor-stroma cross-talk is maintained during metastatic colonization. In circulation, tumor cells are coated with a shield of platelets[85]; an association that promotes an EMT-like transformation of the tumor cells and protects them from shear forces, immune system and oxidative stress[85]. In addition, metastatic cell tropism for specific organs is modulated by signals derived from the primary tumor, which also contribute to the formation of supportive pre-metastatic niches before the arrival of tumor cells[24]. For instance, local expression of certain factors and chemokines prime receptor-expressing tumor cells for extravasation in particular destinations[16]; moreover, specific integrin expression in tumor-derived exosomes educate organ-specific cells and prepare a favorable microenvironment for metastatic colonization[86,87].

Because of the great influence of the stromal compartment in cancer, understanding TME has enabled the identification of new prognostic biomarkers and therapeutic strategies[88]. For instance, a TGF-β-response stromal signature drives a pro-metastatic program in colorectal tumors[89] by influencing several processes such as angiogenesis, immunosuppression or CAFs activation[90–92]; accordingly, novel therapeutic agents that have been developed to block this pathway are currently in clinical trials[92]. Likewise, different components of the stroma modulate the tumor response to therapies[93] and current strategies consist in a combination of drugs to target both stromal and tumor cells[94]. In this regard, a broad list of compounds that target ECM, neovascularization, CAFs, chronic inflammation, macrophages and myeloid-derived suppressive cells recruitment are under investigation[88,95].

2. CANCER ASSOCIATED FIBROBLASTS

Fibroblasts are non-epithelial, non-immune cells that are responsible for ECM production, remodeling and homeostasis; thus, providing a structural scaffold for tissues. Morphologically, they are defined as spindle-shaped cells located in the interstitial space of connective tissues, where they are embedded within ECM as single cells and present no association with the basement membrane[96]. Fibroblasts were first described as collagen-producing cells[97], yet this is not their only contribution to the formation of a basement membrane. These cells are also involved in the synthesis of fibronectin and laminin and to ECM remodeling and degradation by the secretion of MMPs and A disintegrin and metalloproteinases (ADAMs)[96,98]. Moreover, they regulate epithelial cell differentiation, inflammation and wound healing by the secretion of growth factors and cytokines[97].

In normal tissues, fibroblasts are generally quiescent and only become transcriptionally active in some specific situations as wound healing, inflammation and fibrosis[99,100]. This activation is associated to the expression of α-smooth muscle actin (α-SMA) and vimentin, and a gain in contractility and ECM production[97] **(Fig. I5 A-B)**. In addition, activated fibroblasts present higher levels of intracellular adhesion molecule 1 (ICAM1) and vascular adhesion molecule 1 (VCAM1), both involved in the interaction with other cell types[101,102].

In wound healing, fibroblasts are recruited to the site of the injury by factors secreted during local tissue inflammation. These factors (including fibroblast growth factor, FGF-1 and 2; epidermal growth factor, EGF; platelet-derived growth factor, PDGF; and TGF-β) attract and activate fibroblasts, increasing their proliferation and deposition of ECM components[103]. Subsequently, fibroblasts facilitate wound contraction and the maturation of the scar; concretely, they participate in ECM remodeling and in the substitution of collagen III for collagen I by the secretion of proteases and other enzymes[104]. Upon wound closure, fibroblast activation is reversed either by their reprogramming to a resting phenotype or by apoptosis, being replaced in this case by

new resident non-activated fibroblasts[104,105].

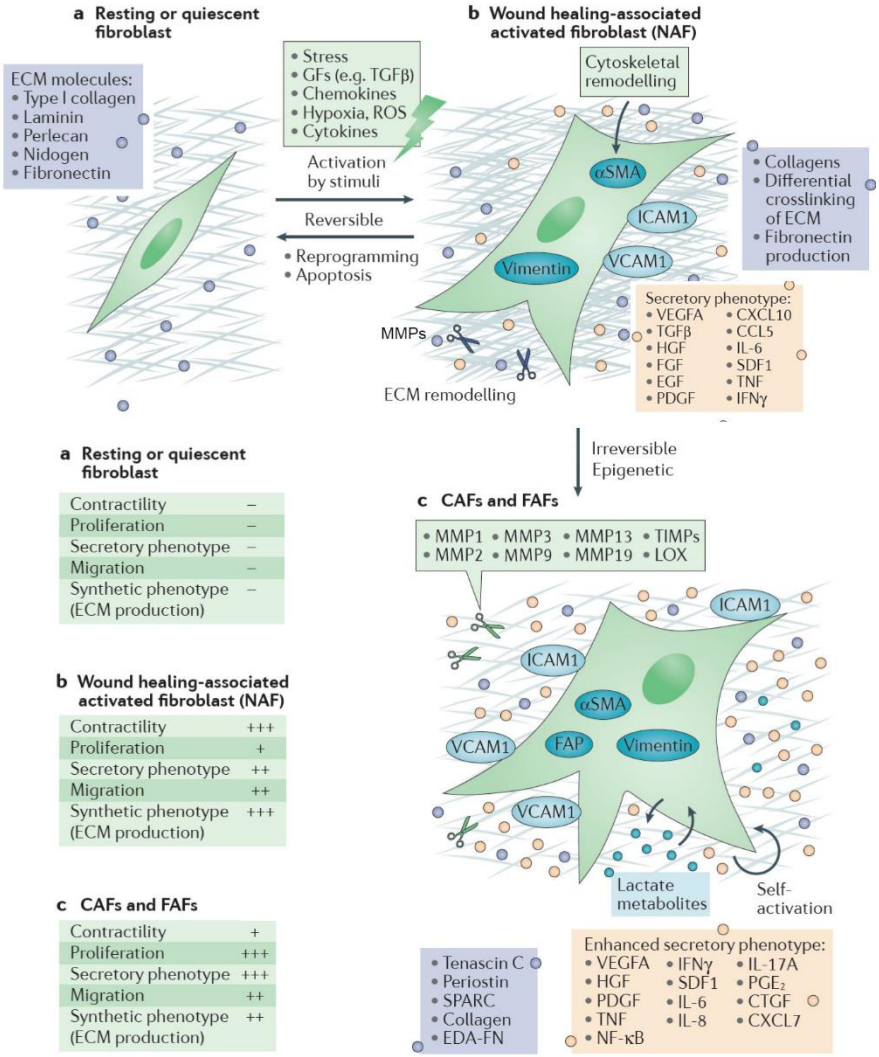

Figure I5. Activation of fibroblasts[97]. A) Resting or quiescent fibroblasts are spindle-shaped cells in the interstitial space between functional parenchyma. **B)** Normal activated fibroblasts (NAFs) participate in wound healing and tissue regeneration. NAFs are characterized by a reversible gain in α-SMA, vimentin, ICAM1 and VCAM1 expression and a stellate shape. They have enhanced ECM production and contractility properties. **C)** Cancer and fibrosis-associated fibroblasts (CAFs and FAFs) exhibit an enhanced secretory phenotype and proliferative properties. Their autocrine activation and the epigenetic regulation of this process limit the reversion of this activation state.

Activated fibroblasts are also a major component of tissue fibrosis, a chronic wound healing condition, and tumors[97,106]. In these two pathological situations, persistent hyperactivation of fibroblasts is likely determined by a combination of chronic inflammation, autocrine stimulation and epigenetic mechanisms that irreversibly enhance anti-apoptotic pathways and proliferation[107,108].

CAFs constitute a dominant component of TME, which encompass highly heterogeneous populations of cells with significant differences in gene expression of ECM-related proteins, cytokines and growth factors[97,109]. In general terms, CAFs present enhanced proliferatory, migratory and secretory phenotypes when compared to non-activated fibroblasts **(Fig. I5 C)** and are characterized by the expression of α-SMA, vimentin, PDGF receptor β (PDGFRβ), S100A4 and fibroblast-associated protein (FAP), although these markers may be not expressed at the same time[97,110]. This broad diversity of CAF markers may depend on the variety of their precursors. As a matter of fact, there is still no consensus in the origin of CAFs; while some studies suggest that they derive from tissue-resident fibroblasts[111], others propose that they come from bone marrow-derived mesenchymal stem cells (MSCs)[112,113]. Other cells of origin might be EMT-transformed cancer cells[114], endothelial cells (that have undergone an endothelial-to-mesenchymal transition)[115] or adipose tissue-derived stem cells[116].

MSCs are multipotent progenitor cells with the ability to differentiate into chondrocytes, osteoblasts, adipocytes or hematopoietic cells upon certain stimulation[117]. Interestingly, MSCs exhibit fibroblast-like markers and properties: they become activated by similar stimuli enhancing ECM production and secretion of growth factors[118]. As they are easily isolated, these cells constitute a good model to study fibroblast activation *in vitro*; yet their value in the study of cancer is not artifactual as MSCs are found in tumors, where they contribute to tumor growth, invasion and transendothelial migration by the secretion of cytokines and MMPs[119,120].

The principal mediators of fibroblast activation in tumors are growth factors released by cancer cells and infiltrating immune cells[121,122]. These include the TGF-β superfamily, PDGFs, EGFs and FGFs, which are also key mediators of chronic tissue damage[121,123]. The exogenous signals determining CAFs functions are highly dynamic among tumor types and time; for instance, they activate either anti-invasive or pro-metastatic functions[97]. In many types of cancer, recruitment and activation of fibroblasts are dependent on TGF-β[91]. As indicated above, its stromal signature is significantly associated with poor prognosis in colorectal[89,124], breast[125] and pancreatic tumors[126]. Once activated, CAFs secrete TGF-β in autocrine fashion, inducing a loop that maintains its activation perpetually and its subsequent contribution to cancer progression[61,91].

2.1. Cancer associated fibroblasts and tumor progression

CAFs contribute to tumor development by the release of secreted paracrine factors but also by physically remodeling the ECM. By these two mechanisms they influence several tumor traits, including neoangiogenesis, inflammation, immunosuppression, tumor growth and invasion[97]. All these effects are summarized in **Fig. I6** and will be next assessed.

On the onset of neoplastic lesions, newly recruited CAFs stimulate pro-survival and self-renewal programs in cancer cells by the release of mitogenic factors such as hepatocyte growth factor (HGF), EGF, connective tissue growth factor (CTGF), insulin-like growth factor (IGF), or interleukin-6 (IL-6)[91]. To overcome the impact of tumor cell overproliferation, CAFs metabolically support tumor cells by the exchange of energy-rich metabolites such as lactate or pyruvate (by the so-called reverse Warburg effect)[127,128]; in addition, CAFs induce angiogenesis by the secretion stromal cell-derived factor 1 (SDF1, also called CXCL12) and the recruitment of endothelial progenitor cells[129].

CAFs interaction with immune cells promotes an immune-suppressive TME. This complex effect is mediated by the secretion of a plethora of factors and cytokines that modulate the different constituents of the immune system[130] (listed in **Fig. I6**). Moreover, CAFs directly interact with immune cells by the expression of ICAM1, which is a docking site for the activation or repression of immune cells[101], and programmed cell death protein ligand 1 (PDL1) and PDL2, that regulate T-cell-mediated immune-suppressive functions[131,132].

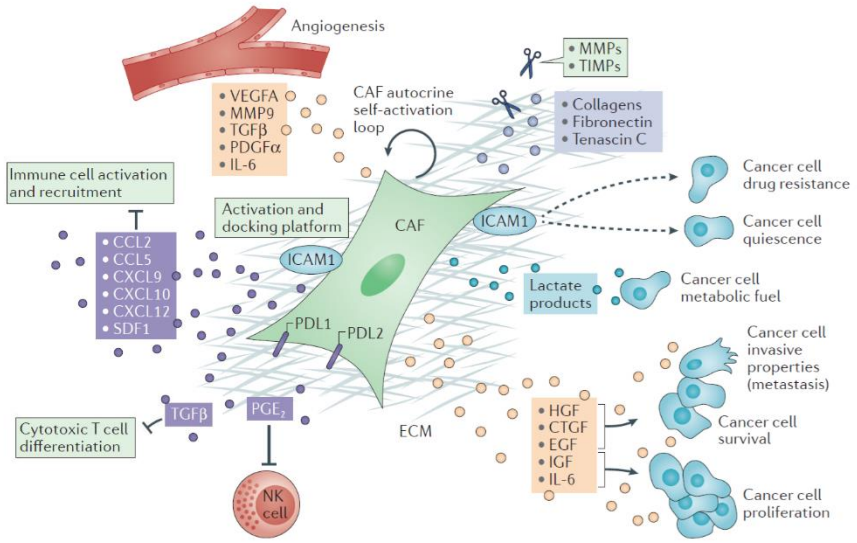

Figure I6. CAFs contribution to tumor progression (adapted from[97]). Activated fibroblasts influence tumor progression by their interaction with tumor cells and other stromal types (immune cells and vasculature). These effects are mediated by CAF-derived secretome, ECM remodeling and cell-cell interactions through the expression of ICAM1, PDL1 and PDL2.

There is also evidence of the contribution of CAFs to stem cell niche formation and its maintenance in lung and colorectal tumors, an effect that is mediated by some of the aforementioned factors[133]. In brief, CAF-derived HGF, IGF, IL-6 and IL-8 confer stemness-like phenotypes in cancer cells by the activation of Wnt, Notch, Nanog or NF-κB signaling[133–135]. Similarly, MSCs promote stemness by the secretion of cytokines and the induction of an aberrant microRNA expression[136].

CAFs have a major influence on tumor cell invasion. As previously described, fibroblasts orchestrate ECM remodeling upon their activation. Importantly they increase the stiffness of the ECM and contribute to the alignment of collagen and fibronectin fibers, thus influencing the directionality of cell migration[137]. By protease-driven degradation, CAFs open tracks into the ECM and lead collective invasion of squamous cell carcinoma cells[138]. EMT-independent collective tumor cell invasion is further enhanced by two other mechanisms: the secretion of chemoattractants, such as prostaglandin E_2 (PGE_2)[139] and chemokine (C-C motif) ligand 5 (CCL5)[119]; or by direct contact between tumor cells and CAFs, which mediates the transmission of mechanical forces through heterotypic E-cadherin/N-cadherin junctions[140]. CAFs also influence EMT by the release of cytokines including tumor necrosis factor α (TNF-α), which induces the EMT-TF Snail1 through NF-κB and Akt signaling pathways[91].

In tumors, the accumulation of a dense fibrillar ECM (desmoplasia) is associated with a poor outcome[141] and, importantly, the modulation of ECM stiffness by CAFs influences cell behavior at different levels[142]. Rigid substrates contribute to tumor invasion and metastasis by promoting EMT[143]; for instance, increased matrix stiffness stabilizes Snail1 in the nucleus of tumor cells[144] and promotes a constitutive nuclear translocation of Twist through its release from the cytoplasmatic binding protein G3BP2[145]. In addition, matrix stiffening increases cyto-skeletal tension and promotes the contractility and migration of tumor cells[146]. Reciprocally, stiff matrices perpetuate the activation of CAFs through ROCK-ERK2 activation and Snail1 nuclear accumulation[144].

The functions of CAFs in metastatic lesions are similar to those in the primary tumor. Specially, they contribute to metastatic niche colonization by promoting tumor growth, *de novo* vasculature formation and cancer cell invasiveness[97,147]. The origin of CAFs in the metastatic site is as heterogeneous as in the primary tumor, as they can derive from bone marrow or tissue-resident fibroblasts and even from the primary tumors; in this case, conferring protection during circulation and a rapid growth advantage to the tumor cells[148].

2.2. The role of Snail1 in fibroblast activation

Activation of CAFs by signals derived from the tumor, such as TGF-β or PDGF, requires the expression of Snail1 transcription factor[149,150]. Studies in our laboratory showed that Snail1 overexpression in these cells enhances the expression of activation markers such as S100A4 and TGF-β[150]. Accordingly, its expression in human malignancies is not limited to cancer cells (in which Snail1 is a crucial factor in triggering EMT) and has been detected in the stroma of epithelial tumors[151,152]. Snail1 stromal signature correlates with a low survival of patients in colorectal[153] and breast tumors, where is mainly expressed in CAFs[137,154]. Snail1 expression in fibroblasts is also relevant for tumor development since its depletion in mice results in a delayed tumor growth[154,155].

Primary colorectal CAFs present higher levels of Snail1 when compared to tissue resident fibroblasts, a difference that is associated with increased levels of α-SMA and FAP[154]. Through a RhoA/α-SMA -dependent mechanism, Snail1 up-regulation in TGF-β-stimulated fibroblasts contributes to fibrillogenesis and production of a stiff ECM with oriented fibers[137]. In a recent publication we demonstrated that induction of Snail1 in fibroblasts by TGF-β derived from tumor cells orchestrates EMT-independent tumor cell invasion; to that end, Snail1 enhances the secretion of MMPs and other paracrine factors including PGE_2, that attract epithelial tumor cells and stimulate their collective invasion[139] **(Fig. I7)**. Concomitantly, orthotopic implantation of breast tumor cells with Snail1-depleted fibroblasts results in a reduction of invasion and metastasis in mice[139].

Snail1 depletion in quiescent fibroblasts does not alter their phenotype[149]; however, a basal Snail1 expression is required for the maintenance of MSCs stemness. *In vitro* Snail1 depletion in these cells accelerates their differentiation to adipocytes or osteoblasts, whereas its depletion in adult mice results in a decrease of bone marrow MSCs[150]. Upon TGF-β stimulation, Snail1 up-regulation in MSCs influences the expression of stemness (CD29 and CD44) and activation

markers (as S100A4); this effect is dependent on Snail1 down-modulation of phosphatidylinositol 3,4,5-trisphosphate 3-phosphatase (PTEN) and its consequent Akt activation[150]. Snail1 also controls the tumorigenic properties of MSCs. For instance, Snail1 depletion in p53 knock-out MSCs prevents sarcomagenesis in immunodeficient SCID mice[156], an effect that correlates with increased Snail1 expression in undifferentiated aggressive sarcomas[151].

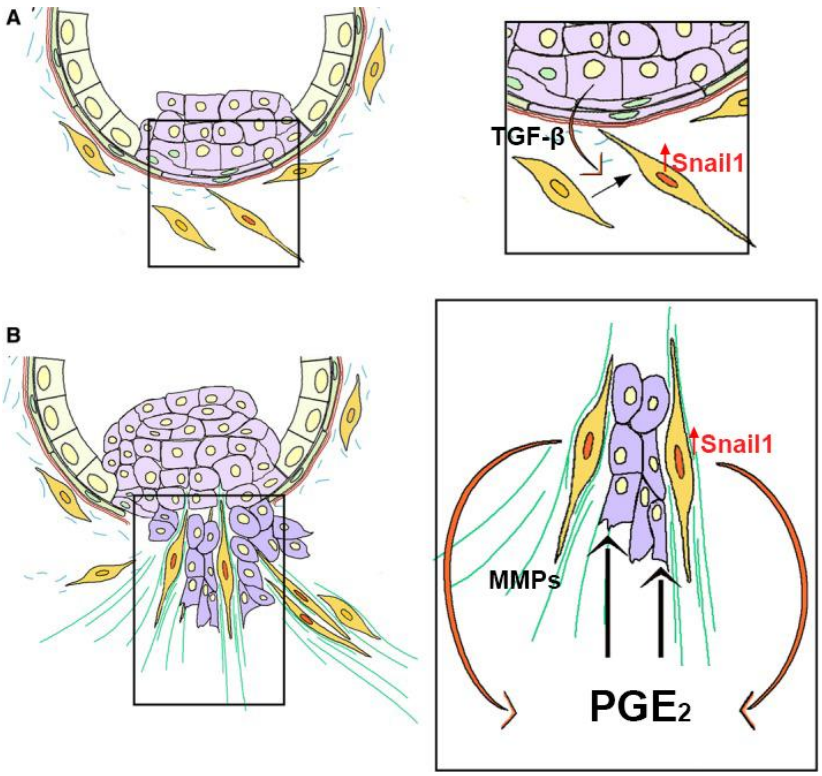

Figure I7. Snail1-dependent activation of CAFs controls epithelial tumor cell invasion (adapted from[152]). (A) Tumor cell-derived TGF-β promotes the activation of CAFs through Snail1 up-regulation. **(B)** Snail1-dependent activation of CAFs enhances the secretion of prostaglandin E_2 (PGE_2) and matrix metalloproteases (MMPs), stimulating epithelial tumor cells collective invasion. Whereas MMPs degrade the matrix creating new tracks for migration, PGE_2 acts as a chemoattractant.

3. TUMOR METABOLISM

3.1. Tumor cell metabolism

In 1923, Otto Warburg first described that under aerobic conditions tumors metabolize approximately ten-fold more glucose than normal tissues[157], a phenomenon known as aerobic glycolysis or the Warburg effect. This seminal observation established the basis for one of the core hallmarks of cancer: reprogramming of energy metabolism[8]. A century on, there is a broad appreciation that tumor metabolism is significantly altered and supports the increased anabolic requirements of over-proliferative malignancies. By these means, tumor cells convert most of their glucose to lactate even in oxygen-rich conditions, in contrast to most non-proliferating differentiated cells, which efficiently produce adenosine triphosphate (ATP) through oxidative phosphorylation[158] **(Fig. I8)**.

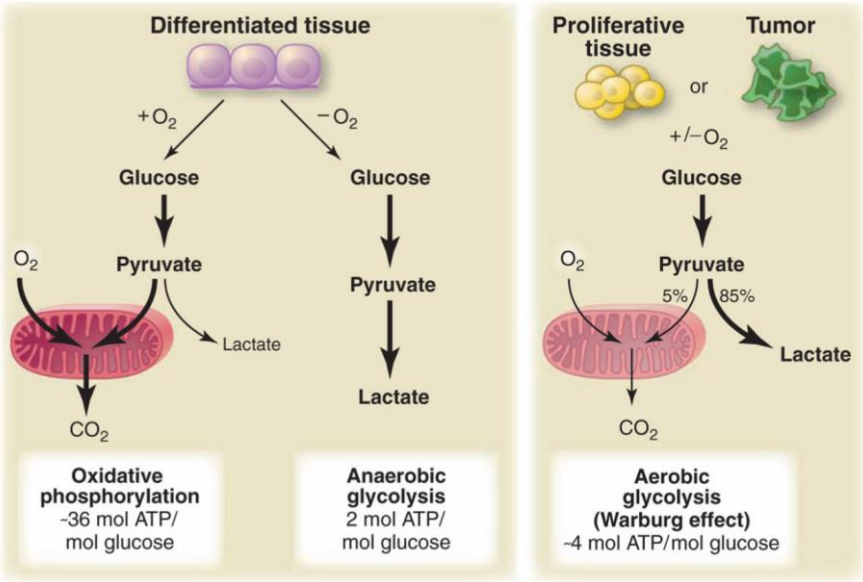

Figure I8. **Metabolism in quiescent versus proliferative cells[158].** Simplistic representation of the differences between oxidative phosphorylation, anaerobic glycolysis and aerobic glycolysis.

In the presence of oxygen, quiescent cells obtain their energy by metabolizing glucose to pyruvate through glycolysis and its complete oxidation to CO_2 through tricarboxylic acid (TCA) cycle, a process that requires oxygen as the final electron acceptor[158]. When oxygen is unavailable, cells undergo anaerobic glycolysis by directing glucose-derived pyruvate to the production of lactate instead. This process is much less efficient and results to low ATP production[158] **(Fig. I8)**. Contrarily, the majority of tumor cells convert most glucose to lactate independently of the oxygen levels[158,159]. This effect is accompanied by an increase in glucose import, which is accomplished by the up-regulation of glucose transporters (notably GLUT1)[160]. In contrast to Warburg's hypotheses (*"the respiration of all cancer cells is damaged"*[161]), aerobic glycolysis is no longer understood as a forced response to overcome mitochondrial defects, but as a mechanism to support enhanced biogenesis, since glycolytic intermediates can derive into various biosynthetic pathways and are fundamental for the generation of nucleosides and amino acids[158,162].

In tumor cells, glucose uptake is regulated by PI3K/Akt signaling[158]. This pathway enhances gene expression of the glucose transporter *GLUT1* and promotes the translocation of GLUT1 protein to the cell membrane[163,164]. Moreover, Akt potentiates the activity of hexokinase (HK) and phosphofructokinase (PFK), two key enzymes of the glycolytic pathway[165], and modulates the reprogramming of mitochondrial citrate metabolism by the activation of ATP-citrate lyase (ACL)[162]. Downstream of Akt, mammalian/mechanistic Target of Rapamycin Complex 1 (mTORC1) promotes mitochondrial biogenesis and stimulates glycolysis by the activation of a transcriptional program that affects hypoxia-inducible factor 1α (HIF-1α) and its target genes[166].

After glucose, glutamine is the most rapidly consumed nutrient in many tumor types[167]. As noted by Harry Eagle in 1955, cancer cells present a high dependence on an exogenous glutamine supply, being consumed ten times more than other aminoacids[168]. Glutamine is also the most abundant amino acid in plasma and the major carrier of nitrogen between organs[169]. Though it can be synthetized by cells, glutamine is the most commonly depleted amino acid in tumors, thus being considered a conditional essential amino acid[170].

Glutamine catabolism exceeds its rates of generation in highly proliferative tumor cells, where it is key for ATP production and for providing intermediates for macromolecular synthesis since it acts both as a carbon and a nitrogen donor[169,171]. Additionally, it contributes to oxidative stress protection by the synthesis of glutathione and NADPH[172]. Glutamine enters the cell through transporters of the solute carrier (SLC) group[173]. Although not all, many glutamine effects are dependent on its conversion to glutamate (Glu) and ammonia by glutaminases (GLS)[169]. Glutamate is then converted to α-ketoglutarate (α-KG) by the action of glutamate dehydrogenases (GLUD) or to various non-essential amino acids via specific aminotransferases[169]. α-KG is shuttled to the TCA cycle, where provides energy or, alternatively, supports the synthesis of lipids through reductive carboxylation (RC)[174]. In addition, glutamine contributes to nucleotides and uridine diphosphate N-acetylglucosamine (UDP-GlcNAc) synthesis[169,175] **(Fig. I9)**.

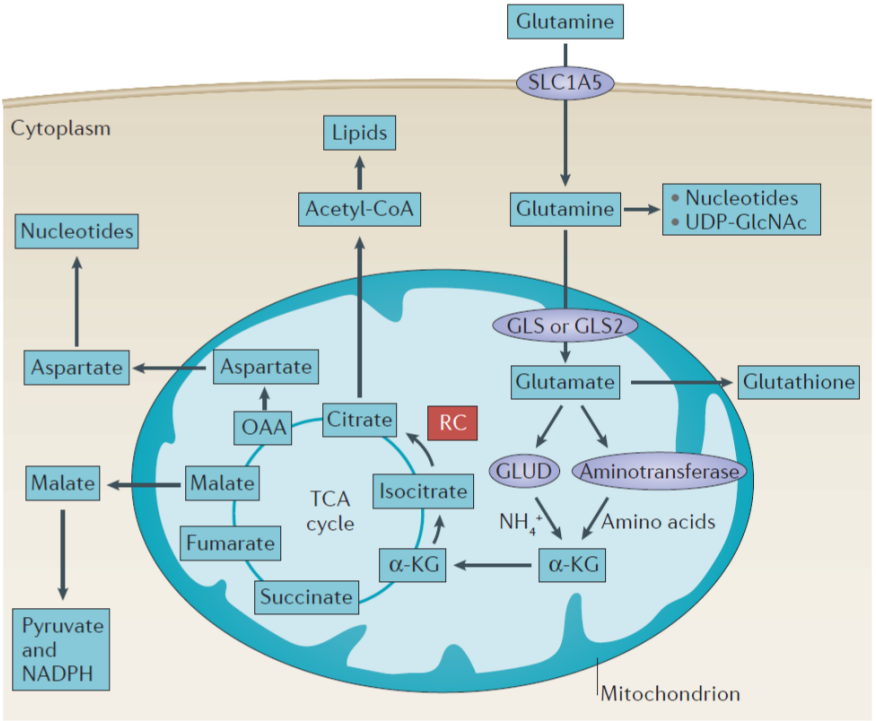

Figure I9. Major metabolic and biosynthetic fates of glutamine[175]. Glutamine enters the cell through SLC transporters and is metabolized to glutamate by glutaminases (GLS). Glutamate is converted to α-ketoglutarate (α-KG) by the action of glutamate dehydrogenases (GLUD) or aminotransferases, causing the generation of NH_4^+ and amino acids respectively. α-KG enters the TCA cycle, where provides energy or, alternatively, supports lipid synthesis through reductive carboxylation (RC). Oxaloacetate (OAA) can be converted to aspartate to support nucleotide synthesis. In addition, glutamine contributes to the synthesis of nucleotides and uridine diphosphate N-acetylglucosamine (UDP-GlcNAc).

Glutamine exerts other effects than supporting amino acid synthesis and ATP production; for instance, it influences cell survival and proliferation by the modulation of signal transduction pathways and gene expression[169]. Several studies determined that glutamine modulates the activity of mTORC1, a serine/threonine protein kinase complex (formed by mTOR kinase and other core components such as raptor and mLST8/GβL) that plays a central role in the regulation of

translation initiation and its efficiency[176]. mTORC1 phosphorylates and activates S6 kinase (S6K), that consequently activates the ribosomal protein S6 promoting ribosome biogenesis and mRNA translation[177]; in addition, mTORC1-dependent phosphorylation of eIF4E binding protein (4EBP) prevents the inhibition of the cap-binding protein eukaryotic translation initiation factor 4E (eIF4E), enabling cap-dependent translation initiation[178] **(Fig. I10)**. Importantly, mTORC1 is considered the main nutrient-sensing protein complex[176]. mTORC1 activation in response to amino acid stimulation is mediated by the p62/TRAF6 complex and the ragulator complex, composed by the family of Rag guanosine triphosphatases (RAGB and RAGC)[179,180]. Upon amino acid availability, p62 recruits TRAF6 to the lysosome, which mediates mTORC1 lysosomal translocation and catalyzes Lys63-polyubiquitination and activation of mTORC1[179] **(Fig. I10)**. In addition, mTORC1 regulates glutamine catabolism by the activation of GLUD and GLS[181,182], which conversely mediate mTORC1 lysosomal translocation and its subsequent activation[183].

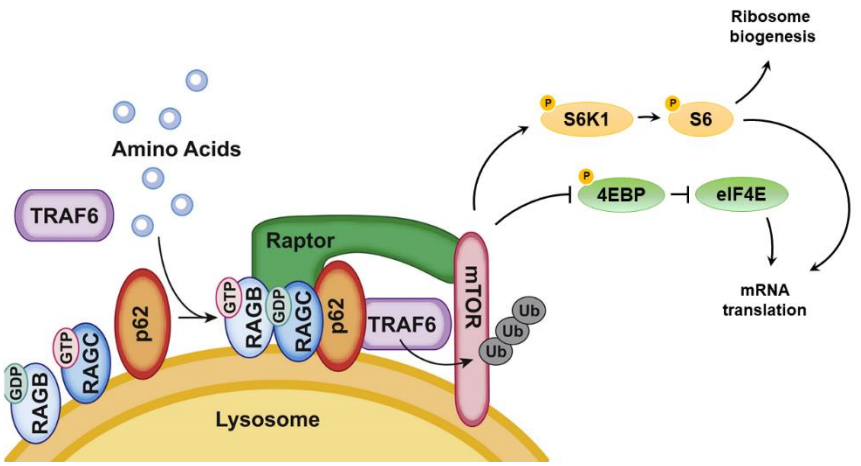

Figure I10. mTORC1 modulates protein synthesis upon changes in amino acid availability (adapted from[179]). In the presence of amino acids, RAGB/RAGC (ragulator) and p62/TRAF6 complexes mediate the translocation of mTORC1 to the lysosome. TRAF6 mediates mTORC1 ubiquitination and its activation. Downstream effects of mTORC1 activation include the phosphorylation of S6K1 and 4EBP, which enhance mRNA translation and ribosomal biogenesis.

Within a tumor, cancer cells conform a very heterogeneous population[184]. This diversity is not limited to their mutational state but to their metabolism. Because of the insufficient supply of oxygen and nutrients that derives from the high metabolic demand of tumor cells and a deficient angiogenesis (an effect known as *metabolic stress*), tumor cells exhibit different rates of mitochondrial respiration and different degrees on reliance on aerobic glycolysis[185]. In addition, oxygen and nutrient availability can change during tumor development, forcing cancer cells to adapt to the new conditions[75]. Therefore, the metabolic phenotype of tumor cells is plastic and depends on their oxygen and nutrient status and their interactions with other tumor and stromal cells[186]. In a simplistic scenario, two populations of cells coexist in a tumor: the first type are glucose-dependent cells that obtain their energy through aerobic glycolysis; the second population imports lactate secreted by the glucose-dependent cells and uses it as its main source of energy[187,188]. A parallel interaction (so called *reverse Warburg effect*) has been demonstrated between tumor cells and fibroblasts[127].

Metabolic stress is a common condition in solid tumors that promotes apoptosis-mediated tumor suppression[189]. Metabolic stress is induced by multiple factors, including the high metabolic demands of unrestrained cell proliferation, their high energy demand and an insufficient blood supply caused by deficient angiogenesis[159]. In this process, tumors that are bigger than 1mm in diameter lack a proper blood supply in the inner part of the tumor, where passive diffusion of nutrients and oxygen is not sufficient for sustaining tumor growth[190]. Metabolic stress is classically characterized by hypoxia and the accumulation of lactate and reactive oxygen species (ROS) that derive from tumor cell metabolism, which induce DNA damage and trigger apoptosis via caspase-mediated activation of p53[189]. Tumor cells survive metabolic stress through autophagy activation, which protects the cells from genetic instability and apoptosis by the clearance of damaged proteins and organelles[189,191]. In addition, tumor cells adapt to glutamine deficiency through proteolytic scavenging of extracellular proteins, debris and apoptotic cells[165]. In glutamine-depleted environments, macropinocytosis of extracellular proteins is dependent

on Ras transformation and EGFR-Pak signaling[192]; in this process, tumor cells overcome their dependence on extracellular glutamine by lysosome-dependent degradation of the uptaken proteins; accordingly, the pharmacological inhibition of macropinocytosis suppresses tumor growth *in vivo*[193].

Moreover, tumor cells confront metabolic stress by their interaction with the TME and the metabolic reprogramming of stromal cells. This reciprocal interaction contributes to the emergence of more aggressive phenotypes[194]. As aforementioned, the high utilization of glucose by cancer cells results in the extracellular accumulation of lactate[158]. It has been reported that increased lactate levels promote the attenuation of T-cell activation, monocyte migration and dendritic cells, as well as the polarization of resident macrophages towards an M2 phenotype, forming an immune-permissive microenvironment and further promoting tumor growth[195]. In addition, lactate promotes angiogenesis by HIF-1α stabilization and vascular endothelial growth factor (VEGF) secretion in other stromal cells; thereby increasing the nutrient supply to the tumor and enhancing tumor cell proliferation[196]. In fibroblasts, accumulation of lactate and the consequent acidification of the extracellular media stimulates hyaluronic acid production and MMPs secretion, thus contributing to tumor invasion[197,198]; on the other hand, tumor cells couple their metabolism with fibroblasts and uptake fibroblast-secreted metabolites as fuel[11].

3.2. Cancer associated fibroblasts metabolism

Like other highly proliferative cell types, CAFs rely on aerobic glycolysis to obtain energy and metabolites[199]. Metabolic reprogramming of these cells is induced upon their activation in order to sustain activated secretome functions, proliferation and cellular motility, and it is mediated by tumor cell-induced oxidative stress, HIF-1α stabilization and growth factors such as TGF-β or PDGF[97,91]. The coordinated effect of TGF-β and reactive oxygen species (ROS) mediates the loss of caveolin 1 (CAV1) in CAFs, which induces autophagy thus enhancing glycolysis in these cells[200]; furthermore, CAV1-defficiencies and autophagy in

fibroblasts are associated with resistance to chemotherapy and poor outcome[201]. As consequence of CAFs metabolic shift, there is an increased production of lactate, fatty acids and ketone bodies that are uptaken by cancer cells or other TME components to fuel their mitochondrial respiration and, ultimately, their proliferation[127,128]. The nature of this relationship can vary depending on the specific characteristics of the tumor and its TME; for instance, in some other cases cancer cells undergo aerobic glycolysis and CAFs uptake tumor cell-secreted lactate[202].

Metabolic coupling between CAFs and tumor cells is not restricted to glucose metabolism but also includes other intermediates such as amino acids. It has been reported that glutamine generation is enhanced in ovarian carcinoma-derived CAFs when compared to tissue resident fibroblasts; contrarily, glutamine catabolism is predominant in ovarian cancer cells, which use CAF-derived glutamine as their source[203]. In the same study, co-targeting glutamine synthetase in the stroma and GLS in tumor cells reduced tumor growth and metastasis[203]. In line with these results, p62 deficiency in prostate CAFs promotes resistance to glutamine deprivation and enhances the generation of asparagine, which constitutes a source of nitrogen for the stroma and sustains the proliferation of epithelial cancer cells[204]. Opposing to these two publications, others have reported glutamine as the major source of carbon for the TCA cycle in CAFs[205]; accordingly, an unpaired proliferation of CAFs is observed upon GLS inhibition and correlates with its over-enhanced activity in CAFs when compared to breast cancer cells[206]. Overall, glutamine metabolism in CAFs may depend on tumor class and specific conditions.

3.3. Tumor metabolism and invasion

Tumor cell metabolism might influence cell migration and invasion by several mechanisms, involving glycolysis and glutamine metabolism. As previously assessed, metabolic stress derived from tumor cell-enhanced aerobic glycolysis and a poor nutrient supply is characterized by the accumulation of lactate in the core of tumors[207]. According to

some authors, this accumulation causes the acidification of the extracellular compartment and provides a favorable microenvironment for the activation of MMPs, which induce ECM degradation and facilitate tumor cell invasion[208,209]. In addition, lactate supplementation in *in vitro* migration models resulted into an increase of β_1-integrin expression and an enhanced motility of squamous larynx carcinoma cells[210]. On the other hand, hypoxia and lactate accumulation trigger HIF-1, a transcription factor that controls multiple cell functions such as survival/apoptosis, metabolism, angiogenesis and invasion. Importantly, HIF-1 induces EMT, enhancing the expression of mesenchymal genes such as vimentin or fibronectin and the secretion of MMPs[211]. In turn, EMT is linked to metabolic reprograming of the tumor cells and enhances glycolytic phenotypes[212]; concretely, Snail1 expression reprograms glucose metabolism by repressing phosphofructokinase (PFKP), thus promoting cancer cell survival under metabolic stress[213].

There are several evidences that the enzymes of the glycolytic pathway play important roles in tumor migration and invasion. For instance, phosphoglucose isomerase (PGI), which catalyzes the conversion of glucose-6-phosphate into fructose-6-phosphate, stimulates cell migration by its function as an autocrine motility factor and by inducing IL-8 production and EMT[214]. In glioma cells, the expression of lactate dehydrogenase has been associated to the secretion of MMP2 and to an enhanced invasiveness, an effect that is mediated by the up-regulation of TGF-β2 expression in these cells[215]

In the case of glutamine metabolism, enhanced glutaminase activity has been associated to highly invasive tumor cells and fibroblasts when compared to non-transformed cells[206]. Moreover, glutaminolysis promotes cancer cell invasiveness by increasing extracellular glutamate[216]; accordingly, high extracellular levels of glutamate have been related with glioma and pancreatic cancer cells invasion and with an up-regulation of ECM remodeling in CAFs[205,217,218].

OBJECTIVES

Metabolic stress in tumors correlates with more aggressive phenotypes[165]. It is also accepted that tumor cells cooperate with the stromal compartment to face the metabolic deficiencies that are consequence of tumor growth[201]. Nevertheless, little is known about the effects of this cooperation on tumor cell invasion and metastasis. Therefore, the aim of this thesis is:

To assess how metabolic stress influences tumor migration.

To achieve this aim, we established two specific objectives:

1. To determine the nutrient requirements of mesenchymal and epithelial cell types.

2. To characterize tumor and stromal cell migration and invasion upon specific nutrient depletion.

RESULTS

1. CANCER-ASSOCIATED FIBROBLASTS PRESENT A HIGHER REQUIREMENT FOR GLUTAMINE THAN EPITHELIAL TUMOR CELLS

1.1. Mesenchymal cells survival is affected by glutamine deprivation

In order to characterize the nutrient requirements of mesenchymal and epithelial tumor cells, we used two stablished cell lines (AT-3 and BTE-136) that had been generated from breast tumors of MMTV-PyMT mice. In this model, polyomavirus middle T oncogene is expressed under control of the mammary MMTV promoter, resulting in the spontaneous generation of luminal B breast tumors that progress through the typical stages of human breast tumors and metastasize to the lung[219]. When we characterized these cell lines, we observed that they differed in their expression of epithelial and mesenchymal markers **(Fig. R1)**. Concretely, AT-3 cells presented a higher expression of E-Cadherin and cytokeratin 14, being more epithelial, whereas BTE-136 showed higher levels of Snail1.

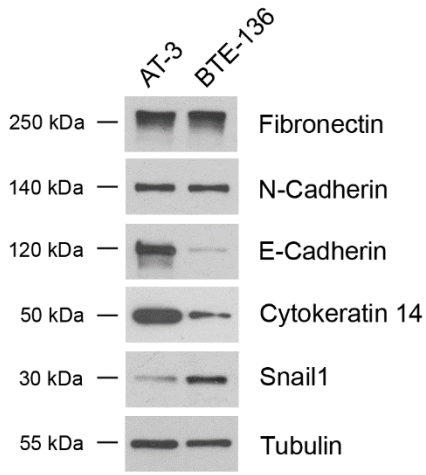

Figure R1. Immortalized MMTV-PyMT tumor cells from different origin show a differential expression of epithelial and mesenchymal markers. Protein levels of the indicated markers were determined by Western blot analysis in AT-3 and BTE-136 cells.

We analyzed the nutrient requirements of these cell lines by their ability to survive to glucose (Glc) and glutamine (Gln) deprivation. For this, we cultured the cells in a low percentage of serum (0.5%) to avoid the effects of growth and we depleted glucose or glutamine in the culture media for 48 hours. As shown in **Fig. R2**, AT-3 were more resistant than BTE-136 to a decrease of glutamine from 2 mM, the standard concentration in cell culture medium, to 0.2 mM. In fact, glutamine deprivation caused a 50% reduction in the number of BTE-136 cells when compared to their culture in 2 mM glutamine.

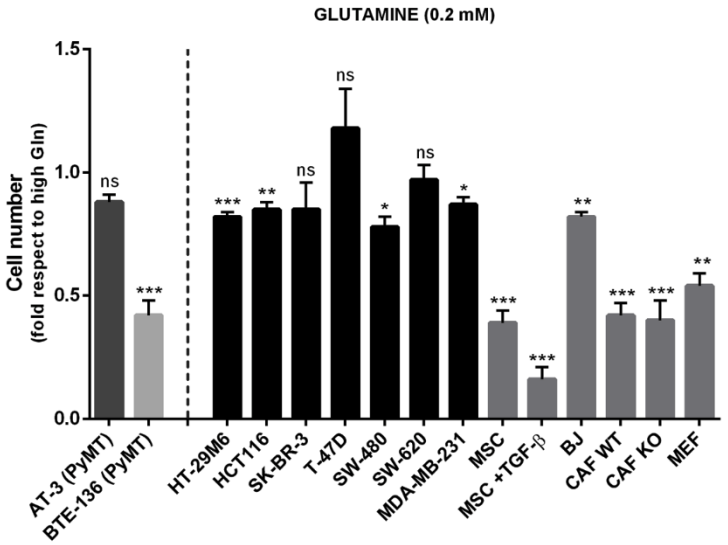

Figure R2. Mesenchymal cell types display a higher sensitivity to glutamine deprivation than epithelial cells. Tumor cells (black bars) and fibroblasts (grey bars) were cultured in low Gln (0.2 mM) for 48 hours. Their viability was measured by crystal violet staining and normalized to its culture in high Gln (2 mM). Data represent mean ± SEM of at least three independent experiments. ns, not significant; * $p<0.05$; ** $p<0.01$; *** $p<0.001$.

In contrast, these two cell lines were almost equally sensitive to a drop in glucose from 1 g/l to 0.1 g/l **(Fig. R3)**. Glucose deprivation did not alter AT-3 viability and it slightly decreased the number of BTE-136 cells, which were much more sensitive to glutamine depletion.

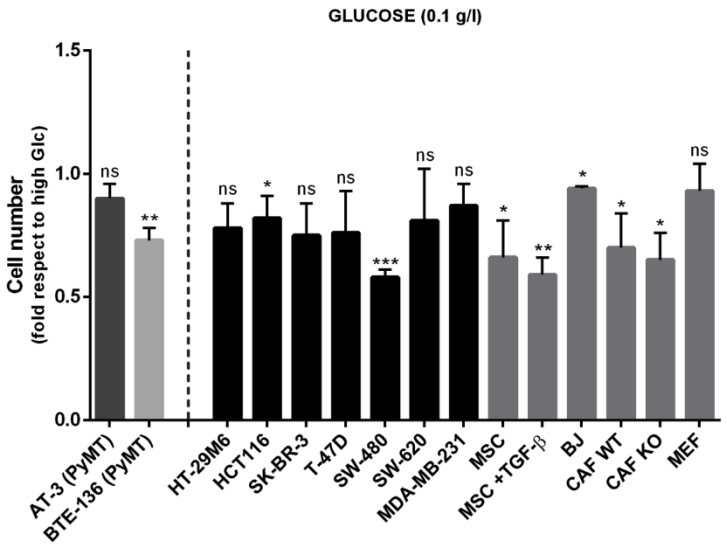

Figure R3. Tumor cells and fibroblasts exhibit a low sensitivity to glucose deprivation. The viability of tumor cells (black bars) and fibroblasts (grey bars) was determined by crystal violet staining after 48 hours in low Glc (0.1 g/l) culture and normalized to its culture in high Glc (1 g/l). Data represent mean ± SEM of at least three independent experiments. ns, not significant; * $p<0.05$; ** $p<0.01$; *** $p<0.001$.

We extended our study to other epithelial and mesenchymal cell lines. Therefore, a panel of breast and colorectal tumor cells as well as fibroblasts from different origin were included in the analysis. Particularly, we analyzed murine mesenchymal stem cells (MSCs), MMTV-PyMT-derived cancer associated fibroblasts (CAFs) and mouse embryonic fibroblasts (MEFs) that were previously established in our laboratory[150,139,137]. Additionally, we used Snail1 knock-out MSCs and CAFs **(Fig. R4)** and TGF-β-stimulated MSCs to check if the activation state of these cells, that is dependent on Snail1 expression, was also influencing their metabolic requirements.

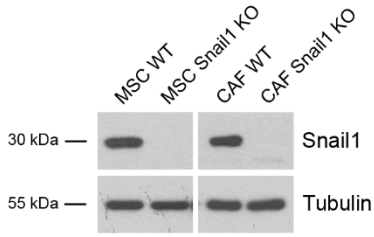

Figure R4. Generation of Snail1 knock-out fibroblasts. MSCs and CAFs derived from Snail1$^{flox/-}$ mice were infected with an empty pBabe retroviral vector (WT) or a pMXCre vector encoding a Cre recombinase (Snail1 KO) and subsequently selected with puromycin. Snail1 depletion was confirmed by Western blot.

When we addressed the survival of these cell types to glutamine deprivation, we found that CAFs were highly sensitive to the depletion of this amino acid. Similarly, MSCs and MEFs viability was reduced to 50% upon glutamine deprivation, whereas epithelial tumor cells were much less affected by this condition **(Fig. R2)**. No significant differences were observed in the viability of Snail1-depleted CAFs (CAFs KO) when compared to their wild-type counterparts, suggesting that the basal levels of Snail1 expression in CAFs are not associated to their glutamine requirement. In contrast, the activation of MSCs by TGF-β further decreased their survival in a glutamine-depleted medium.

Glucose deprivation affected the viability of fibroblastic cells to a lower extent than glutamine depletion. In this case, no significant changes were observed in the culture of MEFs in 1 g/l or 0.1 g/l glucose, whereas its depletion resulted in a slight reduction in CAFs and MSCs survival **(Fig. R3)**. In tumor cells, glucose deprivation only affected the viability of the colorectal SW-480 cells.

As representative of mesenchymal or epithelial cells, CAFs and HT-29M6 viability was further characterized in a set of different glutamine concentrations, going from the standard in cell culture (2 mM) to a complete depletion (0 mM) **(Fig. R5)**. CAF minimally proliferated in a

medium supplemented with 2 mM Gln, but a reduction of Gln to 0.5 mM slightly decreased its cell number, that was severely affected in 0.2 or 0 mM Gln. This effect was noted at 24 hours of culture and it was amplified at 48 hours. On the contrary, only a total depletion of glutamine compromised HT-29M6 epithelial tumor cells viability at both time points.

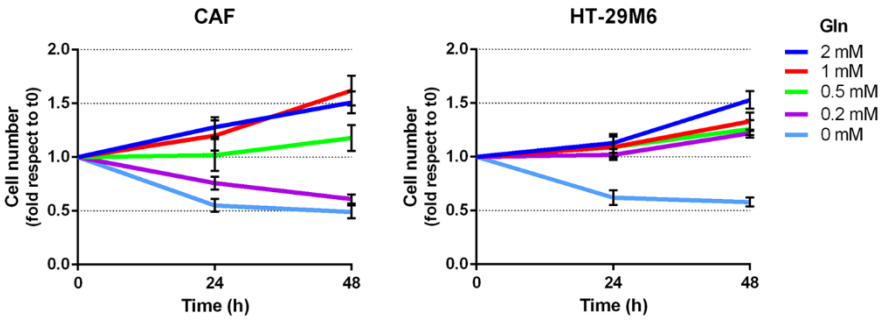

Figure R5. Cancer-associated fibroblast viability is compromised by glutamine depletion. The survival of CAFs and HT-29M6 to different Gln concentrations was assessed by crystal violet staining at 24 and 48 hours and normalized to cell number at t=0h. Data represent mean ± SD of at least three independent experiments.

1.2. Glutamine deprivation enhances apoptosis in fibroblastic cells

We then corroborated our results by assessing apoptosis in some of the previously used cell lines **(Fig. R6)**. Higher levels of cleaved caspase-3, a classical indicator of apoptosis, were detected in low glutamine when comparing mesenchymal BTE-136 with epithelial AT-3 PyMT cells. A similar up-regulation of this marker was observed in glutamine-deprived CAFs and MSCs, but there were no changes in any of the epithelial cells analyzed (HT-29M6, T-47D, SW-480 and HCT116).

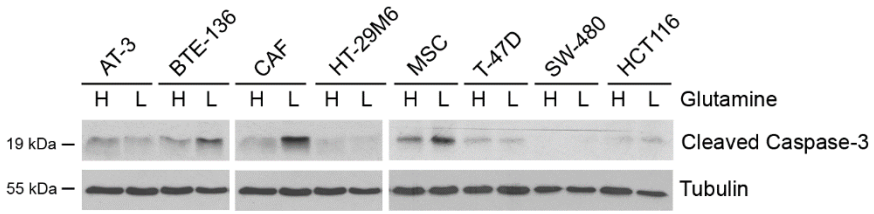

Figure R6. Sensitivity to glutamine deprivation correlates with increased levels of cleaved caspase-3 in fibroblasts. Western blot analysis of cleaved Caspase-3 in epithelial and mesenchymal cell lines cultured in high (H; 2 mM) or low (L; 0.2 mM) Gln for 48 hours.

1.3. Fibroblasts exhibit higher rates of glutamine consumption

The higher sensitivity of fibroblasts to glutamine deprivation was associated to an increased consumption of this amino acid by fibroblasts when compared with HT-29M6, being particularly high in MSC **(Fig. R7)**. Curiously, glutamine consumption was similar in AT-3 and BTE-136 cells, suggesting that BTE-136 were unable to adapt their metabolism in order to overcome glutamine depletion.

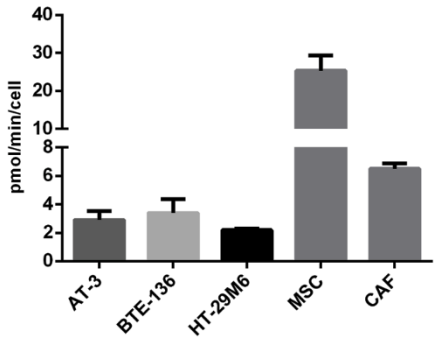

Figure R7. Glutamine consumption is enhanced in fibroblasts. Glutamine concentration was measured in media samples of AT-3, BTE-136, HT-29M6, CAFs and MSCs cultures. Consumption rates were calculated as the difference in concentration between fresh and cell culture media and normalized to cell number and time (minutes) of culture. Data represent mean ± SEM of three independent experiments.

1.4. Glutaminase 1 inhibition affects the viability of mesenchymal cells

Since most glutamine is metabolized to glutamate (Glu) by Glutaminase 1 (GLS1), we checked the effect of an inhibitor of this enzyme on CAFs viability. Addition of CB-839[220] to CAFs or BTE-136 cultures for 48 hours severely decreased cell viability in a similar way as glutamine deprivation **(Fig. R8)**. In these cells, relative IC_{50} values were calculated as the concentration of CB-839 that is required for a half-maximal inhibitory response. In contrast, CB-839 supplementation did not significantly alter HT-29M6 and AT-3 viability, both tumor cells showing an epithelial phenotype.

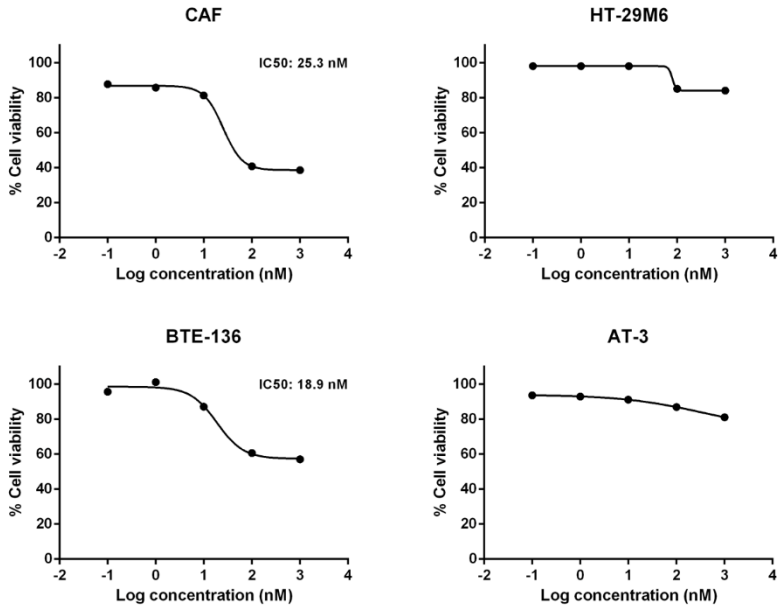

Figure R8. Mesenchymal cells are susceptible to GLS1 inhibition. Cells were treated with increasing doses of CB-839 or dimethyl sulfoxide (DMSO) for 48 hours and their viability was measured by crystal violet staining and normalized to DMSO. Dose-response curves and relative IC_{50} are represented for each cell line. Non-linear curve fits were used to calculate IC_{50} values. Data represent the mean of three independent experiments.

1.5. Cell viability of glutamine-depleted CAFs is not rescued by the addition of other metabolic intermediates

We next assessed if the effects of glutamine deprivation and GLS1 inhibition on the viability of CAFs could be rescued by the addition of other metabolic intermediates. Therefore, we cultured CAFs in low Gln (0.2 mM) and in high Gln (2 mM) plus a CB-839 treatment, and we supplemented both cultures with Glu, lactate (Lac) or Glc.

As shown in **Fig. R9**, the addition of glutamate and lactate to a standard culture medium did not affect the survival of CAFs, whereas glucose slightly increased their cell number. As expected, both glutamine deficiency and CB-839 treatment reduced the viability of CAFs when referred to a high glutamine culture. However, both conditions displayed a different outcome when glutamate was added to the culture medium. In fact, the supplementation of glutamate to CB-839-treated cells improved the survival of CAFs, whereas no significant differences were observed in glutamine-starved cells. Neither lactate or glucose stimulated the survival of CAFs in any of the situations.

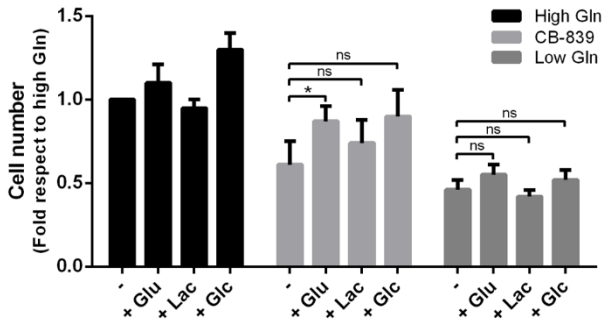

Figure R9. Glutamate, lactate and glucose do not increase the viability of glutamine-depleted CAFs. CAFs were seeded in high Gln (2 mM) or low Gln (0.2 mM) and supplemented with glutamate (Glu; 1 mM), lactate (Lac; 20 mM) and glucose (Glc; 5 g/l) when indicated. In some conditions (represented in light grey bars), high Gln cultures of CAFs were treated with CB-839 (25.3 nM). Cell viability was measured by crystal violet staining after 48 hours. All data was normalized to high Gln condition. Data represent mean ± SEM of at least three independent experiments. ns, not significant; * $p<0.05$

2. GLUTAMINE ORCHESTRATES MIGRATION AND INVASION OF MESENCHYMAL CELL TYPES

2.1. Active fibroblasts migrate towards glutamine

In the previous experiments we demonstrated that fibroblasts present a higher dependence on glutamine than epithelial cells, since the depletion of this amino acid decreases the viability of mesenchymal cells *in vitro*. Therefore, we asked if glutamine could influence the migration capability of fibroblasts. To examine this, we set *in vitro* migration experiments in which we challenged these cells with a glutamine gradient instead of the fetal bovine serum (FBS) gradient that is classically used. Concretely, cells were plated into the upper compartment of Boyden Chambers in media supplemented with either 0.2 mM glutamine (Low Gln) or 2 mM glutamine (High Gln). The lower chamber was filled with 2 mM Gln in all conditions and, in contrast with the usual method, cells were maintained in low FBS during the whole experiment. Hence, cell migration was assessed in the presence (0.2→2 mM Gln) or the absence (2 mM Gln) of gradients. Both conditions are represented in **Fig. 10 A and B**, respectively.

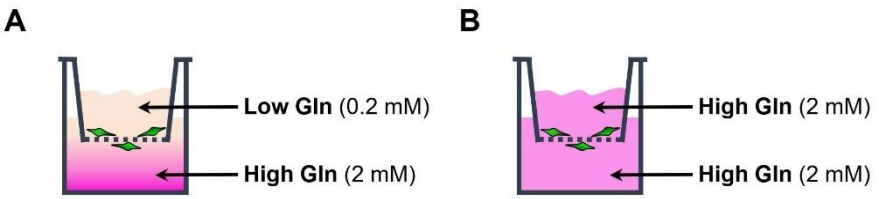

Figure R10. Generation of glutamine-concentration gradients in Boyden chambers. Cell migration was measured as the capability of cells to move from the upper to the lower compartment of Boyden chambers through a porous membrane. Migration was assessed **(A)** in the presence of a Gln gradient (0.2 → 2 mM Gln) or **(B)** in high Gln (2 → 2 mM). Media in both compartments were supplemented with 1g/l glucose and 0.5% FBS.

We evaluated the stability of these gradients by the measure of glutamine concentration in the upper and lower compartment of Boyden chambers at different time points. Differences in glutamine concentration between the two compartments were observed at least for 6 hours **(Table R1)**.

Table R1. Glutamine concentration in Boyden chambers

	Initial	**2 hours**	**6 hours**
Upper chamber	0.25 ± 0.01	1.39 ± 0.13	1.78 ± 0.06
Lower chamber	2.65 ± 0.17	2.13 ± 0.17	2.17 ± 0.09

Glutamine concentration (mM) in samples from the upper and lower compartments of Boyden chambers was determined by Glutamine colorimetric assay kit (K556, BioVision). Data represent mean ± SD of three independent experiments.

As shown in **Fig. R11 A**, the migration of CAFs was enhanced by a glutamine gradient only when cells were stimulated with TGF-β, suggesting that glutamine-driven migration requires fibroblast activation. These results were reproduced in MSCs **(Fig. R11 B)**, in which migration was equally increased by the combination of TGF-β stimulation and a gradient. In both cell lines, Snail1 depletion, which prevented their TGF-β-dependent activation, abrogated glutamine gradient-stimulated migration.

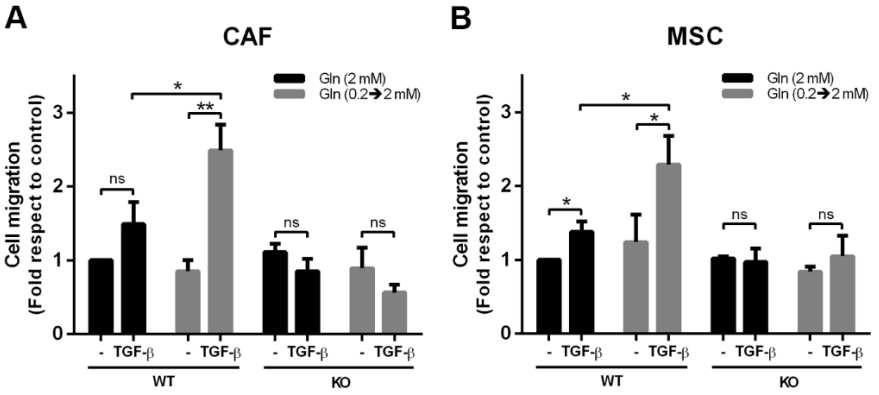

Figure R11. TGF-β-stimulated fibroblasts migrate towards glutamine. Migration assays were performed in **(A)** CAFs and **(B)** MSCs either wild-type (WT) or Snail1 KO (KO) in standard Gln culture (black bars) or in presence of a Gln gradient (grey bars). When indicated, TGF-β (5 ng/ml) was added to the upper compartment. Cells were fixed after 12 h and migration was assessed as indicated in Materials and Methods. Data was normalized in reference to CAFs or MSCs migration in high Gln and represented as the mean ± SEM of at least three independent experiments. ns, not significant; * p<0.05; **p<0.01.

These observations were further confirmed by time-lapse video microscopy using chemotaxis µ-slides (IBIDI). In these slides, MSCs were plated in the central compartment and stimulated with TGF-β. The two reservoirs on the sides of this device were then filled with two different concentrations of Gln (2 and 0.2 mM) **(Fig. R12 A)**.

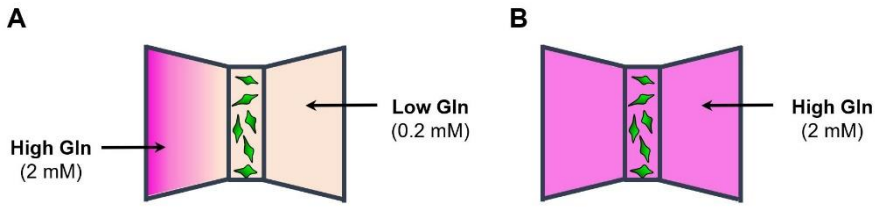

Figure R12. Experimental setup for glutamine-stimulated migration in chemotaxis µ-slides. (A) Gln concentration gradients were generated by high Gln supplementation in one of the lateral compartments of the slide. **(B)** Alternatively, all reservoirs were filled with high Gln (2 mM) media. All the experiments were performed in DMEM 1g/l glucose, 0.5% FBS and 5 ng/ml TGF-β supplementation.

In this device, the stability of glutamine gradients was maintained for more than 24 hours, since we did not observe significant differences in the concentration of glutamine of both central (initially filled with low Gln medium) and side (supplemented with high Gln) compartments among time **(Table R2)**.

Table R2. Glutamine concentration in chemotaxis µ-slides

	Initial	**6 hours**	**24 hours**
Center	0.07 ± 0.01	0.21 ± 0.22	0.27 ± 0.07
Side	1.37 ± 0.07	1.43 ± 0.37	1.39 ± 0.35

Glutamine concentration (mM) in samples from central (low Gln) and lateral (high Gln) compartments of chemotaxis µ-slides was determined by Glutamine colorimetric assay kit (K556, BioVision). Data represent mean ± SD of three independent experiments.

We tracked the migration of glutamine-depleted MSCs to the glutamine-high lateral compartments of chemotaxis µ-slides and compared it to a condition where the two compartments contained 2 mM Gln **(Fig. R12 B)**. As shown in **Fig. R13 A** and **Suppl Videos 1 and 2**, MSCs preferentially migrated into the high Gln reservoir when cultured in low Gln. The migration was less directional when cells were grown in a high Gln culture. Upon gradient stimulation, cells did not show a totally aligned phenotype, but displayed a preference in choosing their direction of migration towards the high Gln compartment. Consequently, the number of cells that arrived at the lateral chamber was higher in Gln gradient than in high Gln **(Fig. R13 B, C).** Small differences were seen in terms of migration speed, being gradient-stimulated cells faster than high glutamine-cultured cells **(Fig. R13 D)**.

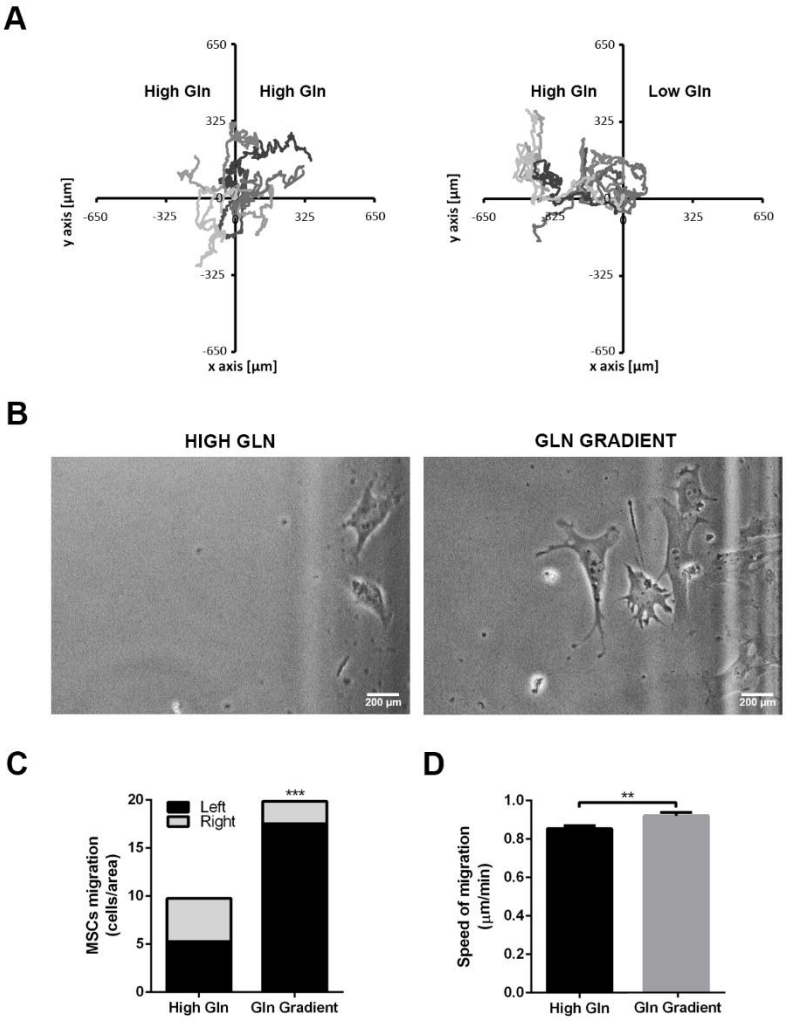

Figure R13. Mesenchymal stem cells migrate towards a glutamine gradient. (A) Plot of single MSCs trajectories. MSCs migration was recorded by time-lapse microscopy and tracked for 12 hours in a Gln-enriched medium (left panel) or in the presence of a Gln gradient (right panel). Chemotaxis µ-slides (IBIDI) were used as indicated in Materials and Methods to generate the gradients. **(B)** Representative pictures of the final time points **(C)** and quantification of the number of cells that migrated into the lateral reservoirs at the final time point. Graph represents total number of cells **(D)** Average speed of migration expressed as the ratio of distance migrated (µm) per minute, in high Gln or Gln gradient conditions. **p<0.01; ***p<0.001.

2.2. Active fibroblasts invade towards glutamine

As in the preceding experiments, fibroblasts also invaded towards glutamine when we performed Matrigel invasion assays. In these assays, both CAFs and MSCs moved towards a Gln-high lower chamber when seeded in low Gln **(Fig. R14 and R15)**. This effect was again dependent on the activation state of the cells, as it was only obtained upon TGF-β stimulation of Snail1-expressig fibroblasts.

To demonstrate the specificity of glutamine gradients in directing fibroblast invasion, we exposed CAFs to glucose and lactate gradients. As seen in **Fig. R14**, neither a 10-fold reduction in glucose in the upper chamber nor the addition of lactate to the lower compartment altered fibroblast invasiveness despite TGF-β supplementation.

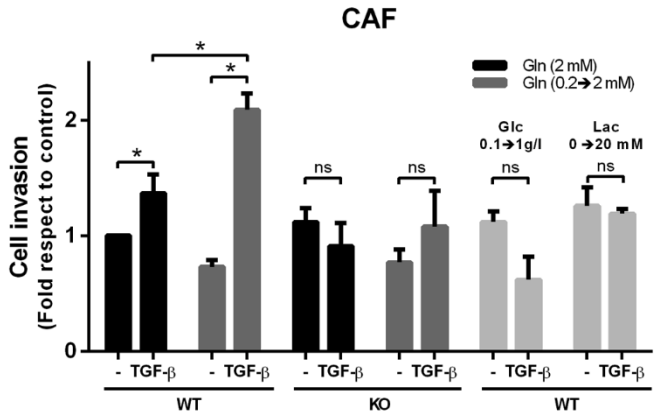

Figure R14. TGF-β/Snail1-dependent activation of CAFs promotes their invasion towards a glutamine gradient. Invasion assays were performed for 12 hours in CAFs WT or Snail1 KO in nutrient-enriched medium (0.5% FBS, 1 g/l Glc, 2 mM Gln) (black bars) or in the presence of Gln, Glc or Lac gradients (grey bars). When indicated, cells were stimulated with TGF-β (5 ng/ml). Data normalization was performed in reference to the invasion of CAFs in the absence of gradients and represented as the mean ± SEM of at least three independent experiments. ns, not significant; *p<0.05.

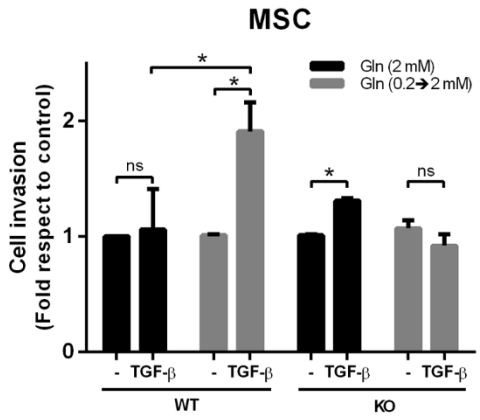

Figure R15. Glutamine-stimulated invasion of MSCs is enhanced upon their Snail1-dependent activation. Invasion of WT and Snail1 KO MSCs was determined after 12 hours upon Gln gradient (0.2 → 2 mM; represented in grey bars) or high Gln (2 mM; black bars) stimulation. When indicated, cells were stimulated with TGF-β (5 ng/ml). Data was normalized in reference to the invasion of MSC in high Gln and represented as the mean ± SEM of at least three independent experiments. ns, not significant; *p<0.05.

Additionally, cell morphology during glutamine-driven invasion was analyzed in TGF-β-stimulated CAFs **(Fig. R16)**. For this reason, CAFs were seeded between two layers of a dense Matrigel/Collagen matrix and included into paraffin. Glutamine (2 mM) was supplemented in the top and bottom compartments (high Gln) or only in the lower chamber (Gln gradient); in this case, 0.2 mM Gln was added to the top. In both conditions, TGF-β was supplemented in the two compartments. After three days, samples were processed as specified in Materials and Methods and Hematoxylin & Eosin (HE) staining were performed. Longitudinal sections of these samples showed that in high Gln cells invaded the matrix in both directions, as single cells and in small aggregates. The same morphology was observed in Gln gradients, but cells moved only towards the compartment that was supplemented with glutamine in this case.

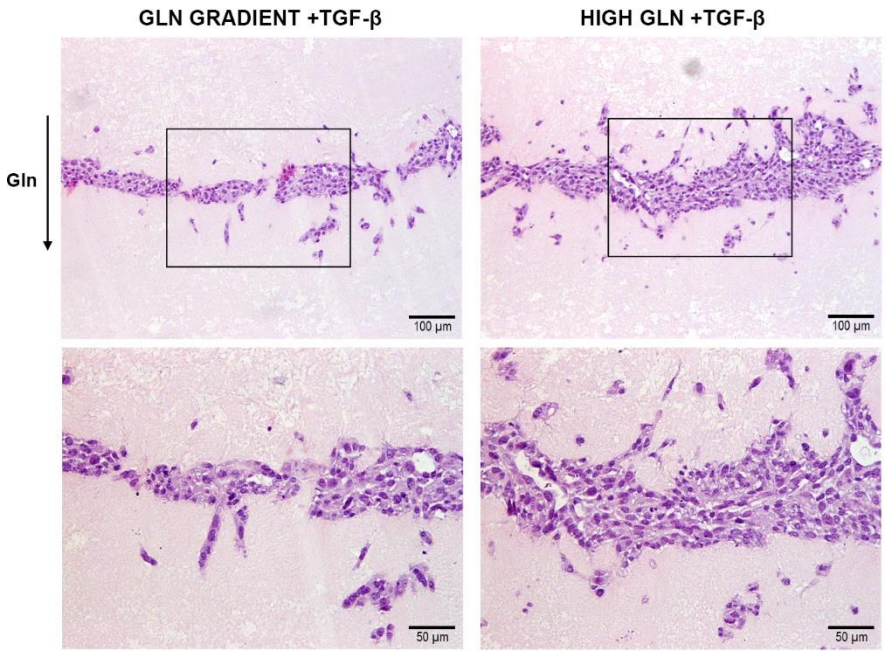

Figure R16. Glutamine dictates the directionality of fibroblast invasion. Representative sections of a 3-days organotypic invasion assay. CAFs were seeded between two matrix layers in the presence of a glutamine gradient or in high Gln. Both compartments were supplemented with TGF-β, and their invasion was measured in HE-stained longitudinal sections.

2.3. Active fibroblasts promote glutamine-driven invasion of epithelial tumor cells

In 2016, our laboratory reported the cooperation between mesenchymal and epithelial tumor cells during FBS-stimulated invasion[139]. In this study, we demonstrated that fibroblasts stimulate tumor cell motility by the secretion of diffusible molecules, such as PGE_2, in response to tumor-derived TGF-β. For this reason, we hypothesized that the capability of fibroblasts to invade towards glutamine might be transferred to epithelial tumor cells when co-cultured.

As in previous assays, we compared glutamine-high to glutamine gradient-stimulated invasion, while we maintained cells in 0.5% FBS in both compartments. In this case, we followed invasion of HT-29M6 cells in co-culture with fibroblasts, as these tumor cells were stably labelled with red fluorescent protein (RFP). We determined that HT-29M6 invasion was not significantly different in high glutamine or in a glutamine gradient but was remarkably increased by CAFs and MSCs only in the presence of a glutamine gradient **(Fig. R17 A-B)**. In accordance with the previous results, both Snail1 depletion in CAFs or MSCs and TGF-β receptor inhibition by SB505124 significantly decreased the action of these mesenchymal cell types on HT-29M6 invasion.

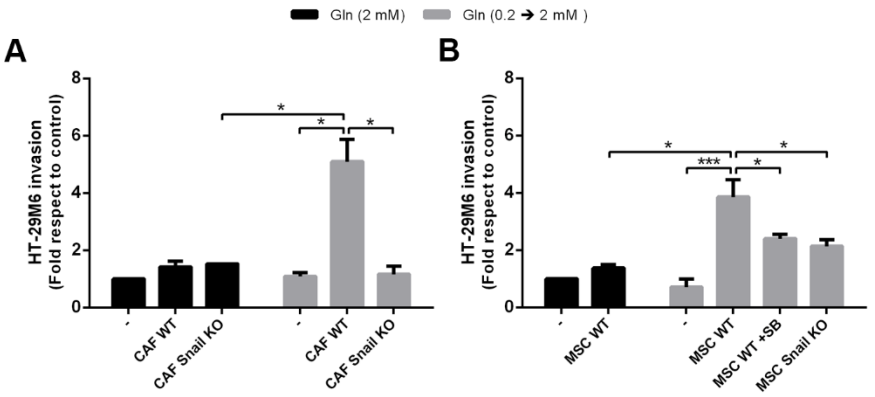

Figure R17. Fibroblast-stimulated HT-29M6 invasion is enhanced by glutamine and is sensitive to Snail1 depletion in fibroblasts. HT-29M6 cells invasion was determined in co-culture with **(A)** CAFs and **(B)** MSCs either WT or Snail1 KO in high Gln (black bars) or in a Gln gradient (grey bars). When indicated, cells were treated with SB505124 (SB; 5 µM). HT-29M6 invasion was measured as the area of RFP-positive cells under the transwell inserts and referred to control condition. Data represent the mean ± SEM of at least three independent experiments. *p<0.05; ***p<0.001.

We also analyzed the morphology of the tumor cells during invasion in longitudinal sections of paraffin-embedded matrices. In this experiment, cell tracks into the matrix were only perceived when HT-29M6 cells were co-cultured with CAFs, both upon glutamine gradient stimulation and in a glutamine-high culture; in these two conditions, cells followed the direction of the gradient or invaded in both directions, respectively. On the contrary, invasion-tracks were not observed in HT-29M6 cultures devoid of CAFs independently of glutamine levels **(Fig. R18).**

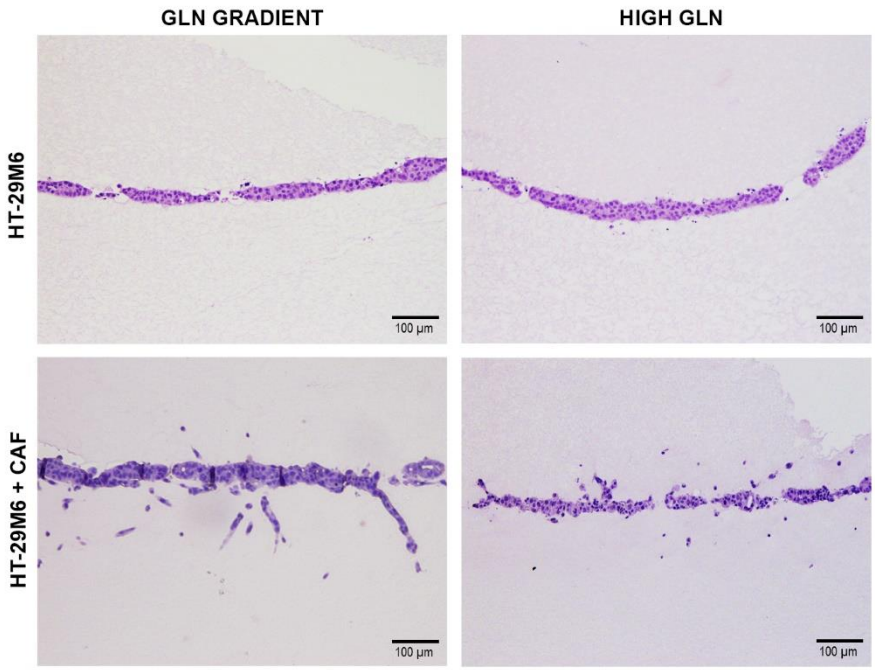

Figure R18. Fibroblasts promote HT-29M6 invasion towards glutamine. Representative HE-stained sections of a 3-days organotypic invasion assay. HT-29M6 were seeded between two matrix layers alone or in co-culture with CAFs, in high Gln or in a Gln gradient.

Again, enhancement of invasion was specific for glutamine, as it was not detected when HT-29M6 and MSCs co-cultures were exposed to glucose and lactate gradients (from 0.1 to 1g/l or from 0 to 20 mM respectively). Depletion of non-essential amino acids (NEAA) in the

upper chamber also increased MSC-stimulated HT-29M6 invasion, although this effect was weaker than in glutamine-driven invasion. The stimulation of HT-29M6 invasion by MSCs was also detected in a gradient of FBS, as previously reported **(Fig. R19)**.

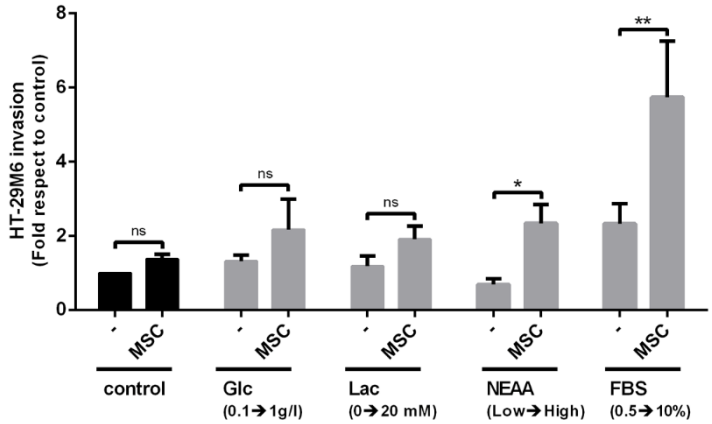

Figure R19. Glucose and lactate gradients do not alter MSC-stimulated HT-29M6 invasiveness. MSCs/HT-29M6 co-cultures were subjected to glucose (Glc), Lactate (Lac), non-essential amino acids (NEAA) and fetal bovine serum (FBS) gradients and HT-29M6 invasion was measured by the amount of RFP staining on each condition. Data represent mean ± SEM of at least three independent experiments, normalized to control condition (absence of gradients; represented in black bars). ns, not significant; * $p<0.05$; ** $p<0.01$.

We then extended the effect of glutamine on invasion to other breast and colorectal tumor cell lines. Invasion was enhanced by a glutamine gradient only in the mesenchymal BTE-136 cells. In contrast, Gln-driven invasion was not stimulated in other glutamine-independent epithelial cell lines, including AT-3, SW-480, T-47D, MCF-7 and HCT116 **(Fig. R20)**. Invasion of all these cell lines was promoted by the co-culture with CAFs **(Fig. R20A)** or MSCs **(Fig. R20 B-C)**; remarkably, AT-3, SW-480 and T-47D cells invaded better in a glutamine gradient than in a glutamine-high medium upon fibroblast co-culture **(Fig. R20 A-B)**.

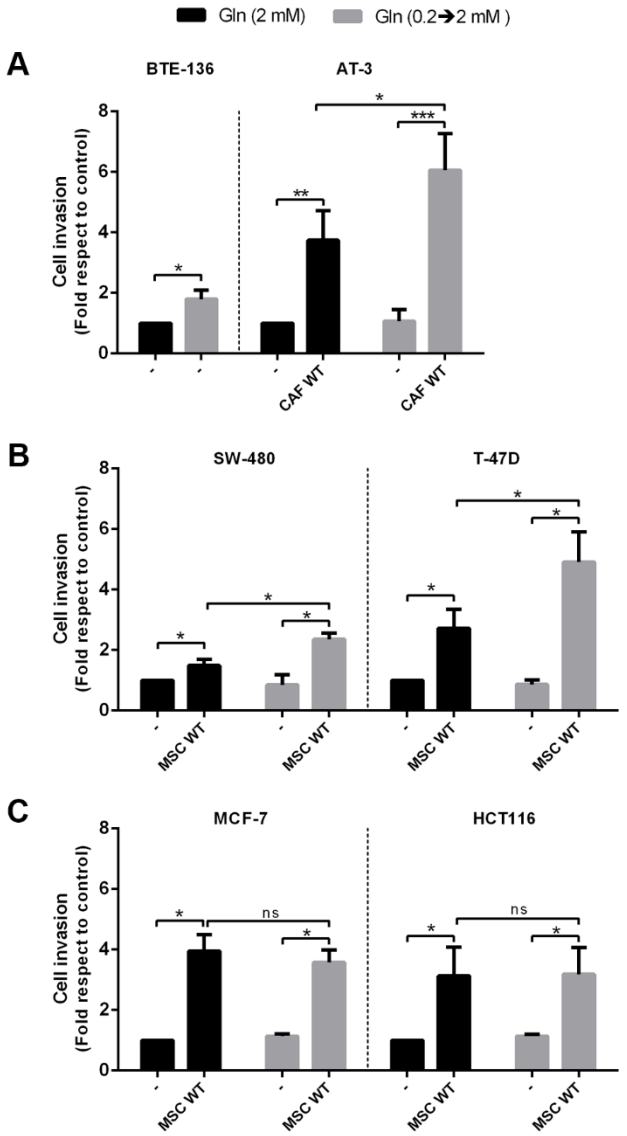

Figure R20. Mesenchymal cells enhance invasion of other tumor cell lines. AT-3, SW-480, T-47D, MCF-7 and HCT116 cells were infected with a retroviral pMSCV-tomato vector and selected with puromycin. Invasion of these cell lines was determined after 48 hours upon high Gln or Gln-gradient culture; when indicated, cells were co-cultured with CAFs or MSCs. In BTE-136 cells, invasion was measured by DAPI staining. In the remaining cell lines, invasion was determined as the area of Tomato-positive cells and referred to invasion in high Gln condition. Data represent mean ± SEM of at least three independent experiments. ns, not significant; * p<0.05; ** p<0.01; *** p<0.001.

2.4. Tumor cells stimulate glutamine-driven invasion of fibroblasts

The sensitivity of MSCs to Snail1 depletion and TGF-β supplementation suggested that these cells were activated by HT-29M6 when co-cultured. For this reason, we tracked the invasion of green fluorescent protein (GFP)-labelled MSCs in co-culture with HT-29M6. We observed that MSCs invasion was stimulated by HT-29M6. This stimulation was higher when cells were exposed to a glutamine gradient and was decreased by TGF-β receptor inhibitor SB505124 **(Fig. R21)**. As expected, MSCs invasion was abrogated by a general metalloprotease inhibitor (GM6001) in our system.

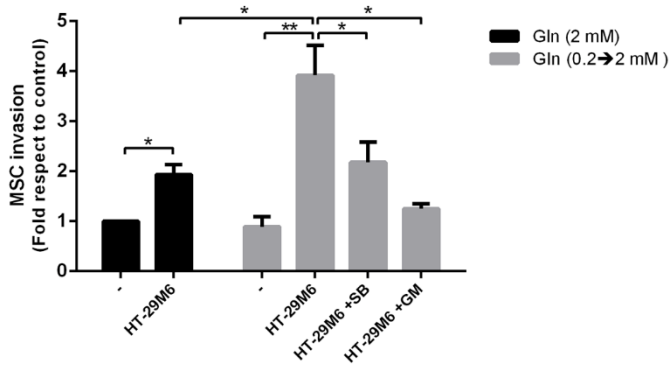

Figure R21. Glutamine-directed MSC invasion is enhanced by co-culture with HT-29M6 cells and is sensitive to TGF-β and metalloprotease inhibitors. MSCs were infected with a pBabeGFP retroviral vector and fluorescent cells selected with puromycin. Cell invasion was measured at 12 hours by the area of GFP-positive cells and referred to high Gln. When specified, MSCs were co-seeded with HT-29M6. SB505124 (SB; 5 μM) and GM6001 (GM; 25 μM) were added to the upper transwell compartment. Data represent mean ± SEM of at least three independent experiments. *p<0.05; **p<0.01

2.5. Tumor cells retain their epithelial phenotype during glutamine-driven invasion

We next assessed the requirement of Snail1 expression in epithelial cells for glutamine-driven invasion. For this, we took advantage of Snail1-KO HT-29M6 cells that were previously generated in our laboratory by CRISPR/Cas9 technology[139]. These cells, that lack almost the entire first exon of *SNAI1* gene, invaded identically to control HT-29M6 when they were co-cultured with MSC in a glutamine gradient **(Fig. R22 A)**, thus suggesting that the expression of Snail1 is not required in HT-29M6 cells for their collective migration with MSCs.

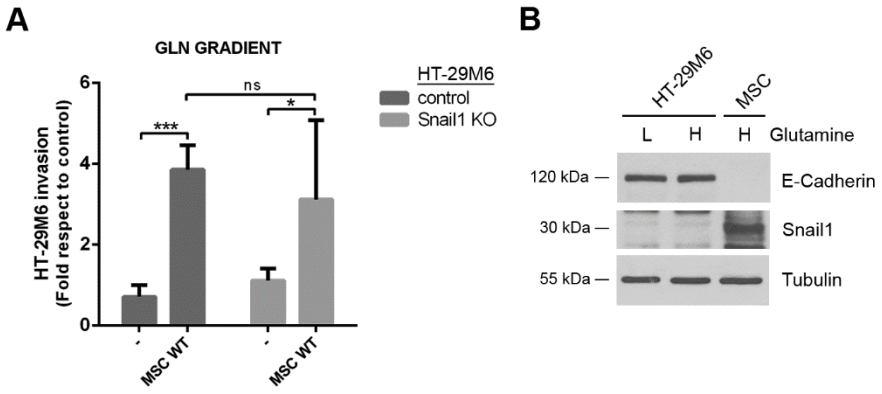

Figure R22. HT-29M6 cells do not lose their epithelial features upon glutamine deprivation. (A) Gln gradient-stimulated invasion was determined as the number of RFP positive cells in HT-29M6 cells control and Snail1 KO, upon MSCs WT co-culture. **(B)** Protein levels of E-cadherin and Snail1 were measured by Western blot in HT-29M6 cells cultured in high (H; 2 mM) or in low (L; 0.2 mM) Gln; MSC were used as positive control for Snail1 expression. Data represent mean ± SEM of at least three independent experiments. ns, not significant; * $p<0.05$; *** $p<0.001$

Accordingly, protein levels of the epithelial marker E-cadherin **(Fig. R22 B)** and RNA levels of the EMT-TFs Snail1, Snail2, Twist and Zeb1, were not altered upon glutamine deprivation in HT-29M6 cells **(Fig. R23)**.

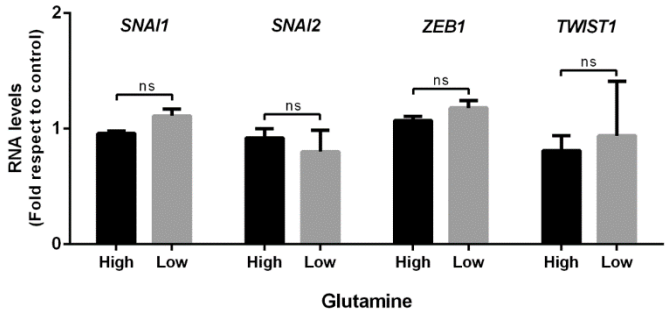

Figure R23. HT-29M6 cells do not undergo EMT-related changes upon glutamine deprivation. RNA levels of Snail1, Snail2, Zeb1 and Twist were analyzed by RT-qPCR in HT-29M6 cells in high or low Gln cultures. Data represent mean ± SEM of at least three independent experiments. ns, not significant.

These results agreed with the morphology of HT-29M6 cells during invasion. In this case, paraffin sections of HT-29M6/CAFs co-culture were analyzed by immunohistochemistry (IHC), since we aimed to determine how these two cell types were organized during glutamine-driven invasion. We corroborated that HT-29M6 cells maintained their epithelial phenotype during glutamine-stimulated invasion, as seen by the high levels of E-cadherin that was indeed present even in some cells inside the matrix. CAFs, which were labelled with the fibroblast-specific protein S100A4, were localized below tumor cells and mainly inside the matrix, likely leading HT-29M6 cells invasion **(Fig. R24)**.

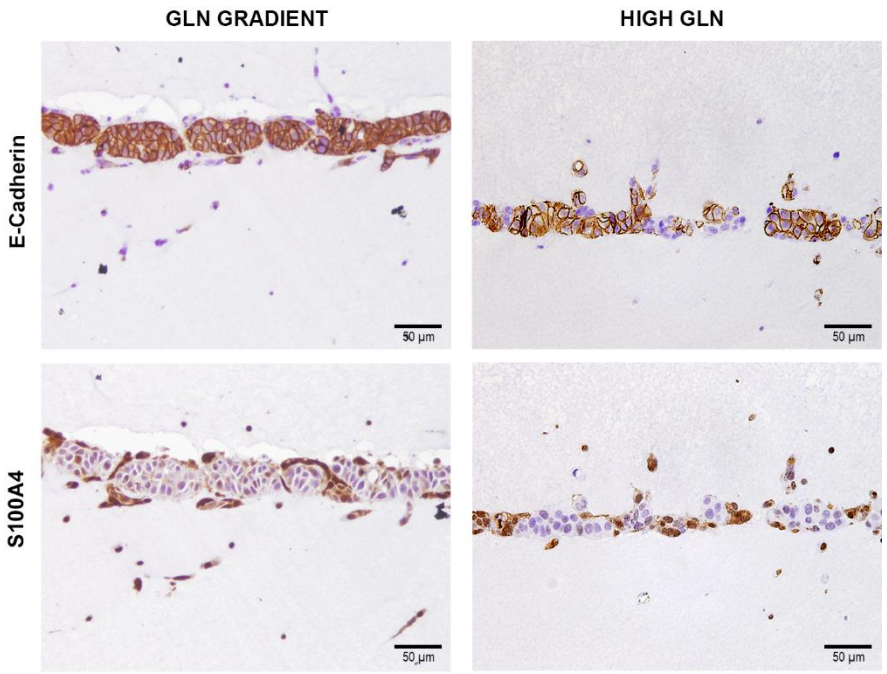

Figure R24. Fibroblasts lead invasion of tumor cells in a glutamine gradient. Organotypic invasion assays of HT-29M6 and CAFs co-cultures were obtained as described in Materials and Methods and analyzed by IHC with antibodies against E-Cadherin and S100A4.

2.6. Fibroblast-derived factors enhance tumor cell migration

It has been widely described that tumor cell migration is enhanced by paracrine signals that derive from the tumor microenvironment[31]. The influence of fibroblast conditioned media on the migration and invasion of tumor cells was then examined. HT-29M6 cells invasion was not affected by MSC-derived media in any of the analyzed conditions **(Fig. R25 A)**, reinforcing the idea that in our system ECM remodeling is basically performed by fibroblasts **(Fig. R18)**. Still, HT-29M6 migration was promoted in a glutamine gradient by conditioned media from MSCs and CAFs when these cells were activated by TGF-β **(Fig. R25 B)**. This suggests that tumor cell migration is stimulated by MSC-secreted factors.

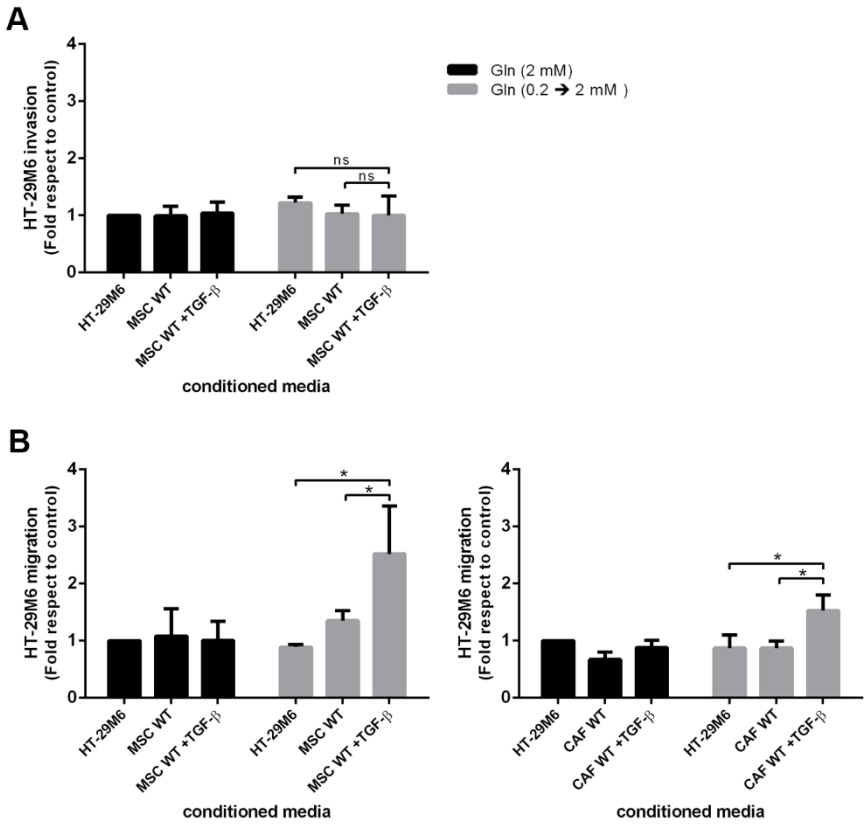

Figure R25. Conditioned media from activated fibroblasts enhances migration but not invasion of glutamine-starved HT-29M6 cells. HT-29M6 **(A)** invasion and **(B)** migration were assessed using conditioned media derived from MSCs and CAFs as chemoattractant. HT-29M6 were seeded in the upper chamber in high (black bars) or low Gln (grey bars). Media from HT-29M6 (as control condition), MSCs or CAFs cultures were treated with TGF-β when specified, supplemented with 2 mM Gln and added to the bottom compartment. Data represent mean ± SEM of at least three independent experiments. ns, not significant; * $p<0.05$.

Curiously, the mechanisms by which MSCs enhanced HT-29M6 cells invasiveness upon glutamine deprivation were not the same as that described for FBS-stimulated invasion. Although PGE_2 secretion by MSCs was stimulated by HT-29 M6 cells also in conditions of glutamine deprivation **(Fig. R26 A)**, its addition to the bottom compartment of

Boyden chambers did not promote HT-29M6 cells invasion when stimulated by glutamine **(Fig. R26 B)**. Similarly, HT-29M6 enhancement of invasion in MSCs co-culture was not abrogated when treated with an EP4 receptor antagonist (L-161). To verify the effect of both PGE_2 and L-161, FBS-gradient invasion experiments were performed in parallel to glutamine-stimulated assays. In this case, we reproduced the published results, as HT-29M6 cells motility responded to both PGE_2 addition and EP4 inhibition.

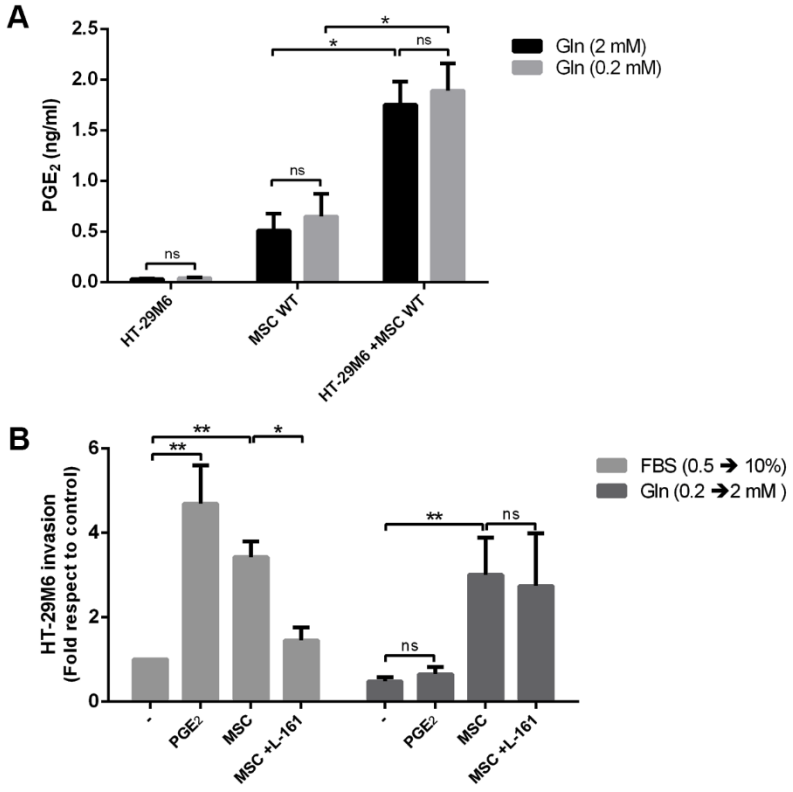

Figure R26. MSC-stimulated HT-29M6 cell invasion is not driven by PGE_2 signaling upon glutamine deprivation. (A) PGE_2 levels were determined by ELISA (RPN222, GE Healthcare Life Sciences) in HT-29M6, MSCs and HT-29M6/MSCs cultures in high (2 mM) and low (0.2 mM) Gln. **(B)** Invasion of HT-29M6 cells was measured in FBS or Gln gradients; MSCs, PGE_2 (100 nM) and L-161 (10 µM) were supplemented when specified. Invasion was quantified as the area of RFP-expressing cells and normalized to FBS-stimulated invasion, Data represent mean ± SEM of at least three independent experiments. ns, not significant; * $p<0.05$; ** $p<0.01$.

We considered the possibility that tumor cell invasion was not stimulated by signaling factors, but by metabolic intermediates derived from activated fibroblasts. Interestingly, it is described that high levels of extracellular glutamate contribute to the invasion of tumor cells[216]; therefore, we evaluated the role of glutamate in HT-29M6 invasion.

Since fibroblasts migrate faster than tumor cells and they exhibit a higher rate of glutamine consumption, we hypothesized that they might generate a glutamate gradient from the lower compartment of Boyden chambers, which would stimulate HT-29M6 cells migration. We assessed whether the addition of glutamate to the lower compartment enhanced the migration of HT-29M6 cells in a similar fashion as MSCs-derived conditioned media did. Although slightly increased, the migration of HT-29M6 cells was not significantly different upon the stimulation with glutamate, either in high or low Gln **(Fig. R27)**.

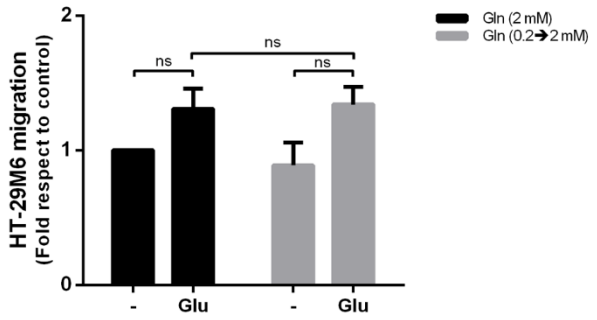

Figure R27. Glutamate stimulation does not enhance tumor cell invasion. Migration of HT-29M6 cells was measured in high Gln (2 mM) or a Gln gradient (0.2 → 2 mM) upon the addition of glutamate (Glu; 1 mM) to the lower compartment. After 48 hours, migration was quantified as the area of DAPI staining and normalized to high Gln, Data represent mean ± SEM of three independent experiments. ns, not significant.

2.7. Glutamine deprivation impairs TGF-β dependent activation of fibroblasts

As aforementioned, glutamine depletion orchestrates TGF-β-stimulated migration and invasion of fibroblasts. In order to elucidate the mechanisms leading to this effect, we assessed how fibroblasts activation was affected by glutamine deprivation. Protein levels of the activation markers Snail1, S100A4 and Fibronectin were decreased in glutamine-deprived CAFs **(Fig. R28)**. These results matched with a decrease in phosphorylated ribosomal protein S6 (phospho-S6) upon low Gln culture, as this protein is a target of mTOR and it is modulated by amino acids. On the other hand, rapid TGF-β-derived changes that did not require *de novo* protein synthesis, such as Smad2 phosphorylation, were not altered in glutamine-depleted cells.

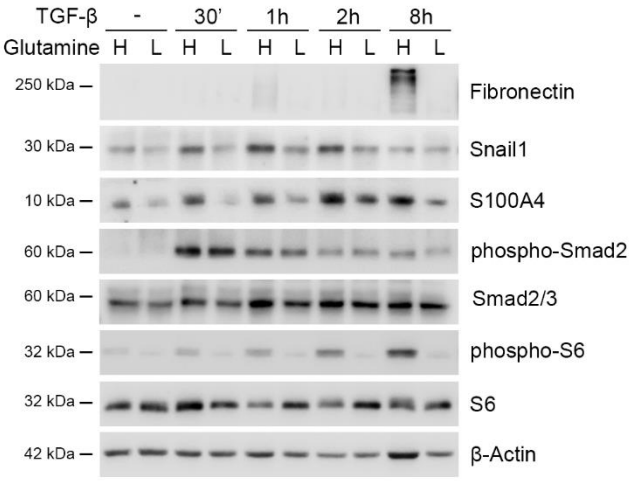

Figure R28. Fibroblast activation by TGF-β is defective in glutamine-deprived cells. Protein levels of the indicated markers were determined by Western blot analysis in CAFs, cultured in high (H; 2 mM) or low Gln (L; 0.2 mM) for 24 hours and stimulated with TGF-β (5 ng/ml) for different time points.

Glutamine depletion impairs *de novo* protein synthesis, resulting in a decrease in the levels of activation markers. We also analyzed if the transcription of those markers induced by TGF-β was affected by glutamine deficiency in MSCs. Whereas *Snai1* and *Tgfb1* mRNA were equally up-regulated in both conditions **(Fig. R29 A)**, other early activation markers as *Usp27x* were affected by the depletion **(Fig. R29 B)**. As we expected, those late markers whose expression depended on Snail1 up-regulation (as the ECM degradation-related gene *Adamts16)* were impaired upon glutamine deprivation.

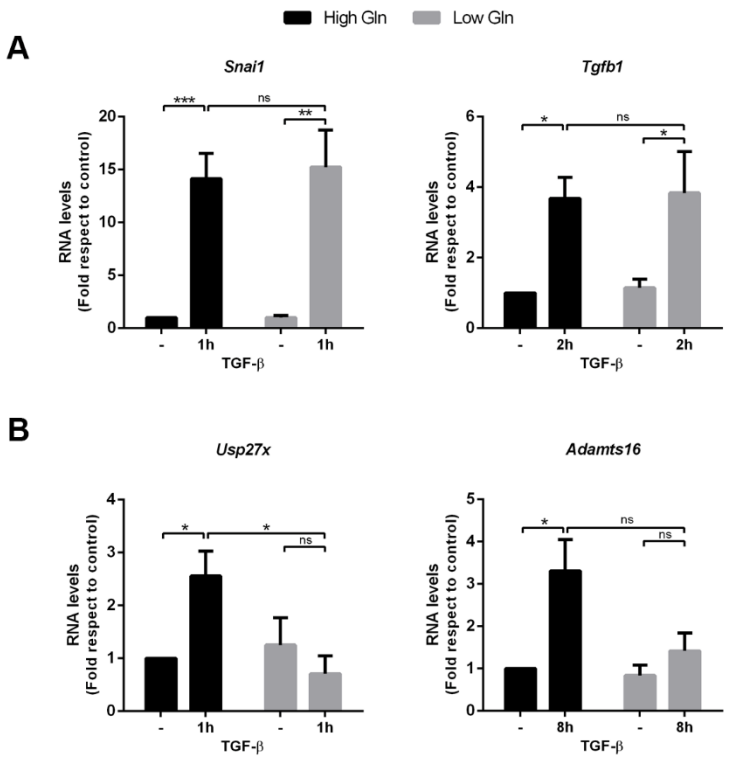

Figure R29. Transcriptional up-regulation of early activation markers is not affected by glutamine deprivation. RNA levels of the indicated markers were determined by RT-qPCR in MSCs. These cells were cultured in high (2 mM) or low Gln (0.2 mM) for 24 hours and stimulated with TGF-β (5 ng/ml) at the indicated time points.

2.8. Glutamine promotes fibroblast migration through Akt2 polarization

As indicated in the introduction, the Snail1-dependent activation of fibroblasts by TGF-β requires Akt activity[150]. However, we did not observe major changes in Akt phosphorylation in CAFs. Indeed, Akt phosphorylation was slightly increased by TGF-β when cells were cultured in a glutamine-high media, but its levels were even lower than the basal when stimulated with TGF-β upon glutamine deprivation **(Fig. R30)**.

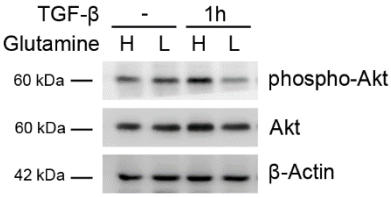

Figure R30. Akt phosphorylation is not affected by TGF-β stimulation in CAFs. CAFs were cultured in high (H; 2 mM) or low Gln (L; 0.2 mM) for 24 hours and stimulated with TGF-β (5 ng/ml) for 1 hour. Protein levels of the indicated markers were determined by Western blot analysis.

Specific activation of Akt has also been reported in the leading edge of migrating cells[221]. To study its distribution during migration, we performed immunofluorescence (IF) staining of CAFs that had been exposed to glutamine gradients in Chemotaxis µ-slides. The results showed a differential polarization of Akt2 in cells of the migration front that was specific for glutamine gradient condition **(Fig. R31 A)**. This distribution was not observed in cells that were not activated, either because the lack of TGF-β or Snail1 **(Fig. R31 B and quantification in C)**.

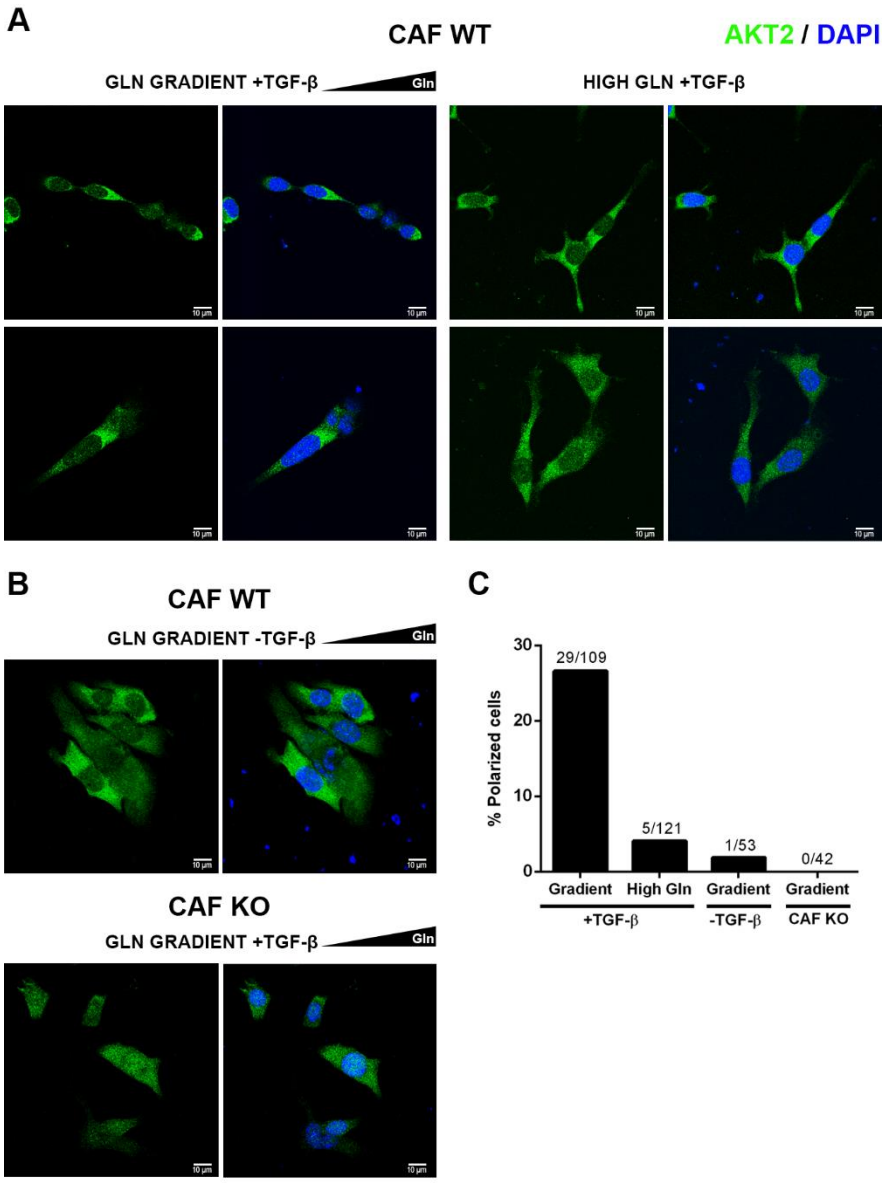

Figure R31. Activated fibroblasts show a subcellular polarized distribution of Akt2 during glutamine-driven migration. IF staining of Akt2 in **(A)** TGF-β-treated CAFs WT, **(B)** untreated CAFs WT (-TGF-β) and CAFs Snail1 KO. Staining were performed after 6 hours of migration in a Gln gradient or in high Gln conditions as described in Materials and Methods. **(C)** Asymmetrical Akt2 localization was quantified and plotted as the proportion of polarized cells in the invasion front. The ratio of polarized cells versus total cell number is specified for each condition.

To ensure that this polarization was not artifactual, we stained for other cytoplasmatic proteins. Neither Akt1 nor total Akt displayed a similar asymmetrical intracellular localization. In addition, we analyzed the distribution of mTOR kinase, since its protein complex mTORC1 is sensitive to the availability of amino acids[179]; however, we did not observe a polarized distribution either **(Fig. R32)**.

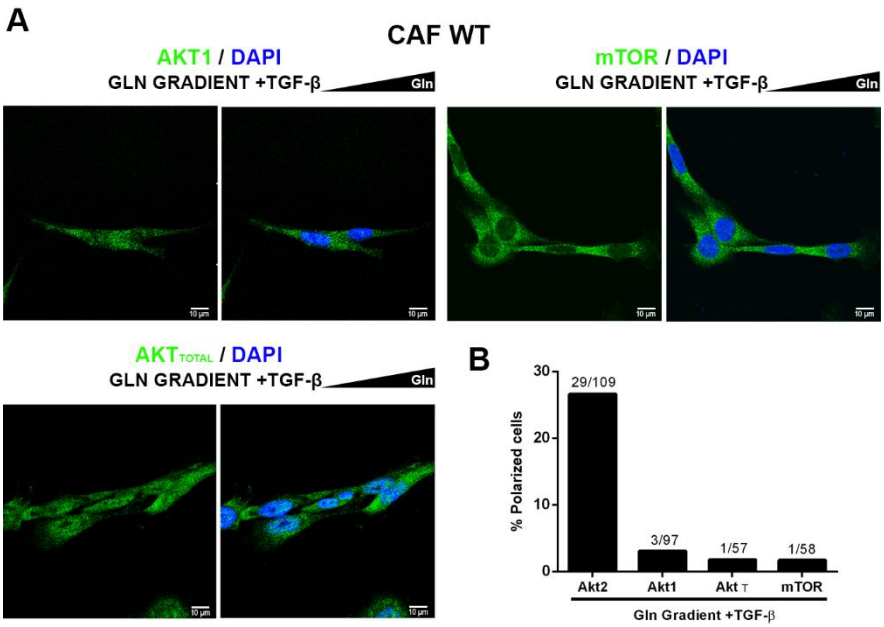

Figure R32. Asymmetrical distribution is not observed in other cytoplasmatic proteins. (A) TGF-β-stimulated CAF migration was stopped after 6 hours in a Gln gradient. After fixation, IF staining of Akt1, mTOR and Total Akt were performed as described in Materials and Methods. **(B)** Quantification of cell polarization was expressed as the ratio of polarized cells versus total cell number and compared to Akt2 polarization of Figure R31.

These results were then validated in other cell types that responded to glutamine in their migration. Akt2 polarization was observed in other mesenchymal types as BTE-136 tumor cells, but it did not appear in epithelial AT-3 cells. Likewise, this asymmetrical distribution was also present in MSCs and MEFs, always depending on their activation by

TGF-β **(Fig. R33 A and quantification in C)**. In all the cell lines, Akt2 subcellular polarization was not found when glutamine was homogeneously enriched in all compartments **(Fig. R33 B)**.

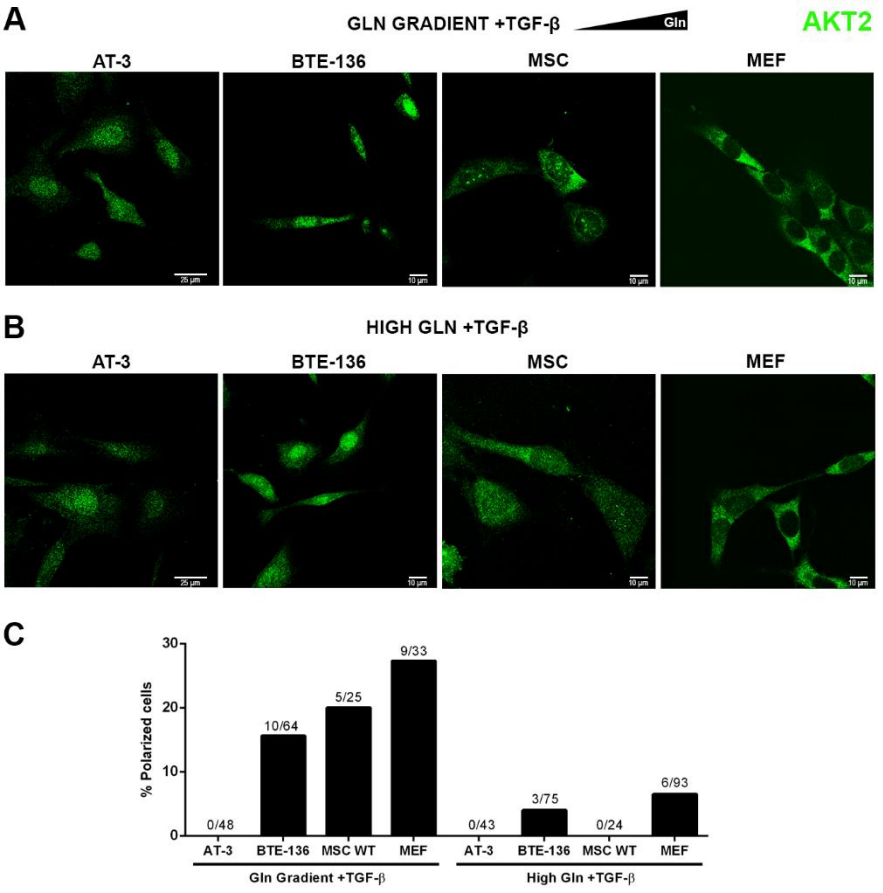

Figure R33. Other mesenchymal cell types exhibit an asymmetrical distribution of Akt2. IF staining of Akt2 were performed in AT-3, BTE-136, MSCs and MEFs after 6 hours of migration in **(A)** Gln gradient or **(B)** high Gln medium, upon TGF-β stimulation. **(C)** Akt2 asymmetrical localization was quantified in all the cell lines and conditions and represented as the percentage of polarized cells respect to total cell number.

We tested the relevance of Akt2 in cell migration by using MEFs that were depleted of this protein[222] **(Fig. R34 A)**. These cells showed a strong reduction in basal and TGF-β-stimulated expression of S100A4. Nonetheless, the depletion of Akt2 slightly decreased Snail1 protein up-regulation and Smad2 phosphorylation upon TGF-β stimulation **(Fig R34 B)**. In contrast, Akt1 depletion only decreased phospho-Smad2 and did not have any effect on the expression of S100A4 or Snail1.

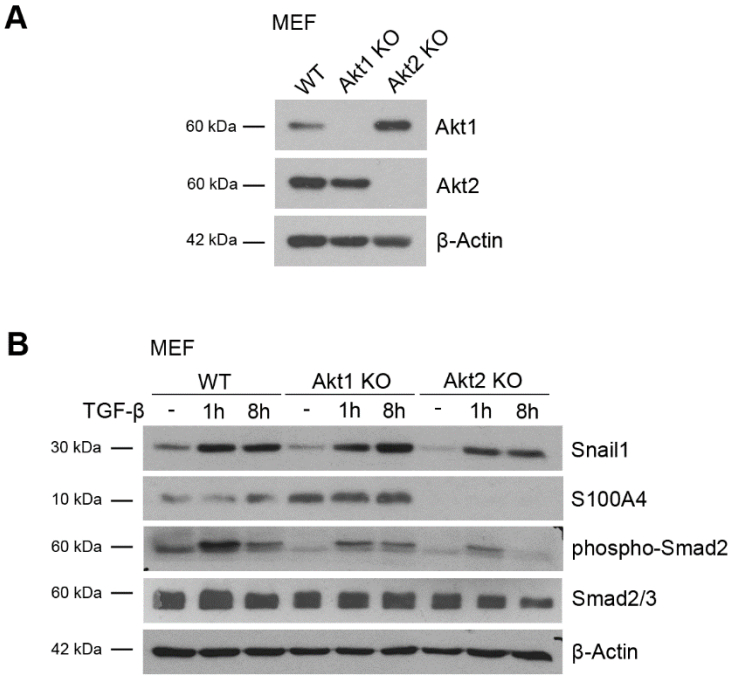

Figure R34. Activation of Akt2-depleted MEFs in response to TGF-β is partially altered. (A) Akt1 and Akt2 depletion in MEFs was validated at protein level by Western blot. **(B)** The indicated proteins were analyzed by Western blot in control, Akt1 and Akt2-depelted MEFs (WT; Akt1 KO; Akt2 KO) when stimulated with TGF-β (5 ng/ml) for 1 or 8 hours in high Gln culture.

As expected, Akt2 KO MEFs were unable to migrate when stimulated with a gradient of glutamine and TGF-β. Conversely, Akt1 KO MEFs migrated as efficiently as control MEFs **(Fig. R35 A)**. In accordance with the low motility shown by these cells, Akt2 KO MEFs were unable to stimulate invasion of HT-29M6 in a glutamine gradient upon their co-culture, in contrast to control or Akt1-depleted MEFs **(Fig. R35 B)**.

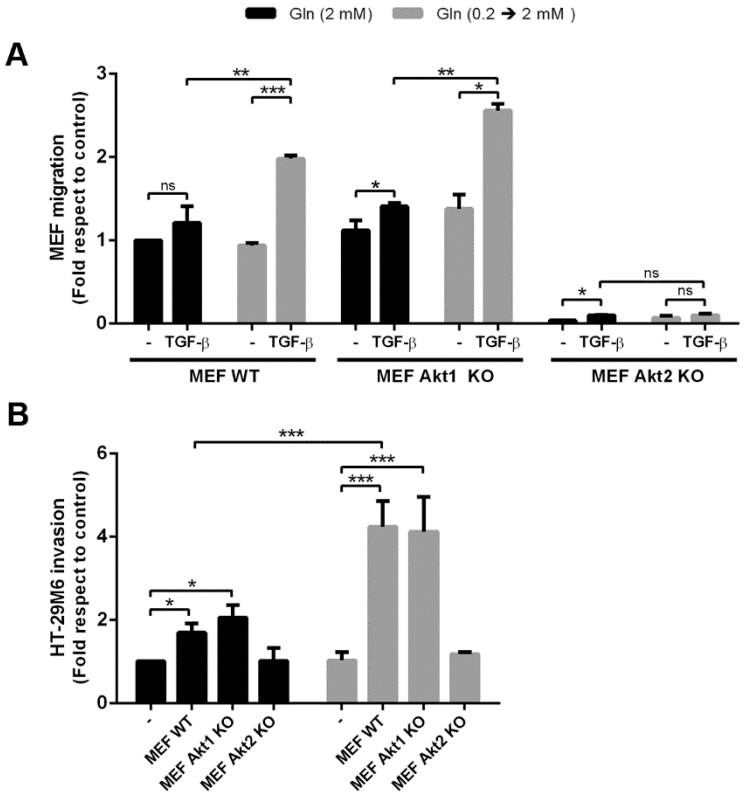

Figure R35. Akt2-depleted MEFs show impaired migration capability and fail to enhance HT-29M6 invasion in a glutamine gradient. (A) Migration of control, Akt1 and Akt2 depleted MEFs (WT; Akt1 KO; Akt2 KO) was assessed at 12 hours in high Gln (2 mM) or in a Gln gradient (0.2 → 2 mM). TGF-β was supplemented when indicated. **(B)** RFP-labelled HT-29M6 cells invasiveness was analyzed in co-culture with MEFs WT, Akt1 KO and Akt2 KO upon high Gln and Gln gradient stimulation. Data represent mean ± SEM of at least three independent experiments. ns, not significant; *p<0.05; **p<0.01; ***p<0.001.

To further validate the importance of Akt2 in glutamine-driven migration of fibroblasts, we rescued the wild-type phenotype in Akt2-KO cells. Migration of Akt2-depleted MEFs was recovered by the ectopic transfection of a full-length Akt2 vector (Akt2-FL), which also restored Akt2 polarized distribution in these cells **(Fig. R36)**. Deficiencies in migration were not improved by the transfection of an Akt2 mutant lacking the pleckstrin homology domain (Akt2-ΔPH), that is necessary for Akt2 cytoplasmatic localization and its subsequent activation.

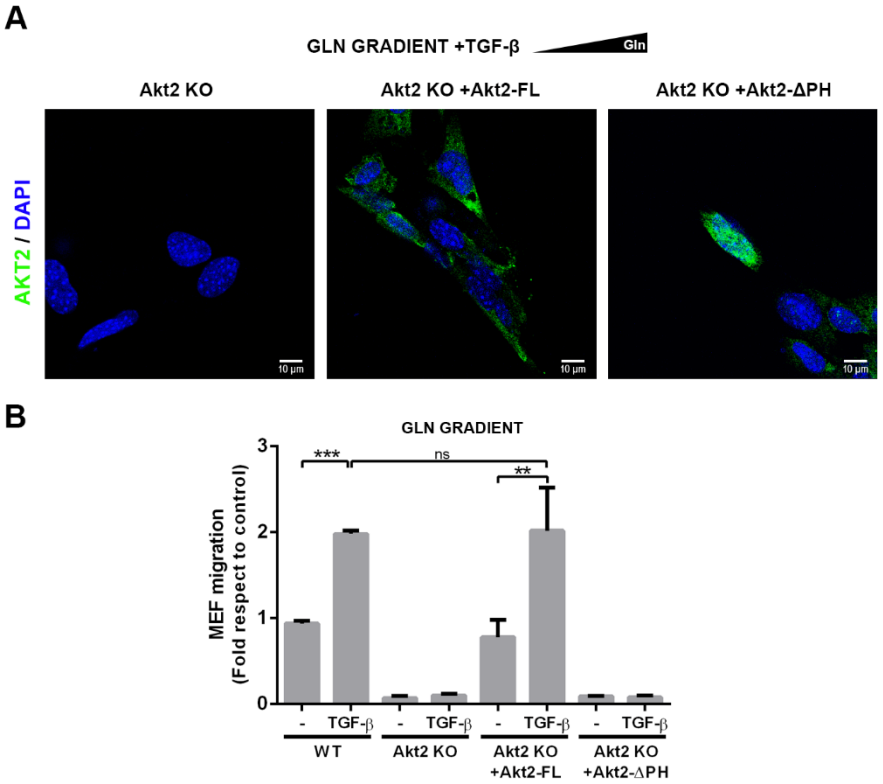

Figure R36. The migration capability of Akt2-depleted MEFs is restored by transfection of a full-length Akt2 vector. Akt2-KO MEFs were transfected with a full length Akt2 vector (Akt2-FL) or Akt2 mutant lacking the plekstrin homology domain (Akt2-ΔPH). **(A)** Akt2 subcellular distribution was determined upon Gln-stimulation by Akt2 IF staining in transfected cells. **(B)** Migration of Akt2-rescued MEFs in a Gln gradient was assessed at 12 hours upon TGF-β (5 ng/ml) treatment. Data represent mean ± SEM of at least three independent experiments. ns, not significant; **p<0.01; ***p<0.001.

2.9. TRAF6 is required for glutamine-dependent Akt2 subcellular polarization

To better understand how the asymmetrical distribution of Akt2 is generated, we focused on its interaction with upstream regulators. Interestingly, Akt2 cytoplasmatic localization is regulated by its ubiquitination in Lysine 63. This ubiquitination is performed by the E3 ubiquitin ligase TRAF6, that is also controlled by nutrients[179].

We detected that, like Akt2, this protein also displayed an asymmetric distribution in CAFs when these cells were exposed to a glutamine gradient. TRAF6 was more abundant in the migration front **(Fig. R37)** and co-localized with Akt2 in polarized fibroblasts **(Fig. R38)**, which suggested its possible effect in regulating Akt2 distribution and subsequently glutamine-driven migration.

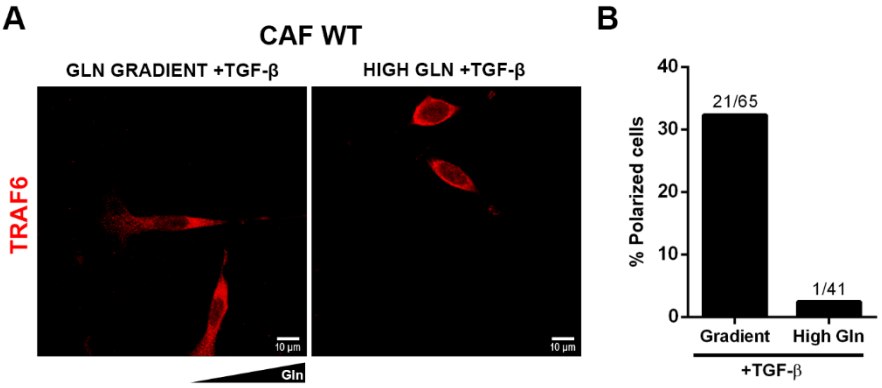

Figure R37. TRAF6 is polarized in CAFs during glutamine-stimulated migration. (A) IF staining of TRAF6 in TGF-β-stimulated CAFs WT. Staining were performed after 6 hours of migration in a Gln gradient or in a high Gln culture. **(B)** Asymmetrical TRAF6 localization was quantified and plotted as the proportion of polarized cells in the invasion front. The ratio of polarized cells respect to total cell number is specified for both conditions.

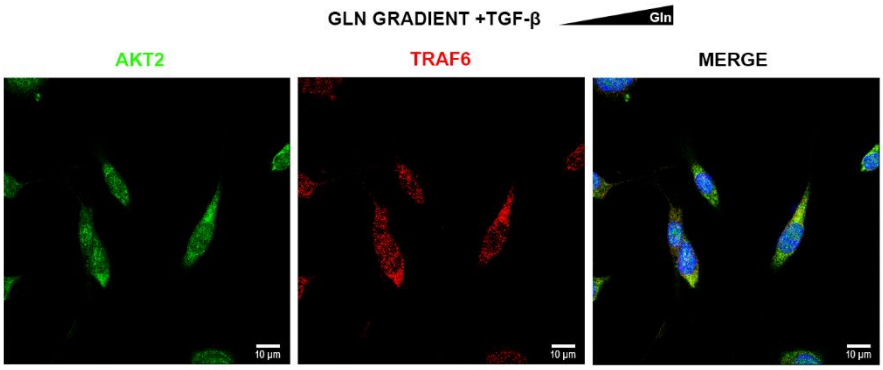

Figure R38. TRAF6 co-localizes with Akt2 in polarized CAFs. Co-IF analysis for detection of Akt2 and TRAF6 in TGF-β-stimulated CAFs. Staining were performed after 6 hours of Gln-driven migration.

To explore the role of TRAF6 in the regulation of Akt2 distribution, we down-regulated TRAF6 in CAFs using two different short-hairpin RNAs (shRNAs). Both knock-down (KD) populations showed similar levels of Akt2 when compared to control cells, but they presented lower levels of phosphorylated Akt2 **(Fig. R39)**.

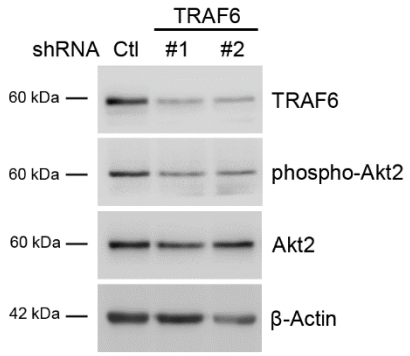

Figure R39. Akt2 phosphorylation is reduced in TRAF6 knock-down CAFs. TRAF6 was knocked-down (KD) in CAFs by lentiviral infection of two different TRAF6 shRNAs (#1 and #2) and its expression determined by Western blot analysis and compared to control shRNA (Ctl).

As in Akt2 KO MEFs, Snail1 and phospho-Smad2 were equally up-regulated by TGF-β in control cells and in TRAF6-KD CAFs **(Fig. R40)**.

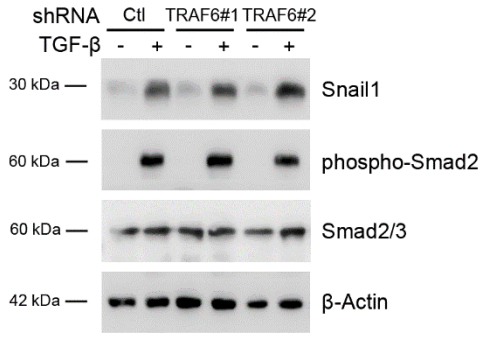

Figure R40. TGF-β-dependent activation of CAFs is not affected by TRAF6 knock-down. CAFs control (Ctl) or TRAF6-KD (TRAF6#1 and TRAF6#2) were cultured in high Gln medium and treated with TGF-β (5 ng/ml) for 1 hour. Expression of the indicated markers was determined by Western blot analysis.

Since TRAF6 is a ubiquitin ligase that regulates Akt by its multi-ubiquitination[66], we studied this modification on Akt2. In order to obtain the ubiquitinated profile of Akt2, we transfected CAFs with a vector of histidine-tagged ubiquitin and we purified ubiquitinated proteins by pull-down assays. Akt2 ubiquitination was then assessed by Western blot. As observed in **Fig. R41**, Akt2 ubiquitination of control CAFs was dependent on TGF-β stimulation. TRAF6 down-modulation decreased the amount of ubiquitinated Akt2 upon TGF-β stimuli. A similar result was obtained when this determination was performed comparing CAFs incubated in low Gln versus high Gln, in accordance with the previous studies indicating that TRAF6 is controlled by amino acids.

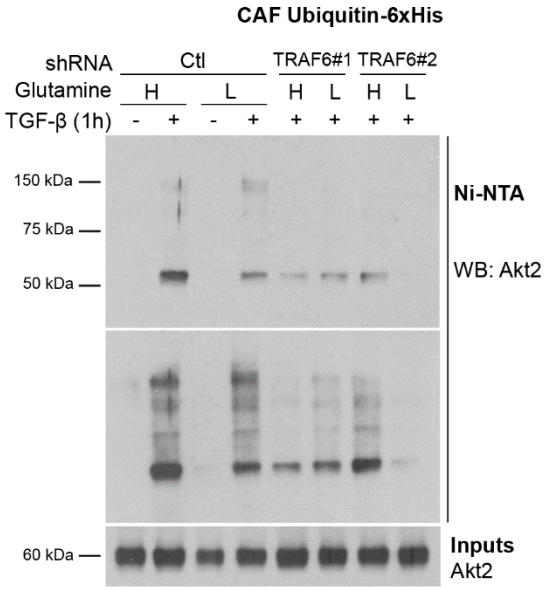

Figure R41. TRAF6 mediates glutamine-dependent Akt2 ubiquitination. CAFs control (Ctl) or TRAF6-KD were transfected with the pMT107 (Ubiquitin-6xHis) vector and cultured in high (H) or low (L) Gln. After 1 hour of TGF-β (5 ng/ml) stimulation, ubiquitinated proteins were purified by Nickel-nitrilotriacetic (Ni-NTA) pull-down under denaturing conditions. Akt2 ubiquitination was determined by Western blot.

By the previous experiments we demonstrated that TRAF6 modulates Akt2 ubiquitination in the presence of amino acids. According to previous studies, this ubiquitination would affect Akt2 subcellular localization by becoming more cytoplasmatic[66]. Because of this, we analyzed if Akt2 polarization was unpaired in glutamine-driven migration of TRAF6-KD CAFs. As expected, Akt2 did not display a polarized distribution in these cells **(Fig. R42)**; in contrast, the nuclear levels of Akt2 were increased.

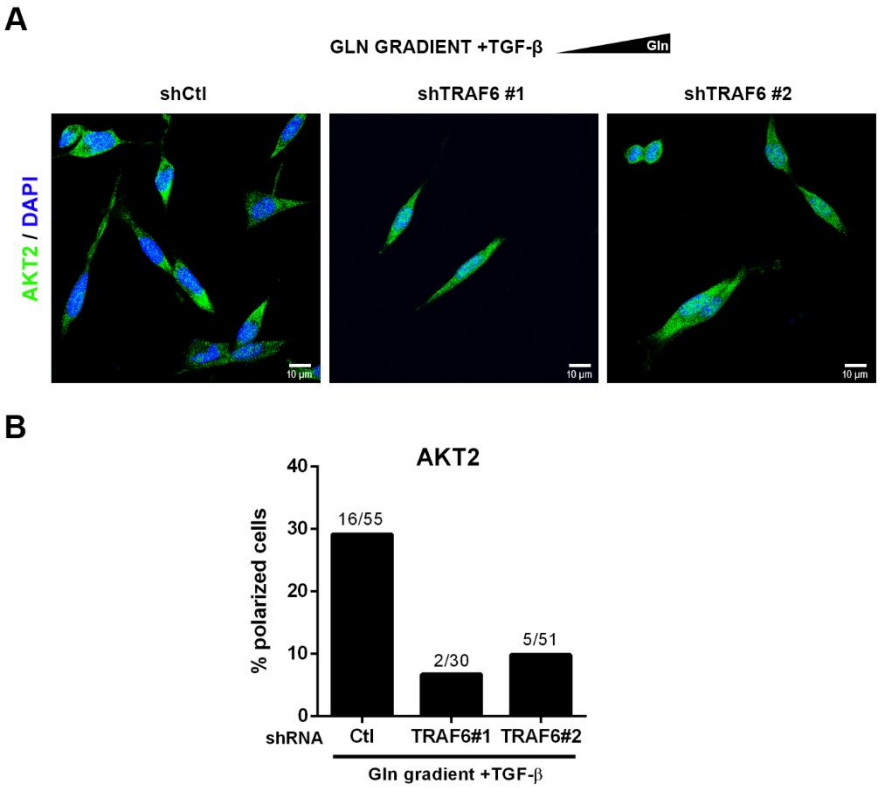

Figure R42. TRAF6 knock-down prevents Akt2 polarization during glutamine-directed CAF migration. (A) Akt2 polarization was determined by IF in CAFs control (Ctl) or TRAF6-KD (shTRAF6#1 and shTRAF6#2). Cells treated with TGF-β and their migration stimulated by a gradient of Gln for 6 hours. **(B)** Akt2 polarization was plotted as the proportion of polarized cells in the invasion front. The ratio of polarized cells versus total cell number is specified for each condition.

Finally, we analyzed the invasion capability of TRAF6-KD CAFs. Again, we seeded these cells in high or low Gln and we assessed their capability to invade through Matrigel towards a glutamine-high chamber. The outcome of this experiment was analogous to our findings in Akt2-KO MEF, as the enhancement of invasion in these cells when activated by TGF-β and exposed to a glutamine gradient was prevented by TRAF6 interference **(Fig. R43)**.

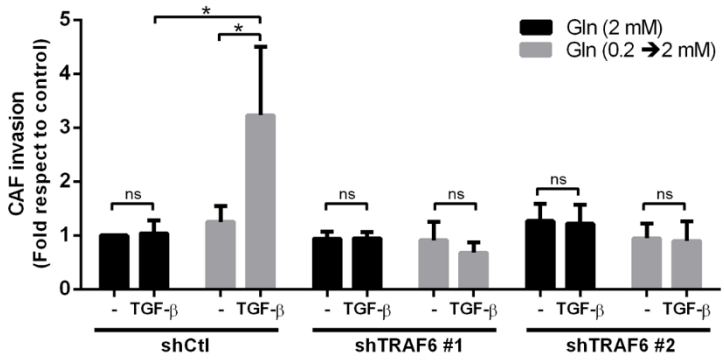

Figure R43. TRAF6 down-regulation prevents TGF-β-stimulated invasion of CAFs. Gln gradient invasion experiments were performed in CAFs control (shCtl) or TRAF6-KD (shTRAF6#1 and shTRAF6#2). TGF-β (5 ng/ml) was supplemented to the upper chamber when indicated and invasion was analyzed after 12 hours. Invasion was normalized respect to invasion of CAFs shCtl in high Gln. Data represent mean ± SEM of at least three independent experiments. ns, not significant; *p<0.05.

DISCUSSION

Acquired motility is a fundamental part of tumor dissemination and metastasis, as it provides tumor cells with the ability to invade the surrounding tissues and spread to the blood vasculature[18]. This process is greatly influenced by CAFs via ECM remodeling, the secretion of signaling molecules or their heterotypic interaction, which leads their collective spread from the tumor[97]. Given the unique metabolic conditions of tumors and their influence in tumor progression[165], my work was focused on the effect of metabolic stress on tumor invasion. In this thesis I determined the ability of TGF-β-activated fibroblasts to migrate following a glutamine gradient, an effect that correlates with the higher dependency of these cells on the uptake of extracellular glutamine.

1. GLUTAMINE METABOLISM IS INDISPENSABLE FOR MESENCHYMAL CELL SURVIVAL

1.1. Mimicking metabolic stress *in vitro*

To more accurately reproduce the behavior of cancer cells *in vitro*, culture conditions must be similar to those in tumors. As mentioned in the introduction, enhanced rates of glucose and glutamine consumption together with a poor inefficient tumor vascularization result in the depletion of nutrients and oxygen in the core of tumors, in contrast with the high nutrient availability of the surrounding tissues[223,224]. In this regard, we adjusted glucose and glutamine concentrations to the levels that are found in human plasma and we assessed the response of tumor cells and fibroblasts to their limitation by further depleting these two nutrients, thus mimicking tumor metabolic stress. All the experiments were performed in low FBS (0.5%), in order to avoid the effects of cell proliferation when comparing high and low nutrient conditions.

In a healthy organism, fasting glucose levels in plasma should be lower than 1.0 g/l[225]. Nevertheless, standard Dulbecco's Modified Eagle Medium (DMEM) contains glucose in a concentration of 4.5 g/l, even exceeding the glucose levels of hyperglycemia. Therefore, we established as our control condition (namely, "high glucose") a culture

medium containing the physiological glucose concentration (1.0 g/l). Since some studies defined that glucose concentration in tumors varies within a range of 0.05 - 0.3 g/l[223,226], we considered our tumor-like condition ("low glucose") a ten-fold reduction respect to the control (0.1 g/l glucose).

Glutamine is the most abundant amino acid in blood. Even though its concentration in plasma is maintained at approximately 0.5 mM[227], culture media contain 2 mM glutamine. Glutamine deprivation was observed in the central part of xenograft tumors when compared with the periphery; concretely, a glutamine concentration of 0.5 mM was reported in the borders of the tumor, whereas its concentration oscillated between 0.1 and 0.2 mM in the core[224]. Accordingly, we used 0.2 mM glutamine ("low glutamine") to mimic the tumor conditions.

1.2. The viability of mesenchymal cells is compromised by glutamine deprivation

When we examined the nutrient requirement of tumor cells, we observed that fibroblasts (including CAFs, MSCs and MEFs) were much more sensitive to a glutamine deficiency than epithelial tumor cells. Accordingly, CAFs and MSCs showed higher rates of apoptosis upon glutamine deprivation, which were associated to an increase in cleaved caspase-3. Glutamine dependence of fibroblasts correlated with enhanced rates of glutamine consumption, suggesting that the uptake of exogenous glutamine is indispensable for the maintenance of tumor associated fibroblasts. Consistent with our data, other authors have reported enhanced glutamine metabolism in CAFs[205,206]. Interestingly, glutamine-based anaplerosis was depicted as a major source of carbon for the TCA cycle in patient-derived CAFs, whereas glutamate was mostly secreted in tumor cells[205].

CAFs undergo metabolic reprogramming upon their activation by several stimuli, including TGF-β, PDGF or hypoxia[128,228,229]. Therefore, we hypothesized that the nutrient dependencies of fibroblasts might be influenced by their activation. Bertero *et al.* demonstrated that rigid

substrates promoted an enhanced glutamine uptake[205], which might be attributed to ECM-mediated fibroblast activation and a consequent metabolic shift[144]. Similarly, we determined that the activation of MSCs by TGF-β further decreased cell survival in a glutamine-depleted medium. Basal levels of Snail1 expression in CAFs did not affect their viability upon glutamine deprivation, since there was no difference in the glutamine dependency of Snail1-depleted and wild-type CAFs.

For its pleiotropic role in cellular functions, glutamine catabolism is considered crucial to sustain tumor cell proliferation[230]. Nevertheless, there is increasing evidence that "glutamine addiction" is highly heterogeneous among tumor cells, as it depends on their tissue of origin[231] and their ability to synthetize glutamine *de novo*[232]. In our study, the majority of the examined tumor cells were not sensitive to glutamine deprivation. In some cases, as in HT-29M6 cells, tumor cells were sensitive to a complete depletion of glutamine but were not affected by a ten-fold reduction of this amino acid, which was sufficient to impair the survival of fibroblasts. Importantly, we correlated glutamine dependence in tumor cells with their mesenchymal features. These results were observed in BTE-136 cells when compared with AT-3, both cell lines derived from MMTV-PyMT tumors with mesenchymal and epithelial phenotypes, respectively. Unexpectedly, these two cell types showed similar rates of glutamine consumption, implying that BTE-136 cells failed to adapt their metabolism in order to confront glutamine deprivation.

On the contrary, either epithelial or mesenchymal cell lines were less sensitive to glucose deprivation, which only affected SW-480 colorectal tumor cells and some of the fibroblastic cells to a lower extent than glutamine starvation. This observations highlight the capability of tumor cells to adapt to new extracellular glucose levels[233]. More likely, the fact that the culture medium contains pyruvate, a product of glucose metabolism, might compensate the effect of glucose restriction, since pyruvate fuels gluconeogenesis, aerobic glycolysis and oxidative phosphorylation[234]. Hence, glucose and pyruvate deprivation should be combined in future experiments.

1.3. Glutaminase1 inhibition impairs the survival of mesenchymal cell types

In tumors, most glutamine is metabolized to glutamate by GLS1[169]. For instance, its expression is a marker of stemness properties and poor prognosis in certain types of tumors[235,236]; thus, targeting glutamine metabolism by GLS inhibition is a therapeutic strategy that is currently in clinical trials[237]. The GLS1 inhibitor CB-839 suppresses tumor growth of triple negative murine tumors[220]; however, not all tumor types are sensitive to GLS inhibition, as CB-839 efficiency is related to the glutamine requirements of each class and the presence of adaptative metabolic networks[238].

None of the aforementioned studies assessed the effect of CB-839 on the stromal compartment. In fact, there is only one publication that describes the sensitivity of CAFs to the GLS1 inhibitor compound 968[206]. In line with our previous results, the high dependency of CAFs on extracellular glutamine correlated with an enhanced sensitivity to GLS1 inhibition. In contrast, HT-29M6 and AT-3 cells, both epithelial tumor cell lines, displayed a lower response to CB-839 treatment, which resulted in a high cell viability.

Enhanced sensitivity to GLS inhibition has been associated to low E-cadherin/high vimentin-expressing mesenchymal cells[239]. Accordingly, CB-839 reduced the viability of the mesenchymal BTE-136 cells, characterized by a high Snail1/low E-cadherin expression, in contrast to AT-3, which present higher levels of E-cadherin and cytokeratin 14. Although not assessed in our study, these differences might be related to EMT. Indeed, it is reported that a down-regulation of GLS1 in breast tumor cells prevents a TGF-β-induced EMT[240]. In addition, GLS1 expression is promoted by TGF-β stimulation in these cells[240], yet the molecular mechanisms of this induction remain to be elucidated.

Taken together, our work highlights the efficacy of GLS inhibition not only to target aggressive tumor phenotypes but also to effectively deplete the stromal compartment, a strategy that might be useful in

combination with other therapeutic agents.

1.4. Glutamine effects on cell survival and growth are not dependent on glutamate

Tumoral “glutamine addiction” has been classically attributed to the role of glutamine in oxidative phosphorylation; nevertheless, glutamine contributes to nucleotides and non-essential amino acids biosynthesis as well[230]. We assessed if the effect of glutamine deprivation on the survival of fibroblasts was rescued by TCA cycle replenishment through the supplementation of culture medium with glutamate. Although the effects of GLS1 inhibition by CB-839 were compensated by the addition of glutamate in a culture of CAFs, this intermediate slightly improved their viability of upon glutamine deprivation. Similar results were obtained when we added glucose or lactate to glutamine-deprived cells, which did not increase the survival of fibroblasts either. These observations suggest that even though glutamine catabolism is important for sustaining energy production in CAFs, glutamine is indispensable for its other functions, either as a nitrogen donor for *de novo* amino acid synthesis, as an exchanger for the import of other amino acids or as a signaling molecule.

Other studies confirmed that glutamine-starved cells are not rescued by other TCA cycle intermediates; instead, recovery of cell proliferation was dependent on the expression of glutamine synthetase (GS), and thus the capability of different cell lines to convert glutamate to glutamine[232]. Interestingly, the same authors determined that the deleterious effect of glutamine deprivation was reduced by the culture in a medium containing nutrient concentrations comparable to human serum but not in regular DMEM[232]. Unlike DMEM, serum-like medium included other non-essential amino acids (such as asparagine, alanine or proline) in its formulation. These observations highlight the role of glutamine in the preservation of intracellular amino acid pool; therefore, it might be interesting to evaluate whether amino acid supplementation compensates the effect of glutamine deprivation.

2. GLUTAMINE DRIVES MIGRATION AND INVASION OF FIBROBLASTS

After determining the essential role of glutamine in the survival of fibroblasts, we assessed the effect of its depletion in cell migration. As previously discussed, glutamine is depleted in the center of the tumors but not in their periphery[224], so we proposed that cells from the tumor core might escape glutamine deprivation-driven apoptosis by migrating to the nutrient-rich surrounding tissues.

Normally, cell migration and invasion are evaluated *in vitro* by challenging cell cultures with a gradient of FBS, which is sometimes combined with the stimulation by other signaling molecules. In contrast, we generated glutamine-concentration gradients that mimic those inside a tumor by two methods: transwell insert-based assays and chemotaxis µ-slides. Transwell assays allowed the quantification of cell migration and invasion, as well as the study of cell morphology in paraffin-embedded samples from matrices containing invading cells; moreover, it was a useful strategy to assess migration and invasion of a co-culture of different cell types, a matter that will be further discussed below. Using chemotaxis µ-slides we tracked the course of single cells and we analyzed their morphological and molecular features during migration. Measuring glutamine concentration at different time points in both devices, we determined that the stability of the gradient was maintained for more than 12 hours in chemotaxis µ-slides. However, the differences in glutamine concentration in the upper and lower parts of Boyden chambers were only maintained for 6 hours.

While previous studies highlighted the connection between glutamine metabolism and invasive tumor phenotypes[241,216], the direct influence of extracellular glutamine levels in tumor invasion had never been explored before. Here we describe that glutamine dependence in CAFs promotes their migration and invasion following a glutamine gradient. This acquired motility is modulated by the activation of fibroblasts upon TGF-β stimulation, since no significant differences were detected in the migration of non-activated fibroblasts in high glutamine or gradient

conditions. Consistent with the previous investigations in our group, which remark the need for Snail1 expression in TGF-β-driven activation of fibroblasts and its importance during invasion and metastasis[139,150], we observed that Snail1-depleted fibroblasts failed to migrate in the direction of the gradient. We extended our observations to other mesenchymal cells (BTE-136, MSCs and MEFs), all of them dependent on glutamine metabolism. In contrast, none of the analyzed epithelial tumor cells, that do not rely on glutamine for their survival, migrated towards this amino acid.

We addressed the causes of glutamine-driven migration and invasion considering two possibilities: first, that fibroblast motility was stimulated by glutamine gradients; and last, that cells were attracted by glutamine towards one single direction. As determined by time-lapse microscopy, TGF-β-stimulated MSCs were almost equally motile in a glutamine-high culture or when challenged with a gradient, being the speed of MSCs migration slightly higher in the second case. The main difference between the two conditions was the directionality of the movement, which was either guided towards the glutamine gradient or random in its absence. These findings were confirmed in longitudinal sections of paraffin-embedded samples of invading CAFs, in which cells were plated between two matrix layers and their invasion was stimulated with glutamine. Again, glutamine-enriched medium enhanced cell invasion in any direction, whereas glutamine gradient directed all the cell tracks towards the high glutamine compartment.

In addition, we demonstrated the specificity of glutamine in the direction of fibroblast invasion by exposing CAFs to glucose and lactate gradients, which did not induce any changes in cell invasiveness. However, there are many studies that correlate the influence of glucose availability in tumor cell invasion and aggressiveness[242–245]. It should be noted that most of this research has been done by the use of 1.0 g/l to 4.5 g/l glucose gradients, which correspond to normal and supra-physiological glucose levels and do not recapitulate metabolic stress in tumors.

3. FIBROBLASTS COOPERATE WITH EPITHELIAL TUMOR CELLS IN GLUTAMINE-STIMULATED INVASION

A growing body of research has examined the influence of CAFs in EMT-independent collective tumor cell invasion, which they mediate by ECM remodeling, heterotypic cell contacts and the secretion of signaling molecules[138–140,154]. Since many of these studies include FBS-stimulated invasion experiments, we addressed the effect of glutamine-driven fibroblast invasion on glutamine-insensitive tumor cells.

We showed that co-culture with fibroblasts promotes invasion of epithelial tumor cells in a glutamine gradient. These results were obtained in colorectal (HT-29M6 and SW-480) and breast (AT-3 and T-47D) tumor cell lines, in their co-culture with either MSCs or CAFs. This effect was not shared by all the tumor cell types, since other cell lines (MCF-7 and HCT116) exhibited fibroblast-stimulated enhanced invasion independently of glutamine levels. We suggest that these cells might have a differential sensitivity to signals derived from CAFs in either high and low glutamine, that would stimulate their invasion in both conditions.

In line with our previous results, tumor cell invasion was blocked by TGF-β receptor inhibition and by Snail1 depletion in our system, indicating that Snail1 expression in fibroblasts is required for induction of collective tumor cell invasion upon glutamine stimulation. Reciprocally, co-culture with HT-29M6 stimulated the invasion of MSCs, which was also conditioned by Snail1-dependent activation of these cells. Although these experiments were not repeated in the current study, in 2016 we determined that TGF-β is produced mainly by the tumor cells in their co-culture with fibroblasts[139]. Therefore, we propose that HT-29M6 cells stimulate Snail1-dependent fibroblast activation by the secretion of TGF-β, a mechanism that is shared in both in FBS and glutamine-driven invasion assays.

Based on the depletion of Snail1 in epithelial cells, we concluded that Snail1 expression in these cells does not contribute to their invasion in

a co-culture with fibroblasts. Concomitantly, glutamine deprivation did not alter the expression of EMT-TFs in cancer cells and, in fact, E-cadherin expression was not altered upon invasion. These results suggest that fibroblasts facilitate tumor invasion without significant EMT-associated changes. Nevertheless, this conclusion does not mean that EMT is irrelevant in glutamine-driven invasion, as we showed that the invasion of Snail1-expressing BTE-136 cells is enhanced without the co-culture with fibroblasts. Hence, Snail1 expression is either required in tumor cells or in fibroblasts for glutamine-dependent tumor cell invasion.

In our latest publication, we demonstrated that TGF-β triggers a Snail1-dependent transcriptional program in fibroblasts that modulates epithelial invasion in different ways[139]. On one hand, it facilitates ECM degradation by the secretion of several MMPs; on the other, it promotes cell migration through the secretion of signaling factors. The most relevant molecule found in this study was PGE_2, as its inhibition completely abrogated the effect of fibroblasts on tumor cell invasion[139]. Surprisingly, PGE_2 did not mediate collective invasion in a glutamine gradient, although its secretion was equally enhanced in FBS and in glutamine conditions.

Conditioned medium from activated fibroblasts enhanced migration but not invasion of tumor cells upon glutamine gradient stimulation; accordingly, HT-29M6 were not capable of generating tracks into the matrix in glutamine-driven organotypic assays. Taken together, these results indicate that, upon glutamine stimulation, CAFs orchestrate tumor cell invasion by physically remodeling ECM, but they also direct their migration by the secretion of soluble molecules that work as chemo-attractants. In fact, some candidates from microarray data of Snail1-dependent TGF-β gene signature in MSCs, including PDGF, FGF and several chemokines, will be evaluated in the future[139]. We also considered the possibility that fibroblasts enhanced tumor cell invasion by the export of glutamine-derived intermediates, since some authors reported that high levels of glutamine consumption contribute to tumor cell invasiveness by generating an extracellular source of glutamate[216].

However, glutamate did not change the outcome of our *in vitro* migration experiments, as its addition to the lower compartment of Boyden chambers did not promote HT-29M6 migration.

4. SNAIL1-DEPENDENT FIBROBLAST ACTIVATION IS IMPAIRED UPON GLUTAMINE DEPRIVATION

Long term amino acid deficiencies result in a decrease of protein synthesis. This process is tightly regulated by mTORC1, since this kinase complex is activated in response to amino acid availability[246,247] and promotes mRNA translation by the phosphorylation of the ribosomal protein S6 and other downstream effectors[177]. According to this well-described mechanism, we observed lower levels of phospho-S6 upon glutamine deprivation. In TGF-β stimulated CAFs, this effect was translated into a decrease in those activation marks that require *de novo* protein synthesis, including Snail1, S100A4 and fibronectin, upon the depletion of this amino acid. Therefore, we concluded that fibroblast activation is impaired upon glutamine deprivation.

In contrast, we did not observe changes in Smad2 phosphorylation in high or low glutamine, thus evidencing that lack of this amino acid hinders *de novo* protein synthesis but does not affect rapid molecular changes such as phosphorylation. Accordingly, gene transcription of activation markers induced by TGF-β remained mostly unaffected by the depletion, which only impaired the expression of those late markers that depend on Snail1 up-regulation. As an exception, the expression of the deubiquitinating enzyme USP27X, which is induced after a short-time TGF-β stimulation, was down-regulated at mRNA level upon glutamine deprivation. For its function in the stabilization of Snail1 protein, Snail1 decay is enhanced in this condition; a phenomenon that might be related to amino acid deprivation-induced autophagy and the recycle of cytosolic materials that are not required to maintain the basic cell functions[248]. In line with our observations with USP27X, glutamine deprivation has been associated to an increased expression of several Snail1-targeting miRNAs in tumor cells[240], implying that Snail1 stability is regulated positively by glutamine metabolism.

5. GLUTAMINE STIMULATES FIBROBLAST MIGRATION ASYMMETRICALLY LOCALIZING AKT2

Akt functions are not only important during the EMT but are required for Snail1 dependent activation of fibroblasts, since these two factors are co-regulated in response to TGF-β[47,150]. Importantly, Akt also mediates cell motility through its many cytoskeletal targets, such as fibrillar actin (F-actin) and vimentin[221]. Here, we report a differential distribution of Ak2 in the migration front of glutamine-sensitive cell types, which was determined by immunofluorescence analysis of mesenchymal cells that had been exposed to glutamine gradients. Concretely, we showed a different distribution of Akt1 and Akt2 in activated fibroblasts: although both proteins were localized mostly in the cytoplasm, only Akt2 was polarized at the leading edge of migrating cells. Interestingly, other authors observed the accumulation of phospho-Akt at the leading edge of postnatal motile cells, where it mediates cell migration by the regulation of cytoskeletal reorganization, front-rear polarity and contractility[221]. Based on this study, we expect that Akt2 co-localizes with some cytoskeletal components in our system and a detailed analysis of this interaction will be performed in the future.

Correspondingly, Akt2 depletion in MEFs completely abrogated their migration capability, highlighting the importance of Akt2 in glutamine-stimulated migration. We considered the possibility that these cells were unable to activate, since Akt inhibition blocks the action of Snail1 in the activation and differentiation of MSCs[150]. When we analyzed the activation of Akt2-depleted MEFs in response to TGF-β we observed that, although slightly reduced, there still was an evident up-regulation of Snail1 expression and Smad2 phosphorylation. In addition, restricting the expression of Akt2 in the nucleus of MEFs, by the transfection of an Akt2 vector lacking its plekstrin homology domain, did not rescue their migration upon a glutamine gradient. Therefore, the differences in migration of Akt2-depleted MEFs are most likely attributed to the role of Akt in the cytoskeleton.

The PI3K/Akt pathway is one of the most frequently mutated signaling

pathways in cancer, as it is involved in the regulation of many functions including cell proliferation, survival and invasion[249]. The relation between Akt2 and tumor invasion has been supported by many publications, which report the role of this protein in the invasion of tumor cells and fibroblasts[250–253]. Conversely, other authors observed that Akt1 but not Akt2 promoted invasion of these cell types [222,254]; implying that Akt-dependent regulation of cell motility might be subject to cell class and specific conditions. In our study, Akt1 depletion in MEFs did not affect their activation, migration nor the enhancement of tumor cell invasion upon glutamine gradient stimulation; thus, validating the specificity of Akt2 in promoting activated fibroblast invasiveness through its asymmetrical distribution.

6. TRAF6 MEDIATES THE GLUTAMINE-DEPENDENT UBIQUITINATION AND POLARIZATION OF AKT2

We demonstrated that Akt2 polarization is regulated by TRAF6, which co-localizes with Akt2 in the cytoplasm of activated fibroblasts upon glutamine stimulation and exhibits an equal asymmetrical distribution. This E3 ubiquitin ligase promotes the cytoplasmatic localization of Akt by its Lys63-linked polyubiquitination[66]. While localized in this cellular compartment, Akt is susceptible to the interaction with other protein kinases, as PDK1 and mTORC2, that activate Akt through its phosphorylation[255]; accordingly, TRAF6 down-modulation in CAFs correlates with a decrease in the basal levels of Akt phosphorylation (see **Fig. R39**).

In addition, TRAF6 interacts with TGFbR and ubiquitinates some downstream effectors of the non-canonical TGF-β pathways[63–65]. In tumor cells, it also contributes to the expression of a pro-invasive gene signature by the ubiquitination of TGFbRI, which is translocated to the nucleus upon its cleavage and modulates the expression of EMT-related genes[256,257]. However, the activation of fibroblasts upon TGF-β stimulation is independent of TRAF6, since the down-modulation of this ubiquitin ligase did not alter the expression of activation markers in these cells.

Other authors demonstrated that TRAF6 ubiquitinates PI3K, promoting its activation upon TGF-β stimulation[65,258]. Although these observations suggest that TRAF6 might contribute to Akt activation indirectly, we reported a decrease in Akt2 ubiquitination upon TRAF6 down-modulation in CAFs. In turn, Akt2 ubiquitination was increased upon TGF-β treatment, implying that fibroblast activation might promote the activity of TRAF6 on Akt2. Based on these results and our co-localization studies, we propose that TRAF6 directly interacts with Akt2. Nonetheless, more experiments need to be performed to fully define this association. For instance, it would be interesting to determine the interactions of TGFbR, TRAF6 and Akt2 by co-immunoprecipitation experiments.

The main criticism of the Ni-NTA pull-down experiments is the impossibility to discriminate Lys63-linked ubiquitination from other types of ubiquitination. Nevertheless, as we performed these experiments without the addition of the proteasome inhibitor MG132, we assume that we are observing a non-degradative ubiquitination that might be the one associated to Lys63. To further discard degradation-related ubiquitination, we could to address Akt2 ubiquitination using Lys63 specific mutants instead of histidine-tagged ubiquitin.

Importantly, we showed that Akt2 ubiquitination depends on glutamine availability in activated fibroblasts, since higher levels of ubiquitinated Akt2 were observed in high glutamine when compared to low glutamine cultures. As already discussed, the ubiquitination of Akt2 in high glutamine is also modulated by TRAF6. However, the mechanisms by which glutamine stimulate TRAF6 activity are still unknown. Notably, TRAF6 associates with p62 in the membrane of the lysosomes and mediates mTORC1 activation through its ubiquitination in response to amino acid availability[179]. This effect is triggered by the phosphorylation of p62 upon amino acid stimulation, which is mediated by the p38δ MAPK through MEKK3/MEK3/6 signaling cascade[247]. When activated, p62 is responsible for the recruitment of mTORC1 and TRAF6 in the lysosomal surface by its interaction with the family of Rag proteins[179,246]. These studies underlined the importance of the p62/TRAF6 complex in

the cellular response to amino acid sensing; therefore, it might be interesting to address if the glutamine-dependent activation of TRAF6 and its downstream effect on Akt2 localization are also mediated by p62.

In contrast to mTORC1, other authors have demonstrated that mTORC2 activity is enhanced upon a short-time glutamine starvation as a mechanism to restore metabolic homeostasis through the modulation of the hexosamine biosynthesis pathway[259]. In the same study, they observed an increase in Akt phosphorylation following acute glutamine withdrawals, but a decrease of Akt phosphorylation when glutamine deprivation was maintained for longer times. We did not analyze the role of mTORC2 in our model, yet we think that the effect of glutamine in the migration of fibroblasts is mainly driven by TRAF6. In this regard, we showed that TRAF6 down-modulation in CAFs abrogated their migration in a glutamine gradient; accordingly, Akt2 polarization was reduced by the loss of TRAF6 in these cells. With these results, we propose that TRAF6 is accumulated in the side of the cell that is in contact with increasing concentrations of glutamine, thus determining the distribution of Akt2 in the same part of the cell.

7. MODEL SUMMARY

Based on all the data discussed above, we propose a physiological *in vitro* model of cancer invasion. Our findings clarify the effect of intra-tumoral glutamine deficiency in tumor invasion, since a gradient of glutamine influences the directionality of the migration of mesenchymal tumor cells and activated fibroblasts. We have determined that these cell types present a high sensitivity to glutamine deprivation, which might be related to the role of glutamine in the synthesis of other amino acids. When challenged with a gradient of glutamine, fibroblasts present an asymmetrical distribution of Akt2 that is modulated by the E3 ubiquitin ligase TRAF6. TRAF6 activity on Akt2 is enhanced by TGF-β stimulation only when glutamine is available. In a glutamine gradient, the cells of the migration front are exposed to increasing concentrations of glutamine. In consequence, TRAF6 is accumulated in the leading edge of these cells and mediates the Lys63-linked ubiquitination of Akt2. This modification promotes a cytoplasmatic localization of Akt2 and increases its kinase activity[66]; accordingly, TRAF6 is responsible for the asymmetrical distribution of Akt2 in this compartment in response to glutamine. Although it was not addressed in this study, the downstream effect of Akt2 polarization in fibroblast migration might be related to its interaction with cytoskeletal proteins, since Akt is an important mediator of cytoskeletal reorganization and cell contractility[221]. Importantly, tumor-derived TGF-β stimulates Snail1-dependent activation of fibroblasts and enhances their migration towards glutamine. This effect drives the collective invasion of fibroblasts and epithelial tumor cells, yet the mechanisms of this cooperation remain to be elucidated. A graphic representation of our proposed model is summarized in **Fig. D1.**

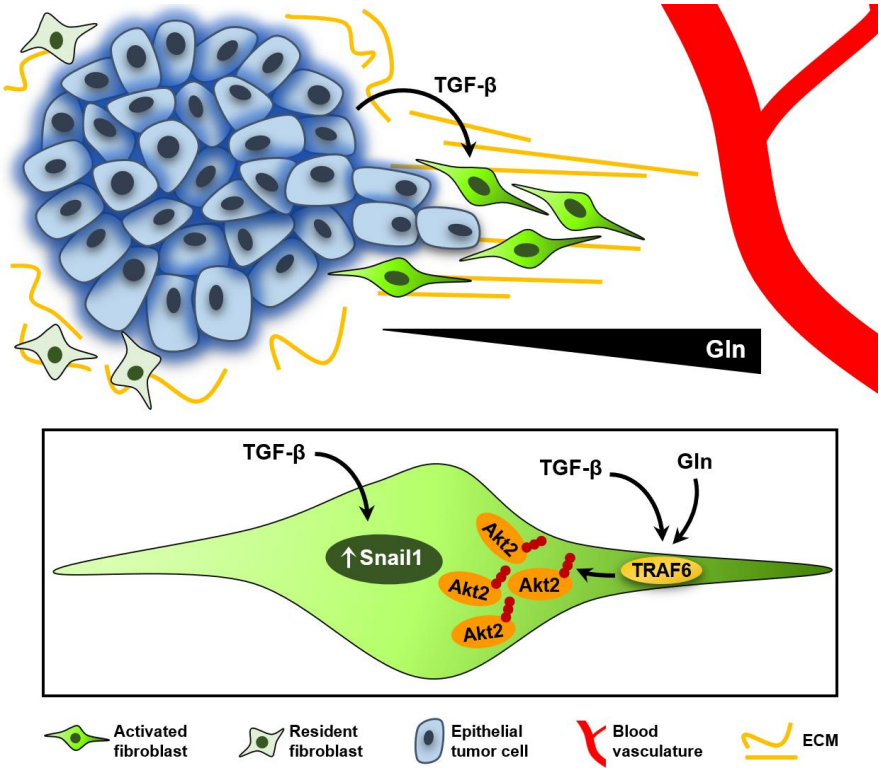

Figure D1. Intra-tumor glutamine deficiency facilitates tumor invasion by promoting cancer-associated fibroblast migration. Glutamine dependence in CAFs promotes their migration towards a gradient of glutamine (Gln), which is generated by the decrease of glutamine in the core of tumors in contrast with the glutamine availability of the surrounding tissues. The secretion of TGF-β by tumor cells is required for Snail1-dependent fibroblast activation and for the collective invasion of both cell types. In the leading edge of migrating cells, TRAF6 is activated in response to the increasing concentration of glutamine and TGF-β stimulation. TRAF6 mediates the Lys63-linked polyubiquitination of Akt2; consequently, Akt2 is accumulated in this part of the cell and mediates the migration of fibroblasts towards glutamine.

CONCLUSIONS

1. Cancer associated fibroblasts (CAFs) and other mesenchymal cells types exhibit a higher glutamine requirement than epithelial tumor cells.

2. Glutamine dependence in CAFs promotes their migration and invasion following a gradient of glutamine.

3. Glutamine-driven migration of CAFs requires TGF-β stimulation and their consequent Snail1-dependent activation.

4. Fibroblasts support the collective invasion of epithelial tumor cells towards a glutamine gradient.

5. Fibroblasts orchestrate tumor cell invasion by ECM degradation and the secretion of signaling molecules. Nevertheless, CAF-derived PGE_2 is not responsible for tumor cell invasion upon glutamine stimulation.

6. The effect of glutamine in the migration of CAFs is associated to an asymmetrical distribution of Akt2 in the leading edge of activated fibroblasts.

7. TRAF6 mediates Akt2 ubiquitination response to TGF-β and glutamine availability and promotes its polarization upon glutamine stimulation.

MATERIALS AND METHODS

1. CELL CULTURE

All cell lines were maintained at 37ºC in a humid atmosphere, containing 5% CO_2. Cells were grown in DMEM supplemented with 4.5 g/l glucose (Invitrogen), 1 mM sodium pyruvate, 2 mM glutamine, 100 IU/ml penicillin, 100 mg/l streptomycin, and 10% FBS (all from GIBCO). All the experiments were performed on cells incubated for at least 24 hours in DMEM 0.1 or 1 g/l glucose (GIBCO), and supplemented with 1 mM sodium pyruvate, 0.2 mM or 2 mM glutamine, 100 IU/mL penicillin, 100 mg/l streptomycin, and 0.5% FBS. When indicated, 1 mM glutamate (G5889, Sigma-Aldrich) or 20 mM L-lactate (71718, Sigma-Aldrich) were added to the culture medium.

NEAA-depleted Minimum Essential Medium (MEM) was produced by the addition of 1 mM sodium pyruvate, 2 mM glutamine, 100 IU/mL penicillin, 100 mg/l streptomycin, 0.5% FBS, 10 mM HEPES (Sigma-Aldrich), 1X MEM vitamin solution, 1X MEM Essential amino acid solution and either 1X (high) or 0.1X (low) MEM NEAA solution (all from Thermo Scientific) into Earle's balanced salt solution (EBSS) (Gibco).

1.1. Cell lines

The human colorectal HT-29M6, HTC116, SW-480 and SW-620, and the breast MCF-7, MDA-MB-231, SK-BR-3 and T-47D cancer cell lines were acquired from the cell line repository of Institut Hospital del Mar d'Investigacions Mèdiques (IMIM). The generation of HT-29M6 Snail1-KO using CRISPR-Cas9 technology has been previously reported[139]. AT-3 cells[260] were a gift from Dr. J. Yélamos (IMIM, Barcelona). BTE-136 cells were kindly provided by Dr. M. Quintela (Centro Nacional de Investigaciones Cardiovasculares, Madrid). Both cell lines were isolated from spontaneous luminal B breast tumors of MMTV-PyMT mice, bearing a polyomavirus middle T oncogene that is expressed under control of the mammary MMTV promoter[219]. CAFs and MSC were established in our laboratory from MMTV-PyMT-derived tumors and bone marrow of Snail1$^{Flox/-}$ mice, respectively. Snail1 depletion in these two cell types was obtained by their infection with a retroviral vector

encoding a Cre recombinase (pMX-Cre)[139,150]; an empty pBabe vector was used as a control. TRAF6-KD CAFs were generated by infection with two different shRNA lentiviral vectors (see **section 2.2**). BJ fibroblasts were a kind gift from Dr. C. Peña (Hospital Puerta de Hierro, Majadahonda). MEFs, either control, Akt1 and Akt2 KO were obtained from Dr. M. J. Birnbaum[222] (University of Pennsylvania, Philadelphia).

In order track cell invasion upon co-culture experiments, many of these cell lines were labeled with fluorescent proteins. HT-29M6 cells were stably infected with pDsRed and maintained in 10 µg/ml G418 (Merk). As specified in **section 2.1**, AT-3, HCT116, T-47D, SW-480 and HT-29M6 Snail-KO cell lines were infected with pMSCV-tomato; GFP-expressing MCF-7, MSC WT and MSC Snail1-KO were also generated. HEK-293T, HEK-293 Phoenix and Plat-E cells from the cell repository in our institution were used for viral production.

1.2. Specific cell treatments

When indicated, culture medium was supplemented with the reagents listed in **Table M1**.

Table M1. Cell culture treatments

Treatment	Concentration
CB-839 (22038, Cayman Chemical Company)	0.1 nM – 1 mM
GM6001 (cc1010, Merk)	25 µM
G418 (345810, Merk)	10 µg/ml
L-161-982 (SML-0690, Sigma-Aldrich)	10 µM
PGE_2 (14010, Cayman Chemical Company)	100 nM
Puromycin (P8833, Sigma-Aldrich)	2 µg/ml
SB505125 (S4696, Sigma-Aldrich)	5 µM
TGF-β1 (100-21, PeproTec)	5 ng/ml

1.3. Conditioned media preparation

HT-29M6, MSCs and CAFs were seeded in 6 well plates in complete growth medium. When cell confluence reached 50-60%, cells were washed twice with phosphate buffer saline (PBS) and culture medium was replaced with DMEM 1g/l glucose, 1 mM sodium pyruvate, 2 mM glutamine, 0.5% FBS at a final volume of 2.5 ml/well. CAFs and MSCs were stimulated with TGF-β for 24 hours. After this time, conditioned media were collected and cell debris was eliminated by the use of 0.45 µm sterile filters (Millipore). Prior to migration and invasion experiments, conditioned media was mixed with fresh DMEM 1g/l glucose, 0.5% FBS at a volume ratio of 4:1. Glutamine was then added at a final concentration of 2 mM. 500 µl of conditioned media were used to fill the lower compartment of Boyden chambers.

2. VIRAL INFECTION

2.1. Retroviral infection

For the infection of human cell lines, viral particles were produced in HEK-293 Phoenix cells, which stably express the HIV-1 *gag* and *pol* viral genes[261]. These cells were plated at 70% confluence and transfected with the indicated plasmids (pMSCV-tomato or pBabeGFP) as well as an adjuvant vector (pCMV-VSV-G) using Lipofectamine Plus reagent (Invitrogen), according to the manufacturer's instructions. Medium from the transfected cells was collected after 24 and 48 hours post-transfection and filtered through a 0.45 µm filter (Millipore). These supernatants were mixed in a 3:1 volume ratio with Retro-X Concentrator (Clontech) and incubated for 24 hours at 4ºC. Viral particles were then pelleted by centrifugation (1,000 x g, 45 minutes) and resuspended in 1ml DMEM, which was aliquoted and stored at -20ºC until use. Subsequently, tumor cells were grown at a 40% confluence and infected with 100 µl of the viral concentrate. After 24 hours, medium was refreshed and the infected cells were selected with 2 µg/ml puromycin (Sigma-Aldrich) for 48 hours. Tomato and GFP-positive cells were further selected by cell sorting.

MSCs were infected with a pBabeGFP vector by the same procedure. In this case, viruses were obtained by the use of Plat-E cells, which stably express the virus structural genes[262]. Since they were generated by retroviral infection with a pMX-Cre vector, MSCs Snail1-KO were already resistant to puromycin; therefore, they were only selected by cell sorting.

2.2. Lentiviral infection

The infection procedure with lentiviral vectors is similar to that of retroviruses. This technique was used to stably down-modulate the expression of TRAF6 in CAFs. The next MISSION® shRNA plasmids (Sigma-Aldrich) were transfected in HEK-293T cells to produce lentiviral particles: non-mammalian shRNA (used as control) SHC002; TRAF6#1 TRCN0000040735; and TRAF6#2 TRCN0000040736.

HEK-239T cells were grown in p100 plates until 90% confluence was reached and transfected with a total amount of 10 µg DNA; 50% of which was the plasmid of interest and the other 50% were those vectors required for lentiviral production (1 µg pCMV-VSV-G, 1 µg pRSV and 3 µg pMDLg/pRRE). Viral particles were purified by Lenti-X Concentrator (Clontech), by the same procedure described for the concentration of retroviruses (see **section 2.1**). CAFs seeded to 40% confluence were infected with the lentiviral concentrates for 24 hours, followed by 2 days of selection with 2 µg/ml puromycin.

3. TRANSIENT AKT2 OVEREXPRESSION

In order to rescue the expression of Akt2 in MEFs Akt2 KO, these cells were transfected with a pCDNA3-HA vector containing the full-length form of Akt2 (Akt2-FL) or a shorter form lacking the plekstrin homology domain (Akt2-ΔPH). For migration assays, MEFs WT were transfected with an empty pEGFP1Ø, which was also used in MEFs Akt2 KO to evaluate the efficiency of the transfection by visualization of GFP positive cells. MEFs WT and Akt2 KO were grown to a 70% confluence and their transfection was performed using Lipofectamine2000

(Invitrogen), following the manufacturers' instructions. Vectors were transfected at a final concentration of 8 µg/plate for pCDNA3-HA vectors and 2 µg/plate of pEGFP1Ø. Migration and invasion experiments were performed 48 hours after the transfection.

4. VIABILITY ASSAYS

4.1. Sensitivity to glucose and glutamine deprivation

The viability of all the aforementioned tumor and fibroblastic cell lines in glucose and glutamine-depleted cultures was determined by crystal violet staining. 50,000 tumor cells/well and 10,000 fibroblasts/well were seeded in 24 multi-well plates in complete growth medium and incubated for 24 hours to enable cell adhesion. Cells were then washed with PBS twice and culture medium was replaced for DMEM 1 mM sodium pyruvate, 0.5% FBS, with either high (1 g/l) or low (0.1 g/l) glucose and high (2 mM) or low (0.2 mM) glutamine supplementation. Cell viability was assessed after 48 hours post-deprivation by crystal violet staining. Cells were washed with PBS and incubated with a 0.5 g/l crystal violet (Sigma-Aldrich), 20% methanol solution on an orbital shaker at room temperature for 30 minutes. Plates were rinsed with tap water until the excess of crystal violet was removed and air-dried. Crystal violet was eluted in 200 µl/well of 30% acetic acid, followed by 1 hour of incubation at room temperature on an orbital shaker. Samples were transferred to a 96 well plate and their optical density was measured at 570 nm in an Infinite 200 microplate reader (Tecan). Cell viability was evaluated as the absorbance in low glucose or glutamine normalized to its culture in high glucose/glutamine. All the analyses were performed in triplicate.

The sensitivity of CAFs and HT-29M6 cells to glutamine deprivation was further evaluated by the same procedure. In this case, cells were cultured in DMEM 1g/l glucose, 1 mM sodium pyruvate, 0.5% FBS supplemented with 2 mM, 1 mM, 0.5 mM 0.2 mM or 0 mM glutamine. Cell viability was analyzed after 24 and 48 hours of glutamine deprivation and referred to the absorbance at the initial time point.

4.2. Sensitivity to GLS1 inhibition

10,000 CAFs, 50,000 HT-29M6, 30,000 AT-3 and 30,000 BTE-136 cells were seeded in 24 multi-well plates. After 24 hours, complete culture media was changed for DMEM 1g/l glucose, 1 mM pyruvate, 2 mM glutamine, 0.5% FBS and. Cells were treated with increasing doses of CB-839 (1 nM, 10 nM, 100 nM and 1 mM; Cayman chemical company) or dimethyl sulfoxide (DMSO) for 48 hours. Cell viability was then determined by crystal violet staining as described in **section 4.1**. and normalized to the corresponding concentration of DMSO. The relative half-maximal inhibitory response (IC_{50}) of CB-839 was calculated for each cell line by non-linear curve fits using Graphpad software.

4.3.Rescue of glutamine sensitivity in CAFs

CAFs were seeded in 24 multi-well plates (10,000 cells/well). After 24 hours, cells were washed with PBS and medium was changed for DMEM 1g/l glucose, 1 mM pyruvate, 0.5% FBS and either high (2 mM) or low (0.2 mM) glutamine. When specified, CAFs were treated with 25.3 nM CB-839 and supplemented with 4.5 g/l glucose, 1 mM glutamate or 20 mM lactate. Cell viability was determined after 48 hours by crystal violet staining and normalized to high glutamine condition.

5. DETERMINATION OF GLUTAMINE CONSUMPTION

Glutamine concentration was measured in media samples of AT-3, BTE-136, HT-29M6, CAFs and MSCs cultures. These cells were seeded in 24 multi-well plates and incubated for 24 hours in DMEM 1g/l glucose, 1 mM pyruvate, 2 mM glutamine, 0.5% FBS. Simultaneously, the same culture medium was incubated without cells. Glutamine concentration was determined in media samples of these cell types by a Glutamine Colorimetric Assay Kit (K556, BioVision). Glutamine consumption rates were extrapolated from the difference in concentration between culture media from empty wells and media from the different cell lines and normalized to cell number and time (minutes) of culture.

The same method was used to determine glutamine concentration in the different compartments of Boyden chambers and chemotaxis µ-slides at different time points.

6. MIGRATION AND INVASION ASSAYS

6.1. Transwell-based migration and invasion assays

100,000 tumor cells or 20,000 fibroblasts were seeded on transwells (3422, Costar) in 150 µl DMEM 1g/l glucose, 0.5% FBS and either 2 mM (high) or 0.2 mM (low) glutamine. In co-culture experiments, DsRed or tomato-labelled epithelial cells and GFP-labelled fibroblasts were mixed, pelleted, and resuspended in 150 µl of high or low glutamine media before seeding. For invasion experiments, transwells were coated with 50 µl of Matrigel (0.5 µg/µl; 354230, Corning) and polymerized at 37ºC for 1 hour before cell seeding. After 4 hours at 37ºC, lower chambers were filled with DMEM 1 g/l glucose, 0.5% FBS, high glutamine. When indicated, treatments were added to the upper compartment except for PGE_2, which was added to the lower chamber. Migration and invasion of fibroblasts were analyzed after 12 hours of gradient stimulation. Alternatively, tumor cell invasion was determined at 48 hours. Both the lower and upper part of the membrane were washed once with PBS, incubated with 4% paraformaldehyde (PFA) at room temperature for 20 minutes and washed again. All the cells in the upper compartment were removed using a cotton swab and membranes were stained with PBS-DAPI (25 µg/ml) for 10 minutes. Membranes were then extracted and mounted in microscope slides with Fluoromount G (Southern Biotech) and coverslips. Invaded cells were photographed with a Nikon Eclipse Ni-E microscope and the cell number and area of invading cells were quantified by the use of ImageJ software. Migration/invasion of all the analyzed conditions was referred to that without gradient stimulation nor treatment.

6.2.IBIDI chemotaxis µ-slides

Cells were seeded in DMEM 1g/l glucose, 0.5% FBS, 2 mM (high) or 0.2 mM (low) glutamine at a final density of 3-5·10^6 cells/ml in the central compartment of chemotaxis µ-slides (80326, IBIDI), according to manufacturer's instructions. After overnight cell adhesion, the two adjacent reservoirs were filled with DMEM either high or low glutamine and glutamine gradients were generated by the addition of 30 µl of DMEM 4 mM glutamine in one of the low glutamine reservoirs. TGF-β was added to all the compartments of the device when specified. Right after generating the gradient, cell migration was recorded by life cell imaging in a Zeiss cell observer microscope, which took pictures in different random areas every 5 minutes for 12 hours. Single-cell coordinates at each time point were tracked by the ImageJ ManualTracking plugin. The average speed of migration was calculated as the ratio of distance migrated (µm) per minute.

Alternatively, slides were fixed with 4% PFA and analyzed by immunofluorescence (IF) after 6 hours of migration. In order to maintain the integrity of the culture, all the following reagents were introduced to the device by the two lateral reservoirs. All the procedure was performed at room temperature. Cells were permeabilized with a 0.1% Triton X-100-PBS solution for 15 minutes. Following two PBS washes of 10 minutes each, samples were blocked with 3% bovine serum albumin (BSA) -PBS for 2 hours and incubated with primary antibodies (listed in **Table M2**) for 1 hour and a half. Slides were washed with PBS twice and incubated with fluorescent secondary antibodies (Alexa 488 and 555-conjugated anti-rabbit or mouse IgGs; Thermo Scientific) for 1 hour. After two more PBS washes, samples were stained with DAPI (25 µg/ml) for 15 minutes and mounted with Fluoromount G (Southern Biotech). Random pictures of the migration front were taken in a Leica TCS-SP5 confocal microscope.

Table M2. Primary antibodies used for immunofluorescence

Antibody	Host	Dilution
Akt (#9272, Cell Signaling)	Rb	1:200
Akt1 (#2938, Cell Signaling)	Rb	1:200
Akt2 (#3063, Cell Signaling)	Rb	1:200
mTOR (#2972)	Rb	1:100
TRAF6 (HPA019805, Sigma-Aldrich)	Rb	1:100
TRAF6 (sc-8409, Santa Cruz)	Ms	1:50

Rb, Rabbit; Ms, Mouse

6.3. Organotypic invasion assays

In this case, transwell inserts were coated with 50 µl of a dense matrix composed by 3 µg/µl Matrigel (354230, Corning) and 2 µg/µl collagen I (354249, Corning) and polymerized at 37ºC for 1 hour. 50,000 CAFs, 100,000 HT-29M6 or a co-culture of both cell types (100,000 HT-29M6 and 20,000 CAFs) were seeded on top. Upon cell adhesion, culture media was removed and cells were covered with 50 µl of the same matrix. Following matrix polymerization, media was added to the upper and lower compartments and invasion was assessed in high glutamine (both compartments filled with DMEM 1g/l glucose, 0.5% FBS, 2 mM glutamine) or glutamine gradient (DMEM 1 g/l glucose, 0.5% FBS, 0.2 mM glutamine in the upper compartment and 2 mM glutamine in the bottom). Additionally, TGF-β was added in both compartments of CAFs culture. Media and TGF-β treatment were refreshed every 24 hours. After 3 days, cultures were fixed with 4% PFA and processed by standard methods for histological analysis. Matrices were transversely mounted into paraffin blocks and processed as indicated in **chapter 7**.

7. ANALYSIS OF INVASION SECTIONS

Paraffin-embedded matrices of organotypic invasion experiments were sliced in 3 µm thick longitudinal sections and transferred to Superfrost™ Plus slides (Thermo Scientific). Upon their use, samples were deparaffined for 1 hour at 65ºC and rehydrated in a battery of xylene (twice for 10 minutes), decreasing ethanol concentrations (5 minutes in each of the following solutions; 100%, 90%, 70% and 50% ethanol) and distilled water. Samples were then processed by HE staining or by IHC.

7.1. Hematoxylin & eosin

Previously rehydrated slides were stained with a 30% hematoxylin solution for 3 minutes and rinsed with tap water and distilled water. Then, they were sequentially submerged in the following battery of solutions: 1) ammoniacal water, 2) distilled water, 3) 0.01% HCl, 4) distilled water (all in and out), 5) 5 minutes in 96% ethanol, 6) 1 minute in eosin, 7) absolute ethanol (three washes), 8) 10 minutes in xylene (twice). Finally, slides were mounted with DPX and coverslips.

7.2.Immunohistochemistry

After sample deparaffination and rehydration, antigen retrieval was performed with citrate buffer at 120ºC for 15 minutes in a pressure cooker. The activity of endogenous peroxidases was quenched with 3% H_2O_2 (Dako) for 10 minutes. Following three TBS-T washes, samples were blocked with 1% FBS/BSA TBS solution for 1 hour at room temperature. E-cadherin (610182, BD Transduction Laboratories) and S100A4 (136784, Millipore) antibodies were diluted in a 1:200 ratio in 1% FBS/BSA and were incubated with the samples at 4ºC overnight. Samples were washed three times with TBS-T and incubated with secondary antibodies (Leica Powervision Poly-horseradish peroxidase (HRP) system, Dako) at room temperature for 30 minutes. After three more TBS-T washes, slides were developed using 3,3'-diaminobenzidine (DAB; Dako) as chromogenic substrate. The reaction was stopped with distilled water and hematoxylin staining were

performed. Samples were mounted with DPX after their dehydration in a battery of increasing concentrations of ethanol (from 50% to absolute) and xylene.

8. PROTEIN ANALYSIS

8.1. Protein extraction

In order to obtain total protein extracts, cells were washed with cold PBS and were scraped off the dish in SDS lysis buffer. Cell lysates were syringed 5 times and boiled at 95ºC for 5 minutes, or until the extracts were completely homogeneous. Protein concentration was determined by the Lowry method (DC protein Assay kit, Bio-Rad).

8.2. Western blot analysis

SDS polyacrylamide gel electrophoresis (SDS-PAGE) was used for the analysis of proteins. Protein samples were mixed with Laemmli Sample Buffer (SB 5X) and boiled for 5 minutes. Protein samples were then loaded to 7.5-15% polyacrylamide gels and run in Tris-Glycin-SDS (TGS) buffer by the use of the Mini-Protean III/Tetra system (Bio-Rad). Precision Plus Protein Dual Color Standards (Bio-Rad) were used for molecular weight estimation on SDS-PAGE gels. Resolved proteins were then transferred to Protran® nitrocellulose membranes (GE healthcare) in transfer buffer at a constant amperage (400 mA) for 60 – 90 minutes, depending on the molecular weight of the proteins of interest. Protein pattern bands were detected by Ponceau S staining, which was added to the membrane for 2 minutes and then rinsed with distilled water until bands were properly visualized. Membranes were blocked for 1 hour at room temperature in either 5% non-fat milk or 3% BSA dissolved in Tris-buffered-saline-Tween (TBS-T) and then incubated with the primary antibody overnight at 4ºC or for 1 hour at room-temperature, depending on the efficiency of the antibody. After two TBS-T washes of 10 minutes each, membranes were incubated with the appropriate secondary antibody (HRP-conjugated anti-IgG; Dako) for one hour at room temperature. Membranes were washed

twice with TBS-T, developed with Immobilon and Luminata Western HRP Substrates (Millipore) and exposed on AgfaCurix films or Hyperfilms (Amersham). The primary antibodies listed in **Table M3** were used in this work.

Table M3. Primary antibodies used for Western blot

Antibody	Host	Dilution
Akt (#9272, Cell Signaling)	Rb	1:1000
Akt1 (#2938, Cell Signaling)	Rb	1:1000
Akt2 (#3063, Cell Signaling)	Rb	1:1000
Cleaved-Caspase3 (9661, Cell Signaling)	Rb	1:1000
Cytokeratin 14 (ab181595, Abcam)	Rb	1:1000
E-Cadherin (610182, BD Transduction Labs)	Ms	1:2000
Fibronectin (ab2413, Abcam)	Ms	1:10000
N-Cadherin (610920, Transduction Labs)	Ms	1:1000
phospho-Akt (S473) (#9271, Cell Signaling)	Rb	1:1000
phospho-Akt2 (S474) (#8599, Cell Signaling)	Rb	1:1000
phospho-Smad2 (S465/467) (#3108, Cell Signaling)	Rb	1:1000
phospho-S6 (Ser235/236) (#4858, Cell Signaling)	Rb	1:2000
Smad2/3 (#8685, Cell Signaling)	Rb	1:1000
Snail1 (#3879, Cell Signaling)	Rb	1:1000
S100A4 (136784, Millipore)	Rb	1:1000
S6 (#2217, Cell Signaling)	Rb	1:2000
TRAF6 (HPA019805, Sigma-Aldrich)	Rb	1:2000
Tubulin (T9026, Sigma-Aldrich)	Ms	1:10000
β-Actin (ab8227, Abcam)	Rb	1:10000

8.3. Ubiquitination assay

Control and TRAF6-KD CAFs were grown in p100 plates to 60% confluence and transfected with a pMT107 vector (8 µg/plate) containing histidine-tagged ubiquitin (ubiquitin-6xHis), following the manufacturer's guidelines for Lipofectamine Plus (Invitrogen) transfection. The efficiency of the transfection was evaluated by the presence of GFP positive cells after the addition of an empty pEGFP1Ø vector (2 µg/plate). Cells were cultured for 48 hours post-transfection and, after two PBS washes, culture media was replaced by DMEM 1 g/l glucose 0.5% FBS, high (2 mM) or low (0.2 mM) glutamine. Following an over-night glutamine deprivation, transfected cells were treated with 5 ng/ml TGF-β for 1 hour. Cells were washed in cold PBS and scrapped off the dish in 500 µl of Buffer I. Cell lysates were collected in 1.5 ml Eppendorf tubes and sonicated twice at 15% amplitude for 15 seconds for further homogenization. 50 µl of each sample were separated, precipitated with trichloroacetic acid (TCA)[263] and resuspended in SB 2X to be analyzed as input. The rest of the samples were incubated with 30 µl of equilibrated Ni-NTA agarose beads (Quiagen) for 3 hours at room temperature. The beads were washed in Buffer I and incubated with Buffer II for 15 minutes at room temperature. To equilibrate pH and salt concentration, an additional wash was performed with PBS. The beads were eluded in SB 2X and heated at 95ºC for 5 minutes. Akt2 was detected in both pull-down and input samples by western blot.

9. RNA ANALYSIS

9.1. RNA extraction

MSCs RNA was extracted with the GenElute TM Mammalian Total RNA Miniprep Kit (Sigma-Aldrich), according to the manufacturer's instructions. Samples were stored at -80ºC until use. Samples were quantified in a NanoDrop™ 1000 spectrophotometer (Thermo Scientific)

RNA from HT-29M6 cells was extracted by the phenol-chloroform RNA extraction method. Cells were washed in cold PBS and lysed in 800 µl TRIzol ® reagent (Invitrogen). Cell lysates were mixed with 200 µl chloroform at room temperature for 2 minutes. The solution was centrifuged at maximum speed at 4ºC for 15 minutes and the aqueous fraction was transferred into a new tube. 500 µl of isopropanol were mixed with each sample and RNA was precipitated by incubation at room temperature for 20 minutes. RNA was pelleted by centrifugation at maximum speed at 4ºC for 15 minutes. The pellet was washed with 1 ml ethanol 75% and centrifuged at 7,500 rpm at 4ºC for 10 minutes. Ethanol was removed and, when all ethanol traces were evaporated, samples were resuspended in RNAse-free water, dissolved for 5 minutes at 55ºC and stored at -80ºC.

9.2. Reverse transcription and real time PCR (RT-qPCR)

For quantitative analysis, RNA samples were retro-transcribed using oligo dT and the Transcriptor First Strand cDNA Synthesis Kit (Roche) following manufacturer's instructions. 100 ng of the obtained cDNA were amplified with specific primers (listed in **Table M4**) using the LightCycler 480 Real Time PCR System (Roche). The amount of amplified cDNA was systematically normalized to the amount of the housekeeping gene *PUM1*. All the analyses were performed in triplicate

Table M4. Primers used for qPCR

Name		Oligonucleotide sequence
Human primers		
PUM1	Forward	5'–GACCAGCAGAATGAGATGGTTC–3'
	Reverse	5'–CATAAGGATGTGTGGATAAGGCA–3'
SNAI1	Forward	5'–GTGCCTCGACCACTATGCC–3'
	Reverse	5'–GCTGCTGGAAGGTAAACTCTGG–3'
SNAI2	Forward	5'–TTTCCAGACCCTGGTTGCTTC–3'
	Reverse	5'–CTCAGATTTGACCTGTCTGCAAATG–3'
TWIST1	Forward	5'–GGAGTCCGCAGTCTTACGAG–3'
	Reverse	5'–TCTGGAGGACCTGGTAGAGG–3'
ZEB1	Forward	5'–TTCACAGTGGAGAGAAGCCA–3'
	Reverse	5'–GCCTGGTGATGCTGAAAGAG–3'
Mouse primers		
Adamts16	Forward	5'–CAGTGAGCAGCAGACACCTG–3'
	Reverse	5'–GTCACAGCTCTTCTCCGACG–3'
Pum1	Forward	5'–CAGGTAATTAACGAGATGGTGCG–3'
	Reverse	5'–ACGGGTGCGTAGACAAAGC–3'
Snai1	Forward	5'–GCGCCCGTCGTCCTTCTCGTC–3'
	Reverse	5'–CTTCCGCGACTGGGGGTCCT–3'
Tgfb1	Forward	5'–CTGCAAGACCATCGACATGG–3'
	Reverse	5'–GTTCCACATGTTGCTCCACA–3'
Usp27x	Forward	5'–CCCACGGAGAAGAAGGATCG–3'
	Reverse	5'–CTGCTAGATGACGAGCGTG–3'

10. ELISA PGE_2

We determined PGE_2 levels in the upper compartment of transwell inserts containing either HT-29M6, MSCs or a co-culture of both cell types, upon high (2 mM) or low (0.2 mM) glutamine culture for 48 hours. These invasion experiments were set up as previously described (**section 6.1**). Cell culture supernatants were immediately frozen after their obtention and samples were stored at -80ºC until use. Prostaglandin E2 Direct Biotrack Assay (RPN222, GE Healthcare Life Sciences) was used according to the manufacturer's instructions. PGE_2 concentration was determined in media from three independent biological replicates.

11. STATISTICAL ANALYSIS

All data represent the relative mean of at least three independent experiments ± standard error of the mean (SEM). Statistical significance was calculated by two-tailed T-test using Graphpad Software and considered when *p < 0.05; **p<0.01, ***p<0.001.

12. BUFFERS AND SOLUTIONS

Buffer I: 6 M Guanidinium-HCl, 0.1 M Na_2HPO_4/NaH_2PO_4 pH 8, 0.01 M Tris-HCl pH 8, 0.2% Triton X-100, 5 mM Imidazole, 10 mM β-mercaptoethanol.

Buffer II: 8 M Urea, 0.1 M Na_2HPO_4/NaH_2PO_4 pH 8, 0.01 M Tris-HCl pH 8, 0.2% Triton X-100, 5 mM Imidazole, 10 mM β-mercaptoethanol.

Citrate buffer: 0.01 M citrate, pH 6.

Crystal violet: 0.5 g/l crystal violet, 20% methanol.

Laemmli sample Buffer 5X: 250 mM Tris-HCl pH 6.8, 10% SDS, 0.02% bromophenol blue, 50% glycerol, 20% β-mercaptoethanol.

SDS lysis buffer: 2% SDS, 50 mM Tris pH 7.5, 10% glycine.

TBS-T: 25 mM Tris-HCl pH 7.5, 137 mM NaCl, 0.1% Tween-20.

TGS: 25 mM Tris-OH pH 8.3, 192 mM glycine, 5% SDS.

Transfer buffer: 50 mM Tris-OH, 386 mM glycine, 0.1% SDS, 20% methanol.

PBS: 137 mM NaCl, 2.7 mM KCl, 10 mM Na_2HPO_4, 1.8 mM KH_2PO_4.

Ponceau S stain: 0.5% Ponceau S, 1% acetic acid.

REFERENCES

1. World Health Organization - Cancer. Available at: http://www.who.int/cancer/en.

2. Noone, A. *et al.* National Cancer Institute SEER Cancer Statistics Review 1975-2012. *JNCI* **103**, 1975–2012 (2015).

3. Greenman, C. *et al.* Patterns of somatic mutation in human cancer genomes. *Nature* **446**, 153–8 (2007).

4. Bedard, P. L., Hansen, A. R., Ratain, M. J. & Siu, L. L. Tumour heterogeneity in the clinic. *Nature* **501**, 355–64 (2013).

5. Stanta, G. & Bonin, S. Overview on Clinical Relevance of Intra-Tumor Heterogeneity. *Front. Med.* **5**, 85–95 (2018).

6. The Cancer Genome Atlas Program (TCGA). Available at: https://portal.gdc.cancer.gov/.

7. Hanahan, D. & Weinberg, R. A. The Hallmarks of Cancer. *Cell* **100**, 57–70 (2000).

8. Hanahan, D. & Weinberg, R. A. Hallmarks of cancer: The next generation. *Cell* **144**, 646–674 (2011).

9. Luo, J., Solimini, N. L. & Elledge, S. J. Principles of cancer therapy: oncogene and non-oncogene addiction. *Cell* **136**, 823–37 (2009).

10. Werb, Z. & Lu, P. The Role of Stroma in Tumor Development. *Cancer J.* **21**, 250–3 (2015).

11. Hanahan, D. & Coussens, L. M. Accessories to the crime: functions of cells recruited to the tumor microenvironment. *Cancer Cell* **21**, 309–22 (2012).

12. Gonzalez, H., Hagerling, C. & Werb, Z. Roles of the immune system in cancer: from tumor initiation to metastatic progression. *Genes Dev.* **32**, 1267–1284 (2018).

13. Grivennikov, S. I., Greten, F. R. & Karin, M. Immunity, inflammation, and cancer. *Cell* **140**, 883–99 (2010).

14. Farhood, B., Najafi, M. & Mortezaee, K. Cancer-associated fibroblasts: Secretions, interactions, and therapy. *J. Cell. Biochem.* **120**, 2791–2800 (2019).

15. Gascard, P. & Tlsty, T. D. Carcinoma-associated fibroblasts: orchestrating the composition of malignancy. *Genes Dev.* **30**, 1002–19 (2016).

16. Massagué, J. & Obenauf, A. C. Metastatic colonization by circulating tumour cells. *Nature* **529**, 298–306 (2016).

17. Steeg, P. S. Targeting metastasis. *Nat. Rev. Cancer* **16**, 201–218 (2016).

18. Jiang, W. G. *et al.* Tissue invasion and metastasis: Molecular, biological and clinical perspectives. *Semin. Cancer Biol.* **35**, 244–275 (2015).

19. Cheung, K. J. & Ewald, A. J. A collective route to metastasis: Seeding by tumor cell clusters. *Science* **352**, 167–169 (2016).

20. Leone, K., Poggiana, C. & Zamarchi, R. The Interplay between Circulating Tumor Cells and the Immune System: From Immune Escape to Cancer Immunotherapy. *Diagnostics* **8**, 59–105 (2018).

21. Paoli, P., Giannoni, E. & Chiarugi, P. Anoikis molecular pathways and its role in cancer progression. *Biochim. Biophys. Acta - Mol. Cell Res.* **1833**, 3481–31 (2013).

22. Al-Mehdi, A. B. *et al.* Intravascular origin of metastasis from the proliferation of endothelium-attached tumor cells: a new model for metastasis. *Nat. Med.* **6**, 100–102 (2000).

23. Nguyen, D. X., Bos, P. D. & Massagué, J. Metastasis: from dissemination to organ-specific colonization. *Nat. Rev. Cancer* **9**, 274–284 (2009).

24. Obenauf, A. C. & Massagué, J. Surviving at a distance: organ specific metastasis. *Trends in Cancer* **1**, 76–91 (2015).

25. Blomberg, O. S., Spagnuolo, L. & de Visser, K. E. Immune regulation of metastasis: mechanistic insights and therapeutic opportunities. *Dis. Model. Mech.* **11**, 1–12 (2018).

26. Peinado, H. *et al.* Pre-metastatic niches: organ-specific homes for metastases. *Nat. Rev. Cancer* **17**, 302–317 (2017).

27. Chaffer, C. L. & Weinberg, R. A. A Perspective on Cancer Cell Metastasis. *Science* **331**, 1559–1564 (2011).

28. Obenauf, A. C. *et al.* Therapy-induced tumour secretomes promote resistance and tumour progression. *Nature* **520**, 368–372 (2015).

29. Chang, J. & Chaudhuri, O. Beyond proteases: Basement membrane mechanics and cancer invasion. *J. Cell Biol.* **218**, 2456–2469 (2019).

30. Nabeshima, K., Inoue, T., Shimao, Y. & Sameshima, T. Matrix metalloproteinases in tumor invasion: role for cell migration. *Pathol. Int.* **52**, 255–64 (2002).

31. Friedl, P. & Alexander, S. Cancer invasion and the microenvironment: plasticity and reciprocity. *Cell* **147**, 992–1009 (2011).

32. Knights, A. J., Funnell, A. P. W., Crossley, M. & Pearson, R. C. M. Holding Tight: Cell Junctions and Cancer Spread. *Trends Cancer Res.* **8**, 61–69 (2012).

33. Brabletz, T., Kalluri, R., Nieto, M. A. & Weinberg, R. A. EMT in cancer. *Nat. Rev. Cancer* **18**, 128–134 (2018).

34. Dongre, A. & Weinberg, R. A. New insights into the mechanisms of epithelial–mesenchymal transition and implications for cancer. *Nat. Rev. Mol. Cell Biol.* **20**, 69–84 (2019).

35. Thiery, J. P., Acloque, H., Huang, R. Y. J. & Nieto, M. A. Epithelial-Mesenchymal Transitions in Development and Disease. *Cell* **139**, 871–890 (2009).

36. Kalluri, R. & Weinberg, R. A. The basics of epithelial-mesenchymal transition. *J. Clin. Invest.* **119**, 1420–1428 (2009).

37. Pastushenko, I. *et al.* Identification of the tumour transition states occurring during EMT. *Nature* **556**, 463–468 (2018).

38. Chen, A. *et al.* E-cadherin loss alters cytoskeletal organization and adhesion in non-malignant breast cells but is insufficient to induce an epithelial-mesenchymal transition. *BMC Cancer* **14**, 552–66 (2014).

39. Solanas, G. *et al.* E-cadherin controls beta-catenin and NF-kappaB transcriptional activity in mesenchymal gene expression. *J. Cell Sci.* **121**, 2224–2234 (2008).

40. Stanisavljevic, J., Porta-de-la-Riva, M., Batlle, R., Garcia de Herreros, A. & Baulida, J. The p65 subunit of NF-κB and PARP1 assist Snail1 in activating fibronectin transcription. *J. Cell Sci.* **124**, 4161–4171 (2011).

41. Zhong, C. *et al.* Rho-mediated Contractility Exposes a Cryptic Site in Fibronectin and Induces Fibronectin Matrix Assembly. *J. Cell Biol.* **141**, 539–551 (1998).

42. Liu, C.-Y., Lin, H.-H., Tang, M.-J. & Wang, Y.-K. Vimentin contributes to epithelial-mesenchymal transition cancer cell mechanics by mediating cytoskeletal organization and focal adhesion maturation. *Oncotarget* **6**, 15966–83 (2015).

43. Wheelock, M. J., Shintani, Y., Maeda, M., Fukumoto, Y. & Johnson, K. R. Cadherin switching. *J. Cell Sci.* **121**, 727–35 (2008).

44. Stemmler, M. P., Eccles, R. L., Brabletz, S. & Brabletz, T. Non-redundant functions of EMT transcription factors. *Nat. Cell Biol.* **21**, 102–112 (2019).

45. Yang, J. & Weinberg, R. A. Epithelial-mesenchymal transition: at the crossroads of development and tumor metastasis. *Dev. Cell* **14**, 818–29 (2008).

46. Garcia de Herreros, A., Peiró, S., Nassour, M. & Savagner, P. Snail family regulation and epithelial mesenchymal transitions in breast cancer progression. *J Mammary Gland Biol Neoplasia* **15**, 135–147 (2010).

47. Villagrasa, P. *et al.* Akt2 interacts with Snail1 in the E-cadherin promoter. *Oncogene* **31**, 4022–4033 (2012).

48. Barberà, M. J. *et al.* Regulation of Snail transcription during epithelial to mesenchymal transition of tumor cells. *Oncogene* **23**, 7345–7354 (2004).

49. Grille, S. J. *et al.* The protein kinase Akt induces epithelial mesenchymal transition and promotes enhanced motility and invasiveness of squamous cell carcinoma lines. *Cancer Res.* **63**, 2172–8 (2003).

50. Vincent, T. *et al.* A SNAIL1–SMAD3/4 transcriptional repressor complex promotes TGF-β mediated epithelial–mesenchymal transition. *Nat. Cell Biol.* **11**, 943–950 (2009).

51. Díaz, V. M., Viñas-Castells, R. & García de Herreros, A. Regulation of the protein stability of EMT transcription factors. *Cell Adh. Migr.* **8**, 418–28 (2014).

52. Comijn, J. *et al.* The two-handed E box binding zinc finger protein SIP1 downregulates E-cadherin and induces invasion. *Mol. Cell* **7**, 1267–78 (2001).

53. Baulida, J., Díaz, V. M. & García de Herreros, A. Snail1: A Transcriptional Factor Controlled at Multiple Levels. *J. Clin. Med.* **8**, 757–778 (2019).

54. Viñas-Castells, R. *et al.* The hypoxia-controlled FBXL14 ubiquitin ligase targets SNAIL1 for proteasome degradation. *J. Biol. Chem.* **285**, 3794–805 (2010).

55. Viñas-Castells, R. *et al.* Nuclear ubiquitination by FBXL5 modulates Snail1 DNA binding and stability. *Nucleic Acids Res.* **42**, 1079–1094 (2014).

56. Lim, S.-O., Kim, H. & Jung, G. p53 inhibits tumor cell invasion via the degradation of snail protein in hepatocellular carcinoma. *FEBS Lett.* **584**, 2231–2236 (2010).

57. Zhou, B. P. *et al.* Dual regulation of Snail by GSK-3β-mediated phosphorylation in control of epithelial–mesenchymal transition. *Nat. Cell Biol.* **6**, 931–940 (2004).

58. Peinado, H., Quintanilla, M. & Cano, A. Transforming growth factor beta-1 induces Snail transcription factor in epithelial cell lines. Mechanisms for epithelial mesenchymal transitions. *J. Biol. Chem.* **278**, 21113–21123 (2003).

59. Zhang, L., Zhou, F. & Ten Dijke, P. Signaling interplay between transforming growth factor-b receptor and PI3K/AKT pathways in cancer. *Trends Biochem. Sci.* **38**, 612–620 (2013).

60. Lambies, G. *et al.* TGFβ-Activated USP27X Deubiquitinase Regulates Cell Migration and Chemoresistance via Stabilization of Snail1. *Cancer Res.* **79**, 33–46 (2019).

61. Massagué, J. TGFbeta in Cancer. *Cell* **134**, 215–30 (2008).

62. Kolosova, I., Nethery, D. & Kern, J. A. Role of Smad2/3 and p38 MAP kinase in TGF-β1-induced epithelial-mesenchymal transition of pulmonary epithelial cells. *J. Cell. Physiol.* **226**, 1248–54 (2011).

63. Sorrentino, A. *et al.* The type I TGF-β receptor engages TRAF6 to activate TAK1 in a receptor kinase-independent manner. *Nat. Cell Biol.* **10**, 1199–1207 (2008).

64. Thakur, N. *et al.* TGFβ-induced invasion of prostate cancer cells is promoted by c-Jun-dependent transcriptional activation of Snail1. *Cell Cycle* **13**, 2400–14 (2014).

65. Hamidi, A. *et al.* TGF-β promotes PI3K-AKT signaling and prostate cancer cell migration through the TRAF6-mediated ubiquitylation of p85α. *Sci. Signal.* **10**, 4186–98 (2017).

66. Yang, W.-L. *et al.* The E3 ligase TRAF6 regulates Akt ubiquitination and activation. *Science* **325**, 1134–8 (2009).

67. Friedl, P. & Wolf, K. Plasticity of cell migration: a multiscale tuning model. *J. Cell Biol.* **188**, 11–19 (2010).

68. Trepat, X., Chen, Z. & Jacobson, K. Cell migration. *Compr. Physiol.* **2**, 2369–92 (2012).

69. Sanz-Moreno, V. & Marshall, C. J. The plasticity of cytoskeletal dynamics underlying neoplastic cell migration. *Curr. Opin. Cell Biol.* **22**, 690–696 (2010).

70. Friedl, P., Locker, J., Sahai, E. & Segall, J. E. Classifying collective cancer cell invasion. *Nat. Cell Biol.* **14**, 777–783 (2012).

71. Mayor, R. & Etienne-Manneville, S. The front and rear of collective cell migration. *Nat. Rev. Mol. Cell Biol.* **17**, 97–109 (2016).

72. Pandya, P., Orgaz, J. L. & Sanz-Moreno, V. Modes of invasion during tumour dissemination. *Mol. Oncol.* **11**, 5–27 (2017).

73. Clark, A. G. & Vignjevic, D. M. Modes of cancer cell invasion and the role of the microenvironment. *Curr. Opin. Cell Biol.* **36**, 13–22 (2015).

74. Balkwill, F. R., Capasso, M. & Hagemann, T. The tumor microenvironment at a glance. *J. Cell Sci.* **125**, 5591–5596 (2012).

75. Reid, M. A. & Kong, M. Dealing with hunger: Metabolic stress responses in tumors. *J. Carcinog.* **12**, 1–6 (2013).

76. Bergers, G. & Benjamin, L. E. Tumorigenesis and the angiogenic switch. *Nat. Rev. Cancer* **3**, 401–410 (2003).

77. Baeriswyl, V. & Christofori, G. The angiogenic switch in carcinogenesis. *Semin. Cancer Biol.* **19**, 329–337 (2009).

78. Krock, B. L., Skuli, N. & Simon, M. C. Hypoxia-induced angiogenesis: good and evil. *Genes Cancer* **2**, 1117–33 (2011).

79. Joyce, J. A. & Pollard, J. W. Microenvironmental regulation of metastasis. *Nat. Rev. Cancer* **9**, 239–52 (2009).

80. Stuelten, C. H. *et al.* Breast cancer cells induce stromal fibroblasts to express MMP-9 via secretion of TNF-alpha and TGF-beta. *J. Cell Sci.* **118**, 2143–2153 (2005).

81. Liu, L., Ye, Y. & Zhu, X. MMP-9 secreted by tumor associated macrophages promoted gastric cancer metastasis through a PI3K/AKT/Snail pathway. *Biomed. Pharmacother.* **117**, 109096–109104 (2019).

82. Liu, Z., Kuang, W., Zhou, Q. & Zhang, Y. TGF-β1 secreted by M2 phenotype macrophages enhances the stemness and migration of glioma cells via the SMAD2/3 signalling pathway. *Int. J. Mol. Med.* **42**, 3395–3403 (2018).

83. Yu, Y. *et al.* Cancer-associated fibroblasts induce epithelial-mesenchymal transition of breast cancer cells through paracrine TGF-β signalling. *Br. J. Cancer* **110**, 724–32 (2014).

84. Patsialou, A. *et al.* Intravital multiphoton imaging reveals multicellular streaming as a crucial component of in vivo cell migration in human breast tumors. *IntraVital* **2**, 25294.1–14 (2013).

85. Labelle, M., Begum, S. & Hynes, R. O. Direct signaling between platelets and cancer cells induces an epithelial-mesenchymal-like transition and promotes metastasis. *Cancer Cell* **20**, 576–90 (2011).

86. Peinado, H. *et al.* Melanoma exosomes educate bone marrow progenitor cells toward a pro-metastatic phenotype through MET. *Nat. Med.* **18**, 883–91 (2012).

87. Hoshino, A. *et al.* Tumour exosome integrins determine organotropic metastasis. *Nature* **527**, 329–35 (2015).

88. Roma-Rodrigues, C., Mendes, R., Baptista, P. V & Fernandes, A. R. Targeting Tumor Microenvironment for Cancer Therapy. *Int. J. Mol. Sci.* **20**, 840–871 (2019).

89. Calon, A. *et al.* Dependency of colorectal cancer on a TGF-β-driven program in stromal cells for metastasis initiation. *Cancer Cell* **22**, 571–84 (2012).

90. Xiong, B., Gong, L.-L., Zhang, F., Hu, M.-B. & Yuan, H.-Y. TGF-β1 expression and angiogenesis in colorectal cancer tissue. *World J. Gastroenterol.* **8**, 496–8 (2002).

91. Calon, A., Tauriello, D. V. F. & Batlle, E. TGF-beta in CAF-mediated tumor growth and metastasis. *Semin. Cancer Biol.* **25**, 15–22 (2014).

92. Haque, S. & Morris, J. C. Transforming growth factor-β: A therapeutic target for cancer. *Hum. Vaccin. Immunother.* **13**, 1741–1750 (2017).

93. Nakasone, E. S. *et al.* Imaging tumor-stroma interactions during chemotherapy reveals contributions of the microenvironment to resistance. *Cancer Cell* **21**, 488–503 (2012).

94. Hirata, E. & Sahai, E. Tumor microenvironment and differential responses to therapy. *Cold Spring Harb. Perspect. Med.* **7**, 1–14 (2017).

95. Valkenburg, K. C., de Groot, A. E. & Pienta, K. J. Targeting the tumour stroma to improve cancer therapy. *Nat. Rev. Clin. Oncol.* **15**, 366–381 (2018).

96. Kalluri, R. & Zeisberg, M. Fibroblasts in cancer. *Nat. Rev. Cancer* **6**, 392–401 (2006).

97. Kalluri, R. The biology and function of fibroblasts in cancer. *Nat. Rev. Cancer* **16**, 582–598 (2016).

98. Bonnans, C., Chou, J. & Werb, Z. Remodelling the extracellular matrix in development and disease. *Nat. Rev. Mol. Cell Biol.* **15**, 786–801 (2014).

99. Darby, I. A. & Hewitson, T. D. Fibroblast Differentiation in Wound Healing and Fibrosis. *Int. Rev. Cytol.* **257**, 143–179 (2007).

100. Enzerink, A. & Vaheri, A. Fibroblast activation in vascular inflammation. *J. Thromb. Haemost.* **9**, 619–626 (2011).

101. Schellerer, V. S. *et al.* Tumor-associated fibroblasts isolated from colorectal cancer tissues exhibit increased ICAM-1 expression and affinity for monocytes. *Oncol. Rep.* **31**, 255–261 (2014).

102. Agassandian, M. *et al.* VCAM-1 is a TGF-β1 inducible gene upregulated in idiopathic pulmonary fibrosis. *Cell. Signal.* **27**, 2467–2473 (2015).

103. Arwert, E. N., Hoste, E. & Watt, F. M. Epithelial stem cells, wound healing and cancer. *Nat. Rev. Cancer* **12**, 170–180 (2012).

104. Hinz, B. Formation and Function of the Myofibroblast during Tissue Repair. *J. Invest. Dermatol.* **127**, 526–537 (2007).

105. Akasaka, Y. *et al.* The mechanisms underlying fibroblast apoptosis regulated by growth factors during wound healing. *J. Pathol.* **221**, 285–299 (2010).

106. Kendall, R. T. & Feghali-Bostwick, C. A. Fibroblasts in fibrosis: novel roles and mediators. *Front. Pharmacol.* **5**, 123–136 (2014).

107. Bechtel, W. *et al.* Methylation determines fibroblast activation and fibrogenesis in the kidney. *Nat. Med.* **16**, 544–50 (2010).

108. Huang, S. K. *et al.* Histone modifications are responsible for decreased Fas expression and apoptosis resistance in fibrotic lung fibroblasts. *Cell Death Dis.* **4**, 621–8 (2013).

109. Sugimoto, H., Mundel, T. M., Kieran, M. W. & Kalluri, R. Identification of fibroblast heterogeneity in the tumor microenvironment. *Cancer Biol. Ther.* **5**, 1640–1646 (2006).

110. Foster, D. S., Jones, R. E., Ransom, R. C., Longaker, M. T. & Norton, J. A. The evolving relationship of wound healing and tumor stroma. *JCI insight* **3**, 99911–28 (2018).

111. LeBleu, V. S. *et al.* Origin and function of myofibroblasts in kidney fibrosis. *Nat. Med.* **19**, 1047–53 (2013).

112. Ishii, G. *et al.* Bone-marrow-derived myofibroblasts contribute to the cancer-induced stromal reaction. *Biochem. Biophys. Res. Commun.* **309**, 232–240 (2003).

113. Quante, M. *et al.* Bone marrow-derived myofibroblasts contribute to the mesenchymal stem cell niche and promote tumor growth. *Cancer Cell* **19**, 257–72 (2011).

114. Petersen, O. W. *et al.* Epithelial to Mesenchymal Transition in Human Breast Cancer Can Provide a Nonmalignant Stroma. *Am. J. Pathol.* **162**, 391–402 (2003).

115. Zeisberg, E. M., Potenta, S., Xie, L., Zeisberg, M. & Kalluri, R. Discovery of Endothelial to Mesenchymal Transition as a Source for Carcinoma-Associated Fibroblasts. *Cancer Res.* **67**, 10123–10128 (2007).

116. Jotzu, C. *et al.* Adipose tissue-derived stem cells differentiate into carcinoma-associated fibroblast-like cells under the influence of tumor-derived factors. *Anal. Cell. Pathol.* **33**, 61–79 (2010).

117. Pittenger, M. F. *et al.* Multilineage Potential of Adult Human Mesenchymal Stem Cells. *Science* **284**, 143–147 (1999).

118. Mishra, P. J. *et al.* Carcinoma-associated fibroblast-like differentiation of human mesenchymal stem cells. *Cancer Res.* **68**, 4331–9 (2008).

119. Karnoub, A. E. *et al.* Mesenchymal stem cells within tumour stroma promote breast cancer metastasis. *Nature* **449**, 557–563 (2007).

120. Waghray, M. *et al.* GM-CSF Mediates Mesenchymal-Epithelial Cross-talk in Pancreatic Cancer. *Cancer Discov.* **6**, 886–99 (2016).

121. Elenbaas, B. & Weinberg, R. A. Heterotypic Signaling between Epithelial Tumor Cells and Fibroblasts in Carcinoma Formation. *Exp. Cell Res.* **264**, 169–184 (2001).

122. Hartupee, J. & Mann, D. L. Role of inflammatory cells in fibroblast activation. *J. Mol. Cell. Cardiol.* **93**, 143–8 (2016).

123. Chaudhary, N. I. *et al.* Inhibition of PDGF, VEGF and FGF signalling attenuates fibrosis. *Eur. Respir. J.* **29**, 976–985 (2007).

124. Hawinkels, L. J. *et al.* Active TGF-β1 correlates with myofibroblasts and malignancy in the colorectal adenoma-carcinoma sequence. *Cancer Sci.* **100**, 663–670 (2009).

125. Richardsen, E., Uglehus, R. D., Johnsen, S. H. & Busund, L. T. Immunohistochemical expression of epithelial and stromal immunomodulatory signalling molecules is a prognostic indicator in breast cancer. *BMC Res. Notes* **5**, 110–20 (2012).

126. Löhr, M. *et al.* Transforming growth factor-beta1 induces desmoplasia in an experimental model of human pancreatic carcinoma. *Cancer Res.* **61**, 550–5 (2001).

127. Pavlides, S. *et al.* The reverse Warburg effect: aerobic glycolysis in cancer associated fibroblasts and the tumor stroma. *Cell Cycle* **8**, 3984–4001 (2009).

128. Martinez-Outschoorn, U. E., Lisanti, M. P. & Sotgia, F. Catabolic cancer-associated fibroblasts transfer energy and biomass to anabolic cancer cells, fueling tumor growth. *Semin. Cancer Biol.* **25**, 47–60 (2014).

129. Orimo, A. *et al.* Stromal Fibroblasts Present in Invasive Human Breast Carcinomas Promote Tumor Growth and Angiogenesis through Elevated SDF-1/CXCL12 Secretion. *Cell* **121**, 335–348 (2005).

130. Harper, J. & Sainson, R. C. A. Regulation of the anti-tumour immune response by cancer-associated fibroblasts. *Semin. Cancer Biol.* **25**, 69–77 (2014).

131. Davies, L. C., Heldring, N., Kadri, N. & Le Blanc, K. Mesenchymal Stromal Cell Secretion of Programmed Death-1 Ligands Regulates T Cell Mediated Immunosuppression. *Stem Cells* **35**, 766–776 (2017).

132. Pinchuk, I. V. *et al.* PD-1 Ligand Expression by Human Colonic Myofibroblasts/Fibroblasts Regulates CD4+ T-Cell Activity. *Gastroenterology* **135**, 1228–1237 (2008).

133. Chan, T. S., Shaked, Y. & Tsai, K. K. Targeting the Interplay Between Cancer Fibroblasts, Mesenchymal Stem Cells, and Cancer Stem Cells in Desmoplastic Cancers. *Front. Oncol.* **9**, 688–703 (2019).

134. Vermeulen, L. *et al.* Wnt activity defines colon cancer stem cells and is regulated by the microenvironment. *Nat. Cell Biol.* **12**, 468–476 (2010).

135. Su, S. *et al.* CD10+GPR77+ Cancer-Associated Fibroblasts Promote Cancer Formation and Chemoresistance by Sustaining Cancer Stemness. *Cell* **172**, 841–856 (2018).

136. Plaks, V., Kong, N. & Werb, Z. The cancer stem cell niche: how essential is the niche in regulating stemness of tumor cells? *Cell Stem Cell* **16**, 225–38 (2015).

137. Stanisavljevic, J. *et al.* Snail1-Expressing Fibroblasts in the Tumor Microenvironment Display Mechanical Properties That Support Metastasis. *Cancer Res.* **75**, 284–295 (2015).

138. Gaggioli, C. *et al.* Fibroblast-led collective invasion of carcinoma cells with differing roles for RhoGTPases in leading and following cells. *Nat. Cell Biol.* **9**, 1392–1400 (2007).

139. Alba-Castellón, L. *et al.* Snail1-Dependent Activation of Cancer-Associated Fibroblast Controls Epithelial Tumor Cell Invasion and Metastasis. *Cancer Res.* **76**, 6205–6217 (2016).

140. Labernadie, A. *et al.* A mechanically active heterotypic E-cadherin/N-cadherin adhesion enables fibroblasts to drive cancer cell invasion. *Nat. Cell Biol.* **19**, 224–237 (2017).

141. Pickup, M. W., Mouw, J. K. & Weaver, V. M. The extracellular matrix modulates the hallmarks of cancer. *EMBO Rep.* **15**, 1243–53 (2014).

142. Lu, P., Weaver, V. M. & Werb, Z. The extracellular matrix: a dynamic niche in cancer progression. *J. Cell Biol.* **196**, 395–406 (2012).

143. Rice, A. J. *et al.* Matrix stiffness induces epithelial–mesenchymal transition and promotes chemoresistance in pancreatic cancer cells. *Oncogenesis* **6**, 352–352 (2017).

144. Zhang, K. *et al.* Mechanical signals regulate and activate SNAIL1 protein to control the fibrogenic response of cancer-associated fibroblasts. *J. Cell Sci.* **129**, 1989–2002 (2016).

145. Wei, S. C. *et al.* Matrix stiffness drives epithelial-mesenchymal transition and tumour metastasis through a TWIST1-G3BP2 mechanotransduction pathway. *Nat. Cell Biol.* **17**, 678–88 (2015).

146. Paszek, M. J. *et al.* Tensional homeostasis and the malignant phenotype. *Cancer Cell* **8**, 241–254 (2005).

147. Wels, J., Kaplan, R. N., Rafii, S. & Lyden, D. Migratory neighbors and distant invaders: tumor-associated niche cells. *Genes Dev.* **22**, 559–74 (2008).

148. Duda, D. G. *et al.* Malignant cells facilitate lung metastasis by bringing their own soil. *Proc. Natl. Acad. Sci. U. S. A.* **107**, 21677–82 (2010).

149. Rowe, R. G. *et al.* Mesenchymal cells reactivate Snail1 expression to drive three-dimensional invasion programs. *J. Cell Biol.* **184**, 399–408 (2009).

150. Batlle, R. *et al.* Snail1 controls TGF-β responsiveness and differentiation of mesenchymal stem cells. *Oncogene* **32**, 3381–3389 (2013).

151. Francí, C. *et al.* Expression of Snail protein in tumor-stroma interface. *Oncogene* **25**, 5134–5144 (2006).

152. Baulida, J. Epithelial-to-mesenchymal transition transcription factors in cancer-associated fibroblasts. *Mol. Oncol.* **11**, 847–859 (2017).

153. Francí, C. *et al.* Snail1 protein in the stroma as a new putative prognosis marker for colon tumours. *PLoS One* **4**, 1–7 (2009).

154. Herrera, A. *et al.* Protumorigenic effects of Snail-expression fibroblasts on colon cancer cells. *Int. J. Cancer* **134**, 2984–2990 (2014).

155. You, J. *et al.* Snail1-expressing cancer-associated fibroblasts induce lung cancer cell epithelial-mesenchymal transition through miR-33b. *Oncotarget* **8**, 114769–114786 (2017).

156. Alba-Castellón, L. *et al.* Snail1 expression is required for sarcomagenesis. *Neoplasia* **16**, 413–21 (2014).

157. Warburg, O. The metabolism of carcinoma cells. *J. Cancer Reserarch* **9**, 148–163 (1925).

158. Vander Heiden, M. G., Cantley, L. C. & Thompson, C. B. Understanding the Warburg effect: the metabolic requirements of cell proliferation. *Science* **324**, 1029–33 (2009).

159. DeBerardinis, R. J. & Chandel, N. S. Fundamentals of cancer metabolism. *Sci. Adv.* **2**, 1–18 (2016).

160. Ancey, P., Contat, C. & Meylan, E. Glucose transporters in cancer – from tumor cells to the tumor microenvironment. *FEBS J.* **285**, 2926–2943 (2018).

161. Warburg, O. On the Origin of Cancer Cells. *Science* **123**, 309–314 (1956).

162. Ward, P. S. & Thompson, C. B. Metabolic Reprogramming: A Cancer Hallmark Even Warburg Did Not Anticipate. *Cancer Cell* **21**, 297–308 (2012).

163. Wieman, H. L., Wofford, J. A. & Rathmell, J. C. Cytokine stimulation promotes glucose uptake via phosphatidylinositol-3 kinase/Akt regulation of Glut1 activity and trafficking. *Mol. Biol. Cell* **18**, 1437–46 (2007).

164. Phadngam, S. *et al.* PTEN dephosphorylates AKT to prevent the expression of GLUT1 on plasmamembrane and to limit glucose consumption in cancer cells. *Oncotarget* **7**, 84999–85020 (2016).

165. Pavlova, N. N. & Thompson, C. B. The Emerging Hallmarks of Cancer Metabolism. *Cell Metab.* **23**, 27–47 (2016).

166. Düvel, K. *et al.* Activation of a metabolic gene regulatory network downstream of mTOR complex 1. *Mol. Cell* **39**, 171–183 (2010).

167. Wise, D. R. & Thompson, C. B. Glutamine addiction: a new therapeutic target in cancer. *Trends Biochem. Sci.* **35**, 427–33 (2010).

168. Eagle, H. Nutrition Needs of Mammalian Cells in Tissue Culture. *Science* **122**, 501–504 (1955).

169. DeBerardinis, R. J. & Cheng, T. Q's next: the diverse functions of glutamine in metabolism, cell biology and cancer. *Oncogene* **29**, 313–24 (2010).

170. Hirayama, A. *et al.* Quantitative Metabolome Profiling of Colon and Stomach Cancer Microenvironment by Capillary Electrophoresis Time-of-Flight Mass Spectrometry. *Cancer Res.* **69**, 4918–4925 (2009).

171. Ahn, C. S. & Metallo, C. M. Mitochondria as biosynthetic factories for cancer proliferation. *Cancer Metab.* **3**, 1–10 (2015).

172. Hensley, C. T., Wasti, A. T. & DeBerardinis, R. J. Glutamine and cancer: cell biology, physiology, and clinical opportunities. *J. Clin. Invest.* **123**, 3678–84 (2013).

173. Bhutia, Y. D. & Ganapathy, V. Glutamine transporters in mammalian cells and their functions in physiology and cancer. *Biochim. Biophys. Acta* **1863**, 2531–9 (2016).

174. Gameiro, P. A. *et al.* In Vivo HIF-Mediated Reductive Carboxylation Is Regulated by Citrate Levels and Sensitizes VHL-Deficient Cells to Glutamine Deprivation. *Cell Metab.* **17**, 372–385 (2013).

175. Altman, B. J., Stine, Z. E. & Dang, C. V. From Krebs to clinic: glutamine metabolism to cancer therapy. *Nat. Rev. Cancer* **16**, 619–634 (2016).

176. Howell, J. J. & Manning, B. D. mTOR couples cellular nutrient sensing to organismal metabolic homeostasis. *Trends Endocrinol. Metab.* **22**, 94–102 (2011).

177. Chauvin, C. *et al.* Ribosomal protein S6 kinase activity controls the ribosome biogenesis transcriptional program. *Oncogene* **33**, 474–483 (2014).

178. Laplante, M. & Sabatini, D. M. mTOR signaling in growth control and disease. *Cell* **149**, 274–93 (2012).

179. Linares, J. F. *et al.* K63 Polyubiquitination and Activation of mTOR by the p62-TRAF6 Complex in Nutrient-Activated Cells. *Mol. Cell* **51**, 283–296 (2013).

180. Sancak, Y. *et al.* Ragulator-Rag complex targets mTORC1 to the lysosomal surface and is necessary for its activation by amino acids. *Cell* **141**, 290–303 (2010).

181. Csibi, A. *et al.* The mTORC1 Pathway Stimulates Glutamine Metabolism and Cell Proliferation by Repressing SIRT4. *Cell* **153**, 840–854 (2013).

182. Csibi, A. *et al.* The mTORC1/S6K1 Pathway Regulates Glutamine Metabolism through the eIF4B-Dependent Control of c-Myc Translation. *Curr. Biol.* **24**, 2274–2280 (2014).

183. Durán, R. V *et al.* Glutaminolysis activates Rag-mTORC1 signaling. *Mol. Cell* **47**, 349–58 (2012).

184. Reiter, J. G. *et al.* An analysis of genetic heterogeneity in untreated cancers. *Nat. Rev. Cancer* 1–12 (2019).

185. Avagliano, A. *et al.* Mitochondrial Flexibility of Breast Cancers: A Growth Advantage and a Therapeutic Opportunity. *Cells* **8**, 401–431 (2019).

186. Chen, X., Qian, Y. & Wu, S. The Warburg effect: evolving interpretations of an established concept. *Free Radic. Biol. Med.* **79**, 253–63 (2015).

187. Kennedy, K. M. & Dewhirst, M. W. Tumor metabolism of lactate: the influence and therapeutic potential for MCT and CD147 regulation. *Future Oncol.* **6**, 127–48 (2010).

188. Semenza, G. L. Tumor metabolism: cancer cells give and take lactate. *J. Clin. Invest.* **118**, 3835–7 (2008).

189. White, E. Role of the metabolic stress responses of apoptosis and autophagy in tumor suppression. *Ernst Schering Found. Symp. Proc.* 23–34 (2007).

190. Forster, J. C., Harriss-Phillips, W. M., Douglass, M. J. & Bezak, E. A review of the development of tumor vasculature and its effects on the tumor microenvironment. *Hypoxia* **5**, 21–32 (2017).

191. Zhao, Y. *et al.* ROS signaling under metabolic stress: Cross-talk between AMPK and AKT pathway. *Mol. Cancer* **16**, 79–91 (2017).

192. Lee, S.W. *et al.* EGFR-Pak Signaling Selectively Regulates Glutamine Deprivation-Induced Macropinocytosis. *Dev. Cell* **50**, 381–392 (2019).

193. Commisso, C. *et al.* Macropinocytosis of protein is an amino acid supply route in Ras-transformed cells. *Nature* **497**, 633–7 (2013).

194. Lopes-Coelho, F., Gouveia-Fernandes, S. & Serpa, J. Metabolic cooperation between cancer and non-cancerous stromal cells is pivotal in cancer progression. *Tumor Biol.* **40**, 1–15 (2018).

195. Colegio, O. R. *et al.* Functional polarization of tumour-associated macrophages by tumour-derived lactic acid. *Nature* **513**, 559–63 (2014).

196. Sonveaux, P. *et al.* Targeting the Lactate Transporter MCT1 in Endothelial Cells Inhibits Lactate-Induced HIF-1 Activation and Tumor Angiogenesis. *PLoS One* **7**, 33418–31 (2012).

197. Rothberg, J. M. *et al.* Acid-mediated tumor proteolysis: contribution of cysteine cathepsins. *Neoplasia* **15**, 1125–37 (2013).

198. Martínez-Zaguilán, R. *et al.* Acidic pH enhances the invasive behavior of human melanoma cells. *Clin. Exp. Metastasis* **14**, 176–86 (1996).

199. Avagliano, A. *et al.* Metabolic Reprogramming of Cancer Associated Fibroblasts: The Slavery of Stromal Fibroblasts. *Biomed Res. Int.* **2018**, 1–12 (2018).

200. Guido, C. *et al.* Metabolic reprogramming of cancer-associated fibroblasts by TGF-β drives tumor growth: connecting TGF-β signaling with Warburg-like cancer metabolism and L-lactate production. *Cell Cycle* **11**, 3019–35 (2012).

201. Lisanti, M. P., Martinez-Outschoorn, U. E. & Sotgia, F. Oncogenes induce the cancer-associated fibroblast phenotype: Metabolic symbiosis and 'fibroblast addiction' are new therapeutic targets for drug discovery. *Cell Cycle* **12**, 2723–2732 (2013).

202. Rattigan, Y. I. *et al.* Lactate is a mediator of metabolic cooperation between stromal carcinoma associated fibroblasts and glycolytic tumor cells in the tumor microenvironment. *Exp. Cell Res.* **318**, 326–35 (2012).

203. Yang, L. *et al.* Targeting Stromal Glutamine Synthetase in Tumors Disrupts Tumor Microenvironment-Regulated Cancer Cell Growth. *Cell Metab.* **24**, 685–700 (2016).

204. Linares, J. F. *et al.* ATF4-induced metabolic reprograming is a synthetic vulnerability of the p62-deficient tumor stroma. *Cell Metab.* **26**, 817–829 (2017).

205. Bertero, T. *et al.* Tumor-Stroma Mechanics Coordinate Amino Acid Availability to Sustain Tumor Growth and Malignancy. *Cell Metab.* **29**, 124–140 (2019).

206. Wang, J.-B. *et al.* Targeting mitochondrial glutaminase activity inhibits oncogenic transformation. *Cancer Cell* **18**, 207–19 (2010).

207. Türkcan, S., Kiru, L., Naczynski, D. J., Sasportas, L. S. & Pratx, G. Lactic Acid Accumulation in the Tumor Microenvironment Suppresses 18F-FDG Uptake. *Cancer Res.* **79**, 410–419 (2019).

208. Kato, Y. *et al.* Acidic extracellular pH increases calcium influx-triggered phospholipase D activity along with acidic sphingomyelinase activation to induce matrix metalloproteinase-9 expression in mouse metastatic melanoma. *FEBS J.* **274**, 3171–3183 (2007).

209. Gatenby, R. A., Gawlinski, E. T., Gmitro, A. F., Kaylor, B. & Gillies, R. J. Acid-Mediated Tumor Invasion: a Multidisciplinary Study. *Cancer Res.* **66**, 5216–5223 (2006).

210. Goetze, K., Walenta, S., Ksiazkiewicz, M., Kunz-Schughart, L. A. & Mueller-Klieser, W. Lactate enhances motility of tumor cells and inhibits monocyte migration and cytokine release. *Int. J. Oncol.* **39**, 453–63 (2011).

211. Yang, S. *et al.* HIF-1alpha induces the epithelial-mesenchymal transition in gastric cancer stem cells through the Snail pathway. *Oncotarget* **8**, 9535–9545 (2017).

212. Sciacovelli, M. & Frezza, C. Metabolic reprogramming and epithelial-to-mesenchymal transition in cancer. *FEBS J.* **284**, 3132–3144 (2017).

213. Kim, N. H. *et al.* Snail reprograms glucose metabolism by repressing phosphofructokinase PFKP allowing cancer cell survival under metabolic stress. *Nat. Commun.* **8**, 14374 (2017).

214. Han, T. *et al.* How does cancer cell metabolism affect tumor migration and invasion? *Cell Adh. Migr.* **7**, 395–403 (2013).

215. Baumann, F. *et al.* Lactate promotes glioma migration by TGF-beta2-dependent regulation of matrix metalloproteinase-2. *Neuro. Oncol.* **11**, 368–80 (2009).

216. Dornier, E. *et al.* Glutaminolysis drives membrane trafficking to promote invasiveness of breast cancer cells. *Nat. Commun.* **8**, 2255–69 (2017).

217. Ishiuchi, S. *et al.* Blockage of Ca2+-permeable AMPA receptors suppresses migration and induces apoptosis in human glioblastoma cells. *Nat. Med.* **8**, 971–978 (2002).

218. Herner, A. *et al.* Glutamate increases pancreatic cancer cell invasion and migration via AMPA receptor activation and Kras-MAPK signaling. *Int. J. Cancer* **129**, 2349–2359 (2011).

219. Lin, E. Y. *et al.* Progression to malignancy in the polyoma middle T oncoprotein mouse breast cancer model provides a reliable model for human diseases. *Am. J. Pathol.* **163**, 2113–26 (2003).

220. Gross, M. I. *et al.* Antitumor Activity of the Glutaminase Inhibitor CB-839 in Triple-Negative Breast Cancer. *Mol. Cancer Ther.* **13**, 890–901 (2014).

221. Xue, G. & Hemmings, B. A. PKB/Akt-Dependent Regulation of Cell Motility. *JNCI J. Natl. Cancer Inst.* **105**, 393–404 (2013).

222. Zhou, G.-L. *et al.* Opposing Roles for Akt1 and Akt2 in Rac/Pak Signaling and Cell Migration. *J. Biol. Chem.* **281**, 36443–36453 (2006).

223. Vaupel, P., Kallinowski, F. & Okunieff, P. Blood flow, oxygen and nutrient supply, and metabolic microenvironment of human tumors: a review. *Cancer Res.* **49**, 6449–65 (1989).

224. Pan, M. *et al.* Regional glutamine deficiency in tumours promotes dedifferentiation through inhibition of histone demethylation. *Nat. Cell Biol.* **18**, 1090–101 (2016).

225. Nathan, D. M. *et al.* Impaired Fasting Glucose and Impaired Glucose Tolerance: Implications for care. *Diabetes Care* **30**, 753–759 (2007).

226. Ettinger, S. N. *et al.* Urea as a recovery marker for quantitative assessment of tumor interstitial solutes with microdialysis. *Cancer Res.* **61**, 7964–70 (2001).

227. Zhang, J., Pavlova, N. N. & Thompson, C. B. Cancer cell metabolism: the essential role of the nonessential amino acid, glutamine. *EMBO J.* **36**, 1302–1315 (2017).

228. Zhang, D. *et al.* Metabolic Reprogramming of Cancer-Associated Fibroblasts by IDH3α Downregulation. *Cell Rep.* **10**, 1335–1348 (2015).

229. Guido, C. *et al.* Metabolic reprogramming of cancer-associated fibroblasts by TGF-β drives tumor growth: connecting TGF-β signaling with Warburg-like cancer metabolism and L-lactate production. *Cell Cycle* **11**, 3019–35 (2012).

230. Bott, A. J., Maimouni, S. & Zong, W.-X. The Pleiotropic Effects of Glutamine Metabolism in Cancer. *Cancers* **11**, 770–786 (2019).

231. Mayers, J. R. *et al.* Tissue of origin dictates branched-chain amino acid metabolism in mutant Kras-driven cancers. *Science* **353**, 1161–5 (2016).

232. Tardito, S. *et al.* Glutamine synthetase activity fuels nucleotide biosynthesis and supports growth of glutamine-restricted glioblastoma. *Nat. Cell Biol.* **17**, 1556–68 (2015).

233. Cannino, G., Ciscato, F., Masgras, I., Sánchez-Martín, C. & Rasola, A. Metabolic Plasticity of Tumor Cell Mitochondria. *Front. Oncol.* **8**, 333 (2018).

234. Gray, L. R., Tompkins, S. C. & Taylor, E. B. Regulation of pyruvate metabolism and human disease. *Cell. Mol. life Sci.* **71**, 2577–604 (2014).

235. Yu, D. *et al.* Kidney-type glutaminase (GLS1) is a biomarker for pathologic diagnosis and prognosis of hepatocellular carcinoma. *Oncotarget* **6**, 7619–31 (2015).

236. Li, B. *et al.* Targeting glutaminase 1 attenuates stemness properties in hepatocellular carcinoma by increasing reactive oxygen species and suppressing Wnt/beta-catenin pathway. *EBioMedicine* **39**, 239–254 (2019).

237. Garber, K. Cancer anabolic metabolism inhibitors move into clinic. *Nat. Biotechnol.* **34**, 794–795 (2016).

238. Biancur, D. E. *et al.* Compensatory metabolic networks in pancreatic cancers upon perturbation of glutamine metabolism. *Nat. Commun.* **8**, 15965–80 (2017).

239. Ulanet, D. B. *et al.* Mesenchymal Phenotype Predisposes Lung Cancer Cells to Impaired Proliferation and Redox Stress in Response to Glutaminase Inhibition. *PLoS One* **9**, 1–22 (2014).

240. Lee, S. Y. *et al.* Dlx-2 and glutaminase upregulate epithelial-mesenchymal transition and glycolytic switch. *Oncotarget* **7**, 7925–39 (2016).

241. Yang, L. *et al.* Metabolic shifts toward glutamine regulate tumor growth, invasion and bioenergetics in ovarian cancer. *Mol. Syst. Biol.* **10**, 728–728 (2014).

242. Liao, Y., Yin, S., Chen, Z., Li, F. & Zhao, B. High glucose promotes tumor cell proliferation and migration in lung adenocarcinoma via the RAGE-NOXs pathway. *Mol. Med. Rep.* **17**, 8536–8541 (2018).

243. Sun, S., Sun, Y., Rong, X. & Bai, L. High glucose promotes breast cancer proliferation and metastasis by impairing angiotensinogen expression. *Biosci. Rep.* **39**, 1–9 (2019).

244. Ding, C. Z. *et al.* High glucose contributes to the proliferation and migration of non-small-cell lung cancer cells via GAS5-TRIB3 axis. *Biosci. Rep.* **38**, 1–10 (2018).

245. Ishida, T. *et al.* Investigation of the Influence of Glucose Concentration on Cancer Cells by Using a Microfluidic Gradient Generator without the Induction of Large Shear Stress. *Micromachines* **7**, 155–170 (2016).

246. Duran, A. *et al.* p62 Is a Key Regulator of Nutrient Sensing in the mTORC1 Pathway. *Mol. Cell* **44**, 134–146 (2011).

247. Linares, J. F. *et al.* Amino Acid Activation of mTORC1 by a PB1-Domain-Driven Kinase Complex Cascade. *Cell Rep.* **12**, 1339–1352 (2015).

248. Zhang, N. *et al.* Increased Amino Acid Uptake Supports Autophagy-Deficient Cell Survival upon Glutamine Deprivation. *Cell Rep.* **23**, 3006–3020 (2018).

249. Mundi, P. S., Sachdev, J., McCourt, C. & Kalinsky, K. AKT in cancer: new molecular insights and advances in drug development. *Br. J. Clin. Pharmacol.* **82**, 943–56 (2016).

250. Irie, H. Y. *et al.* Distinct roles of Akt1 and Akt2 in regulating cell migration and epithelial-mesenchymal transition. *J. Cell Biol.* **171**, 1023–34 (2005).

251. Cichon, A.-C. *et al.* AKT in Stromal Fibroblasts Controls Invasion of Epithelial Cells. *Oncotarget* **4**, 1103–1116 (2013).

252. Attoub, S., Arafat, K., Kamel Hammadi, N., Mester, J. & Gaben, A. M. Akt2 knock-down reveals its contribution to human lung cancer cell proliferation, growth, motility, invasion and endothelial cell tube formation. *Sci. Rep.* **5**, 12759 1–14 (2015).

253. Arboleda, M. J. *et al.* Overexpression of AKT2/protein kinase Bbeta leads to up-regulation of beta1 integrins, increased invasion, and metastasis of human breast and ovarian cancer cells. *Cancer Res.* **63**, 196–206 (2003).

254. Park, B. K., Zeng, X. & Glazer, R. I. Akt1 induces extracellular matrix invasion and matrix metalloproteinase-2 activity in mouse mammary epithelial cells. *Cancer Res.* **61**, 7647–53 (2001).

255. Manning, B. D. & Toker, A. AKT/PKB Signaling: Navigating the Network. *Cell* **169**, 381–405 (2017).

256. Sundar, R., Gudey, S. K., Heldin, C.-H. & Landström, M. TRAF6 promotes TGFβ-induced invasion and cell-cycle regulation via Lys63-linked polyubiquitination of Lys178 in TGFβ type I receptor. *Cell Cycle* **14**, 554–565 (2015).

257. Mu, Y. *et al.* TRAF6 ubiquitinates TGFβ type I receptor to promote its cleavage and nuclear translocation in cancer. *Nat. Commun.* **2**, 330 1–11 (2011).

258. Song, J. & Landström, M. TGFβ activates PI3K-AKT signaling via TRAF6. *Oncotarget* **8**, 99205–99206 (2017).

259. Moloughney, J. G. *et al.* mTORC2 Responds to Glutamine Catabolite Levels to Modulate the Hexosamine Biosynthesis Enzyme GFAT1. *Mol. Cell* **63**, 811–26 (2016).

260. Stewart, T. J., Liewehr, D. J., Steinberg, S. M., Greeneltch, K. M. & Abrams, S. I. Modulating the Expression of IFN Regulatory Factor 8 Alters the Protumorigenic Behavior of CD11b+Gr-1+ Myeloid Cells. *J. Immunol.* **183**, 117–128 (2009).

261. Wang, C. T., Li, J. J., Lai, H. Y. & Hu, B. S. A human cell line constitutively expressing HIV-1 Gag and Gag-Pol gene products. *J. Med. Virol.* **57**, 17–24 (1999).

262. Morita, S., Kojima, T. & Kitamura, T. Plat-E: an efficient and stable system for transient packaging of retroviruses. *Gene Ther.* **7**, 1063–1066 (2000).

263. Ozols, J. Amino acid analysis. *Methods Enzymol.* **182**, 587–601 (1990).